INFORMATION TO USERS

This manuscript has been reproduced from the microfilm master. UMI films the text directly from the original or copy submitted. Thus, some thesis and dissertation copies are in typewriter face, while others may be from any type of computer printer.

The quality of this reproduction is dependent upon the quality of the copy submitted. Broken or indistinct print, colored or poor quality illustrations and photographs, print bleedthrough, substandard margins, and improper alignment can adversely affect reproduction.

In the unlikely event that the author did not send UMI a complete manuscript and there are missing pages, these will be noted. Also, if unauthorized copyright material had to be removed, a note will indicate the deletion.

Oversize materials (e.g., maps, drawings, charts) are reproduced by sectioning the original, beginning at the upper left-hand corner and continuing from left to right in equal sections with small overlaps.

Photographs included in the original manuscript have been reproduced xerographically in this copy. Higher quality 6" x 9" black and white photographic prints are available for any photographs or illustrations appearing in this copy for an additional charge. Contact UMI directly to order.

Bell & Howell Information and Learning
300 North Zeeb Road, Ann Arbor, MI 48106-1346 USA
800-521-0600

THE PRESSURE-VOLUME-TEMPERATURE BEHAVIOR

AND

THE EFFECT OF PRESSURE ON CRYSTALLIZATION KINETICS

OF

POLYETHYLENE RESINS

by

Ludovic CAPT

A Thesis Submitted to the Faculty of Graduate Studies and Research in Partial Fulfillment of the Requirements for the Degree of Master of Engineering

Department of Chemical Engineering
McGill University
Montreal

January, 1999

ABSTRACT

In plastics manufacturing, the morphology and crystallinity are important in the determination of the properties of the final product. They are influenced by several parameters, in particular the pressure and the temperature history during solidification. Therefore, the study of the influence of pressure and temperature on crystallization kinetics is important. In this study, the crystallization kinetics and the PVT behavior of various grades of polyethylene resins were evaluated and compared using a high-pressure dilatometer under both isothermal and isobaric conditions. Also, the PVT behavior was compared to the predictions of the Tait equation of state. It was found that polyethylene chain structure, as determined by branching and branching uniformity, influences nucleation, crystallization kinetics, and the effect of pressure on these processes. In addition, the results confirm the decrease of the surface free energy of the crystal nucleus with increasing pressure.

RÉSUMÉ

Dans la fabrication d'articles en plastique, les propriétés du produit fini sont principalement déterminées par la morphologie et la cristallinité. Ces dernières sont controlées par plusieurs paramètres, en particulier par la pression et la température, pendant la solidification. En conséquence, il est intéressant d'étudier l'éffet de la pression et de la température sur la cinétique de cristallisation. Dans le cadre de cette étude, la cinétique de cristallisation et les diagrammes de Pression-Volume-Température d'une variété de résines de polyéthylene ont été investigués et comparés en utilisant un dilatomètre à haute pression. . De plus, le comportement de l'état fondu a été comparé avec les prédictions de l'équation d'état de Tait. Il a été découvert que les propriétés structurelles de la chaine moléculaire du polyéthylene, en particulier les branches et leur distribution, influencent la nucléation, la cristallisation et l'effet de la pression sur ces deux phénomènes. Les résultats ont aussi confirmé la diminution de l'énergie libre de surface du nucleus avec l'augmentation de la pression.

A la mémoire de mon
grand-père Pierrot.

ACKNOWLEDGEMENTS

I wish to express my deepest appreciation and utmost gratitude for the guidance and encouragement received from my research supervisor, Prof. M. R. Kamal, who stimulated my initial interest in the field of polymer science and engineering.

I also would like to express my sincere appreciation to Mr. M. Samara for his invaluable comments and suggestions during this investigation, and to my colleagues for their help in various aspects.

I am indebted to Nova Chemicals for supplying the materials used in this study.

I also extend my gratefulness to the financial support received from the National Science and Engineering, Research Council of Canada, the Ministère de l'Education du Québec, and the department of Chemical Engineering in the form of teaching and research assistantships.

I am especially grateful to Miss Gloria Vendrell for her encouragement and her suggestions.

Finally, I would like to express my love to my parents for their patience and constant encouragement.

TABLE OF CONTENTS

LIST OF FIGURES

LIST OF TABLES

CHAPTER 1

INTRODUCTION

Polymers are long molecules composed of large numbers of structural units that are chemically bonded. Among the large variety of commercial synthetic polymers, polyethylene is based on the simplest structural ethylene unit, $(-CH_2-CH_2-)_n$. Since 1939, when it was first discovered, polyethylene has evolved into different molecular structures, which give a wide range of properties and end uses. Consequently, polyethylene resins are now classified in three main groups, depending on resin density:

High Density Polyethylene (HDPE)	> 0.94 g/cm^3
Medium Density Polyethylene (MDPE)	0.926 to 0.94
Low Density Polyethylene (LDPE)	0.915 0.925 g/cm^3
Elastomers or Very Low Density Polyethylene (VLDPE)	< 0.915 g/cm^3

The category of LDPE also includes the linear low density polyethylene (LLDPE) resins, which can be distinguished from LDPE resins by the type of chain branching. Special interest is given to LLDPE in this study. LLDPE resins are copolymers based on ethylene and a comonomer (for example, butene, hexene, or octene), that yield short-chain branches. These resins differ in the type and content of comonomers in the copolymer, compositional and branching uniformity, crystallinity and density, and molecular weight and molecular weight distribution (MWD). This large variety of commodity and specialty resins can be obtained by varying the polymerization process conditions, such as polymerization medium, catalysts, and comonomer.

In industry, end user plastics products are manufactured by diverse polymer processing techniques, such as injection molding, blow molding, blow film extrusion,

compression molding, etc.... During these processing operations, polymer resins are exposed to elevated temperatures and pressures, and to stress, strain, etc.... The processing conditions affect the nature of the crystalline structure of polymers, referred to as morphology, which is controlled by the crystallization mechanisms. For a material such as polyethylene, morphology and crystallinity are influenced by the polymer chain structure. Polymer chain structure is defined in terms of: branching size, branching distribution, molecular weight, and MWD. Moreover, morphology and crystallinity determine the ultimate mechanical and physical properties of the final product, such as toughness, brittleness, ductility, elasticity, permeability, transparency, etc.

In view of the above, it is important to investigate the effect of processing conditions and polymer chain structure on crystallization to have a better understanding of the factors affecting the ultimate properties of the end products.

The present work deals with the study of the pressure-volume-temperature (PVT) properties and the effect of pressure on crystallization kinetics for 12 linear low density polyethylene and one high density polyethylene resins. The LLDPE resins consist of various grades of resins prepared by either solution or gas phase polymerization with metallocene or Ziegler-Natta catalysts. They also differ by the content and type of comonomer.

The text is divided into six chapters. Chapters 1 and 2 present the theoretical background. They review the characteristics of the LLDPE resins, polymer crystallization, and polymer PVT properties. Chapter 3 states the objectives of this project. Chapters 4 and 5 describe the experimental procedures and the methods for data analysis. Chapter 6 first presents the results concerning the equations of state, and subsequently, the pressure dependence of crystallization and melting temperatures. Furthermore, the effect of pressure on crystallization kinetic is discussed in light of different theories. Chapter 7 contains the conclusions and suggestions for further work.

Part of the abundant numerical data generated by this work is tabulated in the appendices. An appendix also gives an analysis of error associated with the measurements.

CHAPTER 2

THEORETICAL BACKGROUND

In this chapter, relevant information reported in the literature is presented in three sections. The first section describes briefly the different polymerization processes and their influences on the physical properties of linear low density polyethylene resins. The second section reviews the concepts of polymer crystallization and crystallization kinetics. The last part presents the pressure-volume-temperature properties of polymers.

2.1) LINEAR LOW DENSITY POLYETHYLENE

The large variety of semicrystalline ethylene copolymers, which contain small amount of comonomers (α-olefins), are produced in catalytic polymerization reactions. These copolymers have a lower density than those of ethylene homopolymers. They are usually referred as linear low-density polyethylene (LLDPE) to distinguish them from conventional low density polyethylene (LDPE). LDPE contains long branches, versus short branches for LLDPE, and it is produced in radical polymerization reactions at high pressure.

The large group of commodity and specialty resins collectively known as LLDPE includes a wide range of different resins. Each resin has different properties that depend on the type and content of comonomers in the copolymer, compositional and branching regularity and uniformity, crystallinity, density, molecular weight and molecular weight distribution (MWD). All these resin properties are a consequence of the type of catalyst and polymerization process employed to produce the resin. Figure 2.1 illustrates the various polyethylene types and their simplified chain structures.

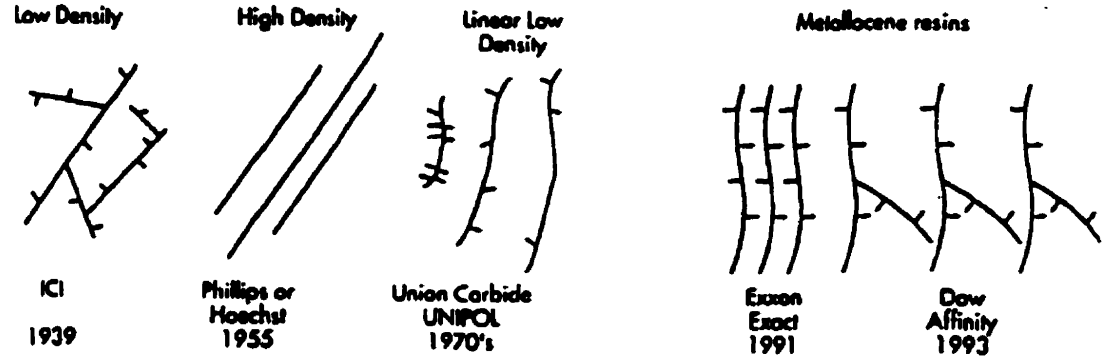

Figure 2.1: Evolution of the polyethylene carbon chain.

2.1.1) Catalysts for LLDPE Production

LLDPE resins are produced in industry with three classes of catalysts: titanium-based catalysts (Ziegler-Natta), metallocene-based catalysts (Kaminsky and Dow), and chromium oxide-based catalysts (Phillips).

2.1.1.1) Ziegler-Natta Catalysts

These catalyst systems represent by far the greatest share of LLDPE resins manufactured. They consist of two components: the first contains as its active ingredient a derivative of a transition metal (usually titanium); the second is an organoaluminum compound. Typical heterogeneous Ziegler-Natta (ZN) catalysts operate at temperature of 70-100°C and pressure of 0.1-2 MPa. The polymerization reactions are carried out in an inert liquid medium (e.g., hexane, isobutane) or in the gas phase. Molecular weight is controlled by using hydrogen as chain-transfer agent.

All solid Ziegler-Natta catalysts contain a mixture of several types of active centers which lead to non-uniform ethylene-α-olefin copolymers, and produce a relatively broad copolymer MWD.

2.1.1.2) Metallocene Catalysts

Three types of metallocene catalysts are presently used in industry: Kaminsky, ionic combination, and Dow catalysts.

Kaminsky catalysts, the original metallocene catalyst systems, contain two components: methylaluminoxane and a metallocene complex of zirconium, titanium, or halfnium with two cyclopentadienyl rings. Most of Kaminsky catalysts contain only one type of active center. Thus, they produce LLDPE with uniform compositional distribution and quite narrow MWDs, which, at their limits, can be characterized by polydispersity indexes (M_w/M_n) of about 2.0 and melt flow ratio (MFR) of about 15. These features of the catalysts determine their use in the synthesis of either uniformly branched very low denisty polyethylene (VLDPE) resins or completely amorphous polyethylene plastomers. They have also been gradually replacing ZN catalysts for the manufacture of certain commodity LLDPE products.

Ionic catalysts are a combination of metallocene complexes of zirconium or titanium and perfluorinated aromatic boron compounds. These catalysts operate over a wide range of temperatures, -70 to 100°C; however, monomers of high purity are required to prevent catalyst poisoning. The LLDPE resins produced by ionic catalysts have a high compositional uniformity.

Dow catalysts, also known as constrained-geometry catalysts, contain only one type of active center and produce uniform LLDPE. They operate at temperature up to 160°C. Dow catalysts have a high capacity to copolymerize linear α-olefins with ethylene. As a result, when these catalysts are used in solution-type polymerization reactions, they also copolymerize ethylene with polymer molecules containing vinyl double bonds at their ends. This auto-copolymerization reaction can produce molecules with very few long-chain branches that yield some beneficial processing properties (cf. fig. 2.1, Dow Affinity 1993).

2.1.1.3) Chromium Oxide-Based Catalysts

Chromium oxide-based catalysts were originally developed by Phillips Petroleum Co. for the manufacture of HDPE resins. LLDPE resins produced with these catalysts have a very broad MWD, characterized by M_w/M_n in the 12-35 range and MFR in the 80-200 range.

2.1.2) Polymerization Processes

The common technologies for LLDPE manufacture include: gas-phase fluidized-bed polymerization, polymerization in solution, high pressure polymerization, and slurry polymerization. Most catalysts are fine-tuned for each particular process. In this present study, special interest will be given to the gas-phase and solution polymerization processes, which are discussed briefly below.

2.1.2.1) Gas-phase Polymerization

The first gas-phase fluidized-bed process for the production of LLDPE was developed by Union Carbide in 1977 (cf. fig. 2.1, Unipol 1977). The Unipol process is suitable for the production of both HDPE and LLDPE. It usually operates at pressure of 1.5-2.5 MPa and temperatures of 70-95°C. The reactor is filled with a bed of dry polymer particles vigorously agitated by a high velocity gas stream, and a mixture of ethylene, comonomers, nitrogen, and hydrogen that is used for molecular weight control. Catalyst particles are continuously fed into the reactor, in which they remain, on average, for 2.5-4 hours.

The gas-phase processes are economical, flexible, and wide-ranging in the use of solid and supported catalysts. Most of the catalysts used for LLDPE production are heterogeneous ZN catalysts, which produce resins containing a pronounced non-uniform branching distribution. The gas phase can also accommodate supported metallocene catalysts that produce compositionally uniform LLDPE resins.

2.1.2.2) Solution Polymerization

Two types of solution polymerization technologies are used for LLDPE synthesis: one uses heavy solvents as a polymerization medium, and the other is carried out in mixtures of supercritical ethylene and molten PE.

In the first process, copolymerization reactions are carried out in the temperature range of 130-250°C, at reactor pressure of 3-20 MPa, and with an ethylene content of 8-10%. It usually operates at residence times of around 5-10 minutes. Three properties of LLDPE are controlled independently: the molecular weight, the copolymer composition, and, in the case of metallocene catalysts, the degree of long-chain branching (Dow Affinity, cf. fig 2.1). The control variables are: temperature, pressure, monomer and polymer concentrations, residence time, and catalyst concentration.

The second type of polymerization concept operates at temperature of 170-350°C and under pressure of 30-200 MPa. The residence time in these reactors is short, from 1 to 5 minutes. Exxon uses metallocene catalysts in a similar solution process to produce uniformly branched ethylene copolymers called Exact resins (cf. fig. 2.1, Exxon Exact).

Solution processes acquired new importance because of their shorter residence times and ability to accommodate metallocene catalysts. Many heterogeneous multi center Ziegler catalysts produce superior LLDPE resins (with better branching uniformity) when the catalyst residence time in the reactor is short. Solution processes, both in heavy solvents and in the polymer melt, are inherently suitable to accommodate soluble metallocene catalysts.

2.1.3) Properties of LLDPE

2.1.3.1) Type of comonomer

Four olefinic comonomers are used in industry to manufacture LLDPE: 1-butene, 1-hexene, 4-methyl-1-pentene, and 1-octene. The content of comonomer in copolymer varies greatly from 1 to 2 mol % (characteristic of medium density polyethylene resins) to around 20 mol % in PE elastomers. The type of comonomer exerts a significant influence on the copolymer properties. For instance, ethylene-1-butene copolymers exhibit inferior mechanical properties to those of ethylene copolymers with other comonomers.

2.1.3.2) Branching Uniformity

Two classes of LLDPE resins are on the market. The metallocene catalyst-based resins have a predominantly uniform branching distribution; that is, all the copolymer molecules have approximately the same composition. In contrast, the Ziegler-Natta catalyst-based resins have pronounced non-uniform branching distributions. Uniformly and non-uniformly branched LLDPE resins differ significantly in physical and mechanical properties.

As a rule, LLDPE resins do not contain long-chain branches. However, some copolymers produced with metallocene catalysts in solution processes can contain about 0.002 long-chain branches per 1000 ethylene units. These branches are formed in auto-copolymerization, as explained above.

2.1.3.3) Crystallinity and density

These two parameters, which are closely related, depend mostly on the content of comonomer in the copolymer. Both density and crystallinity of LLDPE are influenced by the branching uniformity. For instance, an increase in the comonomer content of a copolymer results in a decrease of both crystallinity and density, accompanied by a significant reduction of the stiffness of the polymer.

2.1.3.4) Molecular Weight

The range of molecular weights of commercial LLDPE resins is relatively narrow, usually from 50,000 to 200,000. A typical melt index range for LLDPE resins is from 0.1 to 5.0, but can reach over 30 for some applications. Most commodity-grade LLDPE resins have a narrow MWD, with the M_w/M_n ratios of 2.5-4.5 and MFR values in the 2.-35 range. However, LLDPE resins produced with chromium oxide-based catalysts have a broad MWD, with M_w/M_n of 10-35 and MFR of 80-200.

2.1.3.5) Physical Properties

a) Melting Behavior

Melting points of LLDPE with uniform compositional distributions (prepared with metallocene catalysts) decreases almost linearly with copolymer composition: for instance, from ~ 120°C - for copolymers containing 1.5-2 mol % of comonomer - to ~ 110°C - for copolymers containing 3.5 mol % of comonomer.

In contrast, a copolymer with a non-uniform compositional distribution (e.g., prepared by ZN catalysts) is a mixture that contains copolymer molecules with a broad range of compositions, from almost linear molecules (usually higher molecular weight) to short macromolecules with quite high comonomer content. Melting of such mixtures is dominated by their low branched fractions which are highly crystalline. As a result, the melting points of LLDPE resins with non-uniform branching distribution are not too sensitive to copolymer composition and usually fall in the temperature range of 125-128°C.

b) Thermal and Oxidative Degradation

LLDPE is relatively stable to heat. Thermal degradation starts at temperatures above 250°C and results in a gradual decrease of molecular weight and the formation of double bonds in polymer chains. Oxidation of LLDPE can occur because of heating or sunlight exposure. Thermo-oxidative degredation starts at temperatures above 150°C.

c) Crystalline structure

The presence of short-chain branches in LLDPE molecules inhibits the uniform folding of polymer chains during crystallization. Such inhibition can both decrease the lamellar thickness and increase the number of intermolecular tie molecules, thus resulting in a stronger material. The size of the lamellae for a copolymer of a given composition depends on the degree of branching uniformity. If a LLDPE resin has a uniform branching, all its molecules crystallize poorly due to branching, forming very thin lamellae. Such materials have low rigidity and high flexibility. On the other hand, for a LLDPE resin containing non-uniform branching, its least-branched components crystallize in thicker lamellae; consequently, more branched fractions of the resin remain amorphous and fill the voids between lamellae.

A consequence of the different LLDPE crystalline structures is observed in optical properties. Resins with a uniform branching distribution (metallocene) make highly transparent film with haze as low as 3-4 %. In contrast, films manufactured from compositionally non-uniform copolymers (Ziegler-Natta) are much more opaque, with haze of over 10-15 %; the opacity is due to the presence of large crystalline lamellae consisting of nearly non-branched PE chains.

d) Mechanical Properties

Mechanical properties of LLDPE are attributed to the complex interaction of their structural characteristics: type and content of comonomer, branching uniformity, molecular weight and MWD, and orientation.

2.2) POLYMER CRYSTALLIZATION

A polymer melt can be solidified by lowering the temperature or by increasing the pressure. The resulting crystallization occurs as the macromolecular chains lose their mobility and become frozen in position, where chains are more closely packed than in the melt state. Crystallization behavior depends on the morphological structures that are produced. Morphology is associated with features such as crystallite size and shape, aggregate of crystallites, crystallinity, etc... The first section of the followinf discussion reviews the current models that are used to describe polymer morphology including chain folding, lamellar crystals, and spherulites. The next section discusses briefly the phenomena of nucleation and growth. The last part introduces the common kinetic models used to describe polymer crystallization.

Note: Many reviews on crystallization of polymers have been of considerable help in the preparation of the following section. The early book of Mandelkern[1], was an invaluable source of details. The reviews by Khoury and Passaglia[2], Hoffman et al.[3], and Magill[4] have been very helpful. The three volumes by Wunderlich[5,6,7] were particularly valuable for their exhaustive presentation of polymer physics. Finally, among more recent reviews, those by Chu[8], Mandelkern[9], and Strobl [10]were very contributive.

2.2.1) Polymer morphology

The macroscopic form and structure of the crystal is its morphology. Under a variety of circumstances, commonly encountered in practice, linear macromolecules crystallize into the form of thin platelets, which are known as crystallites. The large upper and lower surfaces consist of an array of macromolecular folds. The morphology of such polymer crystals was first investigated for crystals grown from solution. Nevertheless, crystals crystallized from the melt and their supermolecular structure are now well understood, thanks to the previous studies on solution-grown crystals. Even though this section will mainly outline the morphology of the structures obtained from crystallized melt, some results from solution-grown crystal studies will also be included.

2.2.1.1) Polymer Crystallography

The description of the crystal structure of a polymer is, in most respects, no different from that of a low molar mass compound. A crystal may be defined as a portion of matter within which the atoms are arranged in a regular three-dimensionally repeating pattern. A crystal may be classified into one of the seven large subgroups, referred to as crystal systems, such as triclinic, monoclinic, orthorhombic, etc...

For polyethylene, the orthorhombic crystal form is the most stable at atmospheric pressure. Furthermore, melt crystallization at pressure above 300 MPa (3kbar) leads to the formation of a high-pressure phase, which was discovered by Bassett and Turner[11]. Figure 2.2 illustrates the phase diagram of polyethylene.

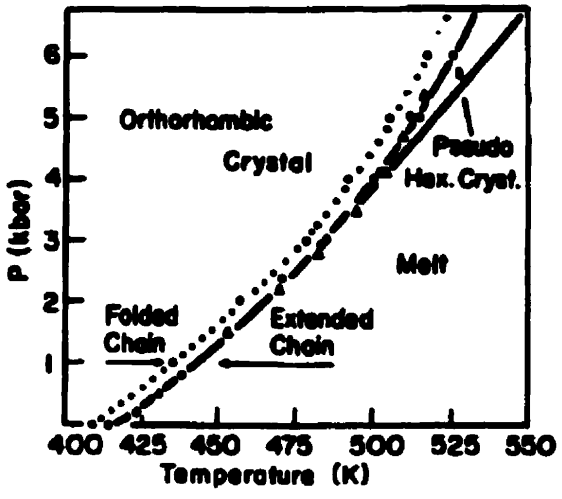

Figure2.2: Phase Diagram of Polyethylene[7].

The high-pressure phase is known as the disordered hexagonal or pseudo-hexagonal phase. The high pressure has been linked to the particular ease of chain extension on crystallization under high pressure. The changes of lattice parameters of polyethylene at 5 kbar pressure going through the transition to the high-pressure phase are shown in Figure 2.3. The crystallographic *a* axis expands continuously to the pseudo-hexagonal phase, while the *c* axis, the chain axis, contracts.

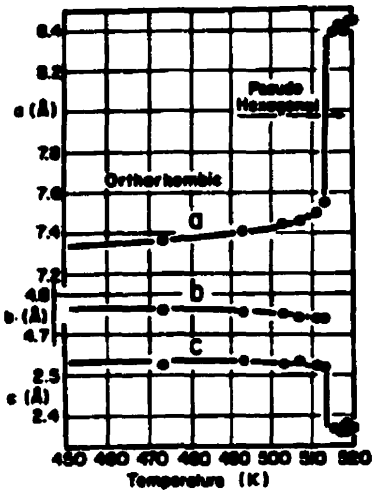

Figure 2.3: Change of lattice parameters of Polyethylene with Temperature at 5 kbar Pressure[7]

2.2.1.2) Chain Folding and lamellar crystals

The chain-folding model was first proposed in the years 1957-1960. Before that time, what was known concerning crystallinity in polymers was interpreted using the "fringed micelle" model, which is sketched in Figure 2.4.

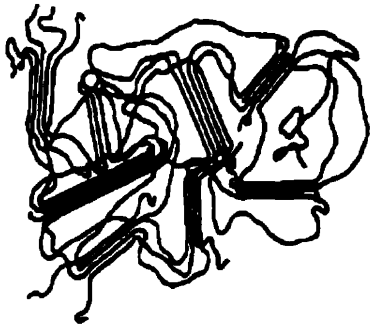

Figure 2.4: A schematic sketch of the fringed micelle model.

The fringed micelle model was supported by the fact that one molecule had to participate in more than one crystallite, because the molecular length was much larger than the known crystallite size. No one seems to have thought of folding the chain back into the crystallite to accommodate the same facts. After ignoring for two decades the early observation of chain folding in thin films of gutta percha by Storks[12], the similar,

yet independent, works of Keller[13], Fisher[14], and Till[15] on the identification of solution-grown polyethylene single crystals led to the concept of chain folding. A schematic chain-folded crystallite is illustrated in Figure 2.5.

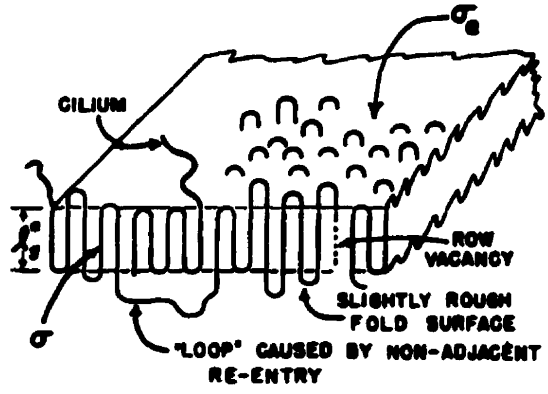

Figure 2.5: Schematic view of a single crystal with possible defects. (Ref. 2)

Figure 2.5 also shows the possible departures from strictly regular folding and defects in a single crystal. The non-adjacent re-entry and loose loop, the slightly rough surface, cilia, and row vacancy can be observed from this sketch. The existence of intercrystalline and interlamellar links shows that the non-adjacent re-entry and long cilia must certainly occur to some extent in melt-crystallized polymers. It should be noted that this sketch does not represent the possible configurations of single crystals, i.e. the hollow pyramid shape that is observed in solution-grown single crystals of polyethylene.

The effect of hydrostatic pressure on crystallization of lamellar crystals has been studied for many years. At sufficiently high pressure (above 300 MPa), polymer crystals show considerably increased thickness along macromolecular chains. These much thicker crystals are commonly known as chain-extended (CE) crystals.

Wunderlich et al.[16] suggested that the CE crystallization process consists of two processes. First, chain-folded lamellae are formed with thickness determined by undercooling, and then the chains are reorganized to CE conformation at high temperature and pressure. Bassett and Turner[11] showed that there are two concurrent competitive processes of crystallization of chain-folded and CE lamellae. Under higher pressure CE crystallization becomes dominant. It was suggested that orthorhombic chain-folded lamellae of polyethylene are formed directly from the melt, while CE crystals of polyethylene result via the intermediate hexagonal phase[11]. Maeda et al.[17] suggested the

existence of different extended-chain (EC) crystal forms: ordinary EC crystals having a lower melting point than that of high melting EC crystals. They proposed three ranges of pressure in which the crystallization is significantly different:

1. Up to 200 MPa. Polyethylene crystallizes directly from melt into chain-folded lamellae.
2. From 200 to 350 MPa. Polyethylene crystallizes into two forms: chain-folded lamellae and extended-chain lamellae.
3. Above 350 MPa, polyethylene crystallizes into low melting ordinary EC hexagonal crystals.

Annealing at elevated pressure causes also thickening of lamellae. Nonetheless, at constant temperature, an increase in pressure decreases the amount of thickening obtained.

It was found that the lamellar thickness depends on crystallization temperature and time, molecular weight, and pressure. Bassett and Turner[11] formulated the following conclusions concerning the lamellar thickness:

1- Increases with the increase of temperature at constant pressure
2- Increases with the increase of pressure at constant supercooling
3- Increases with increasing molecular weight in the range 20,000 to 50,000 g/mol at the same temperature and pressure of crystallization

Recently, Bassett et al.[18] used high-pressure (about 500 MPa) crystallization to compare three linear low-density polyethylenes, because their potential for forming lamellae whith thicknesses equal to the inter-branch separation. Lamellar thickness is much reduced for branched polyethylene containing ethyl or larger branches[18]. In this study, major differences were revealed between metallocene-catalyzed polymers and Ziegler-Natta-catalyzed resins. Butyl-branches were excluded from the hexagonal and orthorhombic lattices, and made the crystal thickness of the metallocene-catalyzed resin invariant.

2.2.1.3) Spherulites

The morphology of melt-crystallized polymers can be described by the following structural hierarchy: the lamellar crystal as the fundamental unit of the lamellar aggregates, which in turn build up various supermolecular structures, which are generally in the form of spherulites. Spherulites consist principally of chain-folded lamellae radiating from a central point, as shown in Figure 2.6.

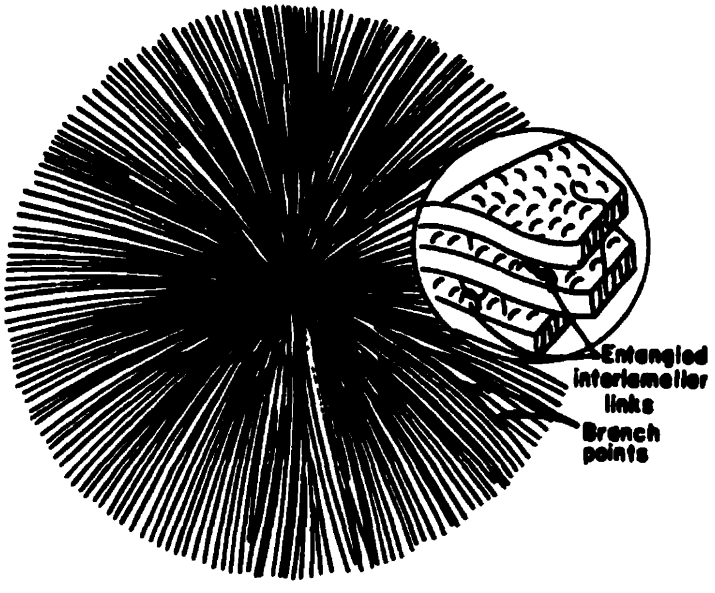

Figure 2.6: Polymer Spherulite with chain-folded lamellae (schematic).

Spherulites are optically anisotropic objects due to molecular orientations within the microscopic regions. The spherulite size may range from submicroscopic to several millimeters. The radial expansion of a spherulite is the result of the formation of lamellar stacks that grow from a common nucleation site, which could be a single crystal or some kind of heterogeneity. The growing spherulites in the crystallizing melt will eventually impinge upon one another.

Pressure, melt temperature, and time are the main parameters that can be used to control spherulite dimensions. Spherulite size increases at a fixed pressure, as the melt temperature is raised. It has been reported that spherulites become smaller with increasing pressure for fixed crystallization conditions[4]. Figure 2.7 reveals how the

spherulite diameter decreases with increasing pressure, which is equivalent to increasing the undercooling. The spherulite dimensions, thus, depend markedly on the degree of undercooling.

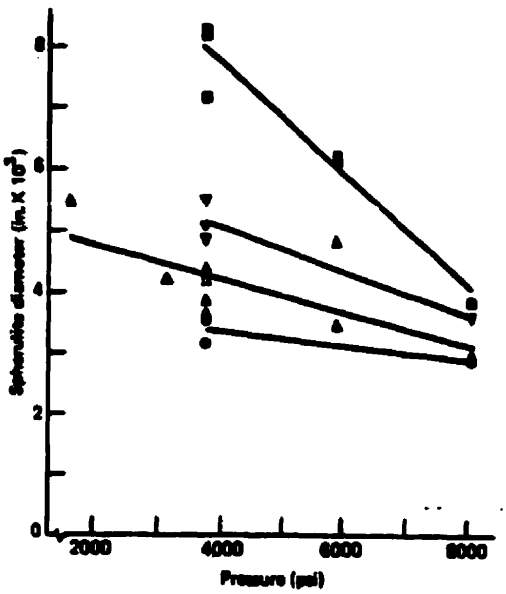

Figure 2.7: Spherulite size-pressure relationship for polypropylene for melt conditions: ●, 11 min at 200oC; ▲, 30min at 200oC; ▼, 120 min at 200oC; ■, 120 min at 220oC. Crystallization temperature 135oC (Reinshagen and Dunlap, 1973)[4].

Hatakeyama et al.[19] studied the crystallization of polyethylene up to 5000 kg/cm^2 (about 500 MPa) and reported that polyethylene crystallized into the spherulitic morphology in the pressure range 1000-2000 kg/cm^2 (100-200 MPa). More recently, Kowalewski and Galeski[20] observed spherulitic crystallization up to about 600 MPa.

The isothermal growth rate of spherulites is a function of crystallization temperature and pressure as well as the molecular weight of the polymer. These different effects on the rate of spherulite growth will be discussed in Section 2.2.2.2).

2.2.2) Nucleation and growth

Crystallization is generally divided into two fundamental processes: nucleation and growth.

2.2.2.1) Nucleation

When a polymer melt is supercooled, there exists an interval of time, depending on crystallization temperature, referred as induction time, during which nuclei start forming randomly and growing to stable crystals. The nature of the nuclei determines the morphology of the subsequent crystallographic form of the growing crystallites[6]. The emergence of nuclei from the melt is called primary nucleation; the later surface nucleation on a crystal face, as a kind of growing mechanism, is referred as secondary nucleation.

Nucleation is divided into two distinct categories: homogeneous and heterogeneous. Homogeneous nucleation occurs in the pure molten phase; small portions of the polymer chains are oriented into regular lattices which give rise to the nuclei as a result of random fluctuations of order. Normally, it is unlikely that homogeneous nucleation would take place upon cooling of polymer melts. For linear polyethylene, only at supercooling greater than 55°C homogeneous nucleation is considered to be significant. Heterogeneous nucleation, however, usually prevails at low levels of supercooling, and the crystallization process is usually completed before reaching a sufficiently low temperature for homogeneous nucleation.

Indeed, heterogeneous nucleation is apparently initiated by heterogeneities present in the melt, such as impurities and foreign surfaces. A foreign surface reduces the nucleus size needed for crystal growth, since the creation of the interface between polymer crystal and substrate may be less hindered than the creation of the corresponding free polymer crystal surfaces.

Turnbull and Fisher[21] expressed the steady state nucleation rate in the form:

$$\dot{N} = \dot{N}_0 \exp\left(-\frac{E_D}{kT}\right)\exp\left(-\frac{\Delta G_m}{kT}\right) \qquad (2.1)$$

where $\dot{N}$ is the nucleation rate (in nuclei/sec.cm^3),

$\dot{N}_0$ is a pre-exponential factor, depending on molecular structure and crystal geometry

E_D is the free energy barrier opposing transport of segments across the melt-crystal interface (in ergs),

ΔG_m is the free energy required to form a critical nucleus in the melt (in ergs),

k is the Boltzmann's constant (in ergs/K),

T is the crystallization temperature.

The term $exp\left(-\frac{E_D}{kT}\right)$ expresses the probability that a segment of chain of critical length would reach a surface of a growing crystal in the local diffusive transport process at constant temperature and pressure. The nucleation term, $exp\left(-\frac{\Delta G_m}{kT}\right)$, corresponds to the probability that a surface nucleus would reach a critical size. Since the influence of the term E_D becomes significant around the glass transition temperature[22], and, on the other hand, ΔG_m is strongly dependent on temperature during crystallization[23], the nucleation rate is dominated by the nucleation term, and subsequently is a function of crystallization temperature.

The critical free energy, ΔG_m, of formation of a rectangular heterogeneous nucleus of thickness b_0 to a pre-existing flat surface is dependent on supercooling and surface free energy as shown below[8]:

$$\Delta G_m = \frac{16\sigma\sigma_e(\Delta\sigma)T_m^{0^2}}{\Delta h_u^{\,2}\Delta T^2} \qquad (2.2)$$

where σ is the specific free energy of the surface parallel to the chain axis

σ_e is the specific free energy of the crystal fold surface

$\Delta\sigma$ is the specific interfacial free energy difference parameter

T_m^0 is the equilibrium melting point

ΔT is the degree of supercooling, $T_m^0 - T$, at which the crystallization takes place

Δh_v is the enthalpy of fusion per unit volume of a large perfect crystal at T_m^0

Furthermore, the surface free energies, σ and σe of the crystal nucleus have been reported to depend on pressure[24,25,26].

2.2.2.2) Crystal Growth

A spherulite, as described earlier, may be considered as a system consisting of lamellae that radiate from a central point. It may be, therefore, assumed that spherulitic growth proceeds through repeated depositions of molecular layers of constant thickness. This means that linear crystal growth rate is linked to the secondary or molecular nucleation rate.

The growth rate, G, is described by an equation of the form[27]:

$$G = G_0 \exp\left(-\frac{E_D}{RT}\right)\exp\left(-\frac{\Delta G_m}{kT}\right) \qquad (2.3)$$

where G_0 is a pre-exponential constant, which is not strongly dependent on temperature and on molecular weight[28]. The ΔG_m term describes the free energy of the nucleus growing in an m-dimensional space. A two-dimensional lamellar crystal model seems to represent most polymer system adequately[29].

Based on the secondary nucleation growth rate of the Lauritzen-Hoffman model[3], the linear growth rate can also be written as:

$$G = G_0 \exp\left(-\frac{U^*}{R(T - T_\infty)}\right)\exp\left(-\frac{K_g}{T(\Delta T)f}\right) \qquad (2.4)$$

where U^* is the activation energy which governs the mobility of the polymer with respect to the temperature. T is the crystallization temperature, T_∞ is the WLF temperature at which the mobility of the molecules converges to zero, R is the gas constant, K_g is the nucleation factor, ΔT is the degree of supercooling, and f is a factor to correct the temperature dependence of the heat of fusion.

a) Influence of Crystallization Temperature on Growth Rate

The Lauritzen-Hoffman model has contributed to the study of the effect of temperature or the degree of supercooling on the spherulite growth rate. Hoffman et al.[3] reported that the growth rate of spherulite as a function of ΔT passes through a maximum, as illustrated in Figure 2.8.

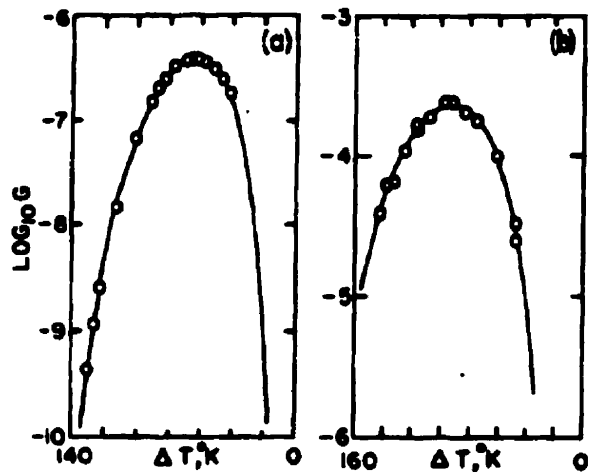

Figure 2.8: Temperature dependence of the growth rate of spherulite in isotactic polystyrene (a) and polyamide 6 (b). (Ref. 3)

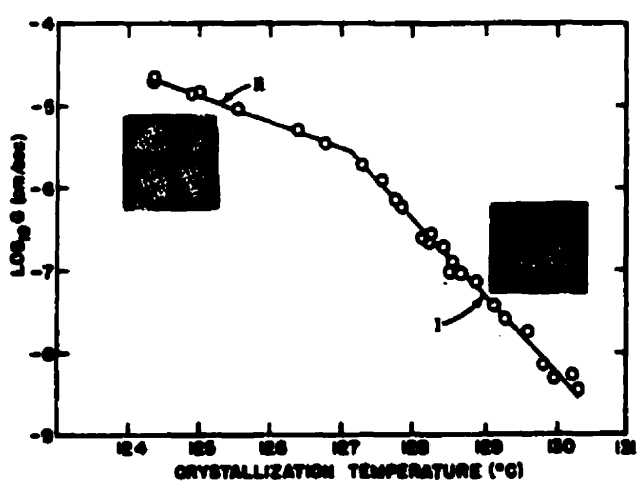

Figure 2.9: Dependence of the growth rate on crystallization temperature in polyethylene. (Ref. 3).

In addition, Hoffman et al.[3] experimentally reported two growth regimes depending on crystallization temperature. Regime I leads to axialite morphology, whereas regime II corresponds to spherulitic growth, as shown in Figure 2.9.

b) Influence of Molecular Weight on Growth rate.

The isothermal spherulite growth rate is a function of crystallization temperature, undercooling, pressure, and molecular weight of the polymer. The influence of molecular weight was studied by Magill[4]. Some of his results are presented in Figure 2.10.

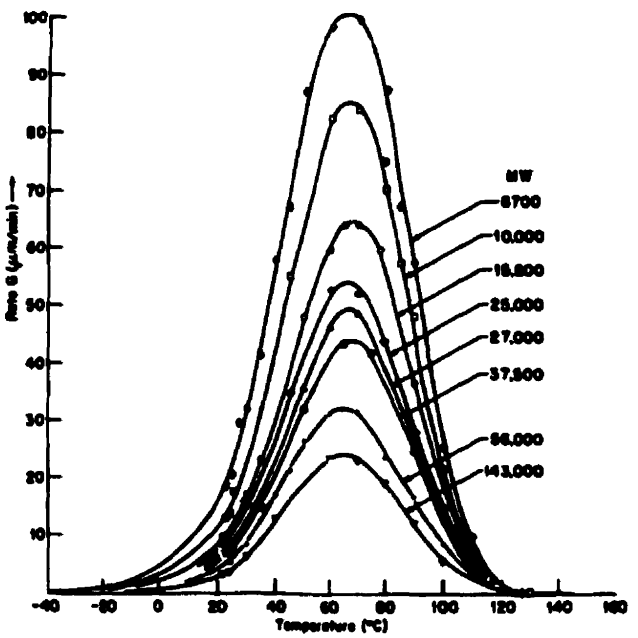

Figure 2.10: Dependence of Spherulitic Growth Rate on Temperature for Different Molecular Weights, (Ref. 4).

From this figure, it can be seen that the growth rate is increases as molecular weight decreases, at constant temperature.

c) Influence of Pressure on Growth rate.

Edwards and Phillips have reported that the rate of growth of row-nucleated lamellae in cis-polyisoprene passes though a maximum, as a function of pressure at constant temperature, as shown in Figure 2.11.

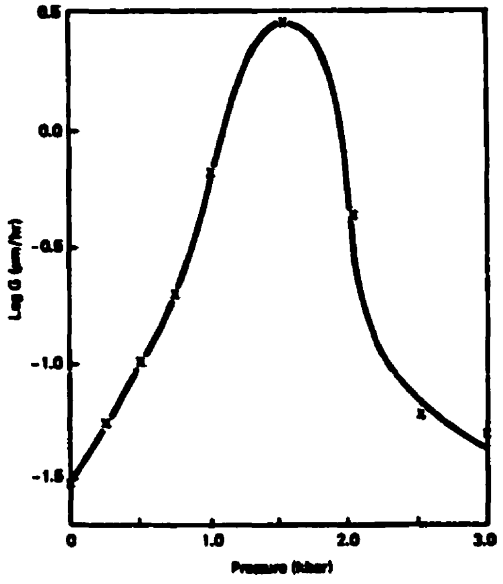

Figure 2.11: Logarithm of lamellar growth rate versus pressure for cis-polyisoprene at 0°C (Ref 4).

The growth rate was about six times larger than that experienced at the temperature corresponding to the maximum rate at atmospheric pressure. This increase can be explained by an increased G_0 with pressure and/or by the dependence of melting point on pressure[4]. Edwards and Phillips also found that the lamellar growth rate is constant for a given supercooling, but that it increases as the pressure is lowered at constant temperature, as presented in Figure 2.12. They also observed a similar trend for spherulite growth[30].

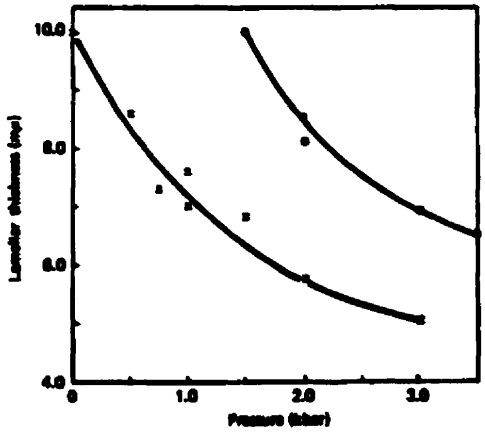

Figure 2.12: Lamellar crystal thickness versus pressure at 0°C for cis-polyisoprene (Ref. 4).

It is known that the crystallization of polyethylene under pressure is governed by primary nucleation since the dominant supermolecular structures are spherulites[20].

2.2.2.3) Secondary Crystallization and Crystal Perfection

The process that comprises the initial nucleus formation and the following spherulitic growth is generally called primary crystallization. At this stage, more than half of the final crystallinity of the polymer has been reached. Any further crystallization, which is largely associated with slow thickening and lateral growth of the lamellae in the crystal stacks, is labeled secondary crystallization. The term secondary crystallization is frequently applied to all effects that increase the crystallinity after the primary crystallization is over. The secondary crystallization is characterized by a linear increase of the degree of crystallinity with the logarithmic time[31].

Secondary crystallization involves two processes: further perfection of the poorly crystallized polymer in the spherulites and further crystallization of the remaining amorphous phase.

Strobl[10] proposed a slightly different definition of secondary crystallization, namely further crystallization that occurs when the sample is cooled from the crystallization temperature to room temperature. Investigating the effect of this additional crystallization on polyethylene, Strobl[10] reported different behavior for linear and branched polyethylene. The 'insertion mode' of secondary crystallization of branched polyethylene provided a larger part (35%) than that of the isothermal primary crystallization (15%). On the other hand, secondary crystallization of linear polyethylene was characterized by a surface crystallization-process that only caused a 10% increase in crystallinity. Secondary crystallization will thus depend on the branching content of the macromolecular chains.

2.2.3) Crystallization Kinetics

Study of crystallization kinetics at high pressure has been carried by a variety of techniques. Matsuoka[32] studied polyethylene crystallization dilatometrically up to pressure of 2 kbar. Martin and Mandelkern[33] investigated crystallization of rubber at pressure up to 800 bar by observing a dilatometer through a window in a pressure vessel. The dilatometric technique was extended to a maximum pressure of 5.3 kbar with the improved high-pressure dilatometers used by Hatakeyama et al.[19], Kyotani and Kanetsuna[24], and Hoehn et al.[34] in studies of polyethylene and polyethylene fractions. Calvert and Uhlmann[35] conducted differential scanning calorimetry on pressure-quenched samples, and Wunderlich and Davidson[16] and Sawada and Nose[25] constructed a high-pressure differential thermal analysis cell for their study of polyethylene. Although the above methods are the most commonly used techniques, several others have been explored. Edwards and Philips[30] obtained kinetic information on *cis*-polyisoprene using transmission electron microscopy by chemically staining the samples at high pressure. X-ray, infrared studies, and Raman spectroscopy were also performed using the diamond anvil cell. Eckel, Buback, and Strobl[36] performed a combined high pressure Raman and dilatometric study on polyethylene. Bridges, Charlesby, and Folland[37] used pulsed NMR to measure crystallization kinetics of polyethylene at atmospheric pressure. Brown and Jonas[26] extended the NMR technique for their study of polyethylene crystallization kinetics under high pressure.

To represent crystallization kinetic data at atmospheric or high pressure, there are several kinetic equations. The theory of Lauritzen, Hoffman and co-workers[3] can also be applied to high pressure crystallization for further interpretation, as reported by Kyotani and Kanetsuna[24], Sawada and Nose[25], and Brown and Jonas[26], for polyethylene.

The influences of temperature and pressure on crystallization kinetics are reviewed in the second part of this chapter. The induction time dependence on temperature and the melting point dependence on pressure are also discussed.

2.2.3.1) The Kinetic Equations

The analysis of crystallization kinetics of polymers can based depending on phase transformation conditions, on isothermal or non-isothermal experiments. Isothermal experimental data have been generally represented with the generalized Avrami equation. The Avrami equation has been found useful to describe accurately the primary crystallization, which starts at the end of the induction time, and ends at the beginning of the secondary crystallization.

Modifications of the Avrami equation have been proposed to describe secondary or non-isothermal crystallization. Tobin[38], Dietz[39], Malkin et al.[40] and Kim and Kim[41] suggested models to describe crystallization kinetics when secondary crystallization was observed. For non-isothermal kinetics, Nakamura[42] and Kamal and Chu[43] developed techniques, also based on the Avrami equation.

a) The Generalized Avrami Equation

The Avrami[44,45] equation is applicable to any type of crystallization. It describes the time evolution of the overall crystallinity. The Avrami equation has been commonly applied to describe the overall isothermal transformation kinetics, and it is expressed as follows:

$$x(t) = 1 - exp(-kt^n) \tag{2.5}$$

where $x(t)$ is the relative crystallinity achieved after some time t. The constant n represents the mode of nucleation and k the growth rate, known as the rate constant of crystallization. It should be noted that the Avrami equation was derived under several assumptions such as that the crystallization goes to completion, and that the kinetics remains the same during crystallization. Mandelkern[46] introduced, for isothermal conditions, the generalized Avrami equation expressed as:

$$X(t) \equiv \frac{x(t)}{x_\infty(t)} = 1 - exp\left[k(T)t^n\right] \tag{2.6}$$

where $x(t)$ is the actual fraction of the crystallized polymer at time t, $x_\infty(t)$ is the ultimate crystallinity fraction achieved at temperature T, and $X(t)$ is known as the relative

crystallinity that varies from 0 at the beginning of crystallization to 1 at the end. The crystallization half time $t_{1/2}$:

$$t_{1/2} = \left(\frac{ln2}{k}\right)^{1/n} \tag{2.7}$$

is the time at which half of the conversion has taken place, which is a convenient measure for the speed of crystallization.

The Avrami exponent n was first limited to integer values because it is thought that the values of n could give an indication of particular types of nucleation and crystal growth. In most of recent research, the Avrami equation was used as a convenient equation to represent and compare kinetic data, therefore, the restriction on n was released.

b) Tobin's Model

Tobin[38] proposed a new model based on the generalized Avrami equation, by pointing out that the phase transition problem must be cast into the form of the Volterra integral equation. This relation was derived for two separate cases: homogeneous and heterogeneous nucleation and growth.

For conversion below 50% and for $1 \leq n \leq 4$, Tobin's equation is expressed in the form:

$$\frac{X(t)}{1-X(t)} = kt^n \tag{2.8}$$

The advantage of Tobin's model is that it represents the secondary crystallization phenomenon, with a slightly better accuracy than that of Avrami.

c) Dietz's model

Dietz[39] modified the Avrami equation by introducing an additional parameter to describe the secondary crystallization:

$$\frac{dX(t)}{dt} = nkt^{n-1}[1-X(t)]exp\left[\frac{-aX(t)}{1-X(t)}\right] \tag{2.9}$$

Here a is the new introduced parameter.

d) Kim and Kim's model

Kim and Kim[41] derived a new crystallization kinetics equation by considering the decrease of the growth rate with crystallinity. Their modified Avrami equation is:

$$X(t) = 1 - exp\left[-kf(t)^n\right] \tag{2.10}$$

$$f(t) = \int_0^t \left[1 - X(t)\right]^m dt \tag{2.11}$$

where $X(t)$ and k have the same definition as those in eq. (145) and f(t) is a growth function. For m=0, the relation reduces to the Avrami form. For $m>0$, the growth rate decreases with time.

e) Hillier's Model

Based on the assumption that the secondary crystallization is a slow first-order process, Hillier[47] proposed a modified two-stage model:

$$X(t) = X_p^{\infty}\left[1 - exp(-k_p t^n)\right] + X_s^{\infty} k_s \times \int_0^t \left[1 - exp(k_p \theta^n)\right] \times \left[exp(-k_s(t-\theta))\right] d\theta \tag{2.12}$$

where the subscripts p and s refer to primary and secondary crystallization, respectively. The secondary crystallization starts when the primary crystallization is assumed to be completed. This is indicated by a change in the order of crystallinity-time dependence.

2.2.3.2) Factors influencing crystallization kinetics

Crystallization kinetics of polymers can be significantly affected by several factors such as crystallization temperature, pressure, stress, flow, and induction time. The temperature and pressure effects will be discussed in the following section.

a) Influence of Temperature

Crystallization rates in polymers are strongly dependent on temperature, pressure, and stress (molecular orientation). At atmospheric pressure, the crystallization rate constant, k, is equal to zero above the equilibrium melting point and below the glass transition temperature. In the intermediate region, it exhibits a maximum, which was observed[29] for a variety of polymers at $T_{max} = 0.82T_m^0$. It has been shown that the logarithm of the crystallization rate versus temperature appears in a parabolic form[48]. Furthermore, Ziabicki[49] proposed an empirical equation for the temperature dependence of the crystallization half-times as follows:

$$\left(\frac{1}{t_{1/2}}\right) = \left(\frac{1}{t_{1/2}}\right)_{max} exp\left[-4\ln(2)\frac{(T-T_{max})^2}{D^2}\right] \qquad (2.13)$$

where $(1/t_{1/2})_{max}$, T_{max} and D can be determined from experimental data.

b) Influence of Pressure

The Avrami equation has been commonly used to represent isothermal crystallization kinetic data at atmospheric pressure and high pressure. The range of Avrami exponent *n* observed for polyethylene under atmospheric pressure is exceedingly broad, covering the range from 1 to 4[6]. Hatakeyama et al.[19] observed an Avrami exponent close to 1 for crystallization of polyethylene at 500 MPa. Kyotani and Kanetsuna[24] found values of *n* decreasing from approximately 2 at 840 kbar to 1.2 at 5 and 5.2 kbar. Hoehn et al.[34] observed values centered in the region 2.0-2.2. Sawada and Nose[25] found values of *n* between 1.8 and 2.3 for extended-chain crystals in the range 2.49-3.0 kbar. Their results for folded-chain crystals in this pressure range fell between 2.9 and 3.4. Brown and Jonas[26] observed values of *n* between 1.3 and 1.7 in the pressure range from 1.0 to 4.5 kbar. They found that the Avrami exponent was not dependent on pressure, but rather on undercooling; it decreased with increasing supercooling. This was also observed by Kyotani and Kanetsuna[24]. Exact agreement among the different studies is not expected, since crystallization behavior is well known to be dependent on molecular weight and polydispersity.

The effect of pressure on the crystallization rate is generally explained by its effect on melt temperature, i.e. an increase of the degree of supercooling with pressure. However, the crystallization rate has been found to be dependent on pressure at constant supercooling. Wunderlich and Davidson[16] found that the degree of supercooling necessary for crystallization increased by 50% in going from atmospheric pressure to 5 kbar, indicating that under identical supercooling, crystallization was retarded by pressure. On the other hand, Hatakeyama et al.[19] observed that the crystallization rate, estimated from the half-time of crystallization, was increased when pressure was raised from 1.0 to 2.0 kbar and from 4.0 to 5.0 kbar at constant supercooling. The results of Kyotani and Kanetsuna[24] were in agreement with this observation.

The theory of Lauritzen and Hoffman[3] has also been used for further interpretation. Brown and Jonas[26] plotted the Avrami rate constant k versus $T_m^2/T(\Delta T)^2$ and versus $T_m/T(\Delta T)$ to distinguish between rate control by the process of diffusion or by nucleation and growth. They observed that the logarithm of the crystallization rate was linearly dependent on both temperature variables, and that the slopes of these lines decreased by increasing pressure. These results are in agreement with the ones found by Kyotani and Kanetsuna[24] and Sawada and Nose[25]. Brown and Jonas concluded that the crystal nucleus surface energies were decreasing with increasing pressure. This observation is in contradiction with the observation of Calvert and Uhlmann[35], which indicates an increase of the surface energy of the lamellar crystal with increasing pressure.

2.2.3.3) Others aspects of Crystallization Kinetics

a) Induction Time

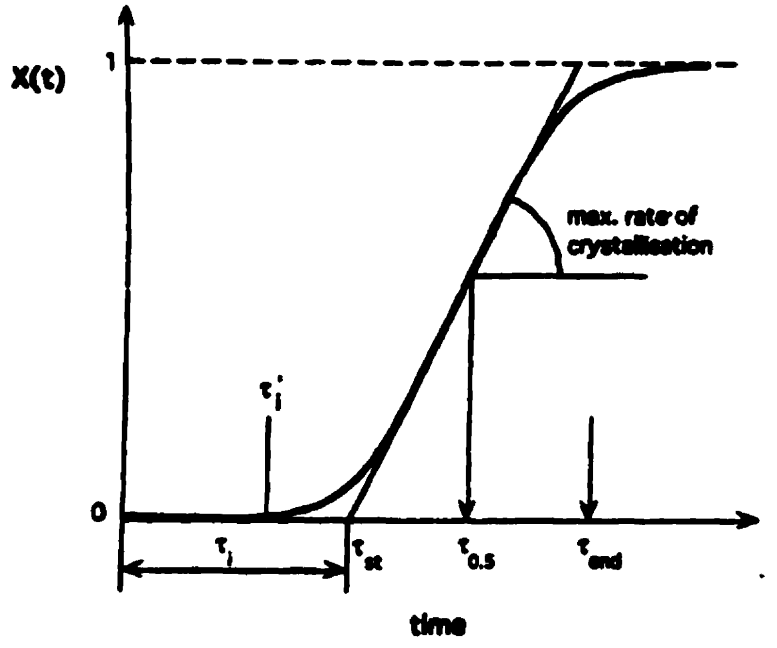

Figure 2.13: Schematic diagram of the crystallization process as a function of time, with a definition of certain quantities.

Figure 2.13 illustrates the graphical inflection method that can be used to define three characteristic quantities. The tangent to the curve at the inflection point defines the maximum crystallization rate; the half time of crystallization, $\tau_{0.5}$ at which half of the crystallization has occurred; and the incubation period, τ_i. In this graph, there is another incubation period, τ_i', indicating the point at which the curve deviates from zero value. The induction time, τ_i', is defined as the time interval required at a supercooled state before the critical equilibrium nucleus dimension is established, and τ_i is defined as the time to reach the steady state of nucleation. There exists also a time interval before spherulites can be resolved with the optical microscope and this is referred as the apparent incubation period. There is no valid reason to prefer one definition to another, except that the induction times defined by the construction in Figure 2.13 are less dependent on experimental technique.

The dependence of the induction time, τ, on the degree of supercooling, ΔT, has been formulated by Godovsky and Slominsky[29] as:

$$\tau = P(\Delta T)^{-\varepsilon} \tag{2.14}$$

where P and ε are constants. The values of ε ranged between 8 and 15 for a variety of synthetic polymers.

b) Pressure Dependence of Temperature

The main effect of pressure on crystallization kinetics is attributed to the effect of pressure on melting point, thus the degree of supercooling. The increase of melting point, T_m, and crystallization temperature, T_c, with pressure has been investigated for many years. The values of T_m and T_c exhibit an almost linear dependence on pressure up to 200 MPa, which is in agreement with the Clausius-Clapeyron equation, defined as follows:

$$\frac{dT_m}{dP} = \Delta V_f^0 \frac{T_m^0}{\Delta H_f^0} = constant \tag{2.15}$$

where ΔV_f^0 is the volume change on fusion, ΔH_f^0 is the heat of fusion, and T_m^0 is the equilibrium melting point. For polyethylene, the values of $\frac{dT_m}{dP}$ were found to be in the range from 0.22°C/MPa for folded-chain crystals, to 0.35°C/MPa for extended-chain crystals[16]. Wunderlich and Davidson[16] calculated a theoretical value of $\frac{dT_m}{dP}$ at atmospheric pressure for a hypothetical perfect crystal, and reported a value of 0.32°C/Mpa. In addition, Saeki et al.[50] demonstrated that the Clausius-Clapeyron equation was useful to calculate values of the entropy of fusion under high pressure.

However, it has been shown that for large pressure increase, the melting curve of polyethylene decreases in slope with increasing pressure[16,51]. Takamizawa et al.[51] showed that the dependence of the melting point for large pressure increases was best represented by the Simon equation[52]:

$$P - P_0 = a\left[\left(\frac{T_m}{T_{m,0}}\right)^c - 1\right] \tag{2.16}$$

where T_m is the melting temperature at pressure P, and $T_{m,0}$ that at atmospheric pressure; a and c are constants that depend on each substance. For polyethylene, the authors found that the constants a and c depended on the molecular weight. These parameters were found to range from 315 to 362 MPa for a and from 3.85 to 422 for the parameter c. It must be noted that the Simon equation does not, however, predict the maximum point in the T_m-P curve.

2.3) PRESSURE-VOLUME-TEMPERATURE PROPERTIES OF POLYMERS

A Pressure-Volume-Temperature (PVT) study consists of analyzing the significant effect of pressure and temperature on the specific volume of polymers. The understanding of the PVT behavior of a polymer system is important for the analysis and understanding of processing operations, in which shrinkage and compressibility effects are significant. Compressibility, thermal expansion coefficient, and the temperature region in which crystallization, glass formation or melting take place are easily assessed from PVT measurements. A PVT investigation also contributes to the understanding of the thermodynamics of polymers through the equations of state.

2.3.1) Pressure-Volume-Temperature Apparatus

Several suitable techniques exist to study the PVT behavior of polymers. The latest reported technique uses an injection molding machine to generate PVT data for thermoplastics[53]. Nevertheless, most of the published PVT data were obtained using the classical bellows technique. This methodology is divided into two available methods that differ by the manner in which pressure is applied to samples. In the first method, which has been used mainly in the past, pressure is axially applied to the sample by the use of a cylindrical piston. However, except for true liquid samples, recent research[54] reveals that, generally, this direct measuring technique does not provide an accurate method for

determining the response of semicrystalline polymers to pressure, especially for the solid state. There is an alternative technique that subjects the material to a true hydrostatic pressure through the use of a confining fluid, usually mercury. This last technique, which is utilized in the apparatus adopted for this work is described in detail in Chapter 4.

2.3.2) Equations of State

The equilibrium pressure-volume-temperature (PVT) properties of a melt can be described by an equation of state: V=V(P,T). Several empirical and theoretical equations of state are available to describe polymer melts, glasses and crystals, reviewed by Zoller[55] and Bhateja and Pae[56]. The most useful equations are the empirical Tait equation[6] for melts and glasses, the theory of Simha and Somcynsky[57] for melts and glasses, and of Simha and Jain[58] for crystals. In addition, there is the Inverse-Volume equation, developed by Kamal and Levan[59], which yields consistent values for the prediction of the thermal expansion coefficient and compressibility of polymers. For its simplicity and for the sake of comparing the accuracy of our experiments with literature, the empirical Tait equation was chosen to represent the melt behavior of the resins under investigation. In addition, the inverse-volume equation was utilized in order to describe the compressibility and the thermal expansion coefficient of the materials.

The empirical Modified Tait equation and Inverse-Volume equation are briefly introduced in this section.

2.3.2.1) The Modified Tait equation

The Tait equation[60] was originally proposed to explain the compressibility behavior of seawater. It was later found to describe the PVT response, except at high pressure, of some liquid hydrocarbons and also of some crystalline hydrocarbons. Simha et al.[57] also found the Tait equation to apply well to amorphous polymers such as PS, PMMA, and PVC. The Tait equation is usually expressed in the form:

$$V(P,T)=V(0,T)\{1-C\ln[1+\frac{P}{B(T)}]\} \qquad (2.17)$$

$V(P,T)$ is the specific volume at pressure P and temperature T, C is a constant, which is dependent on the structure and molecular weight in the case of hydrocarbons, and $B(T)$ is a material constant that is written as:

$$B(T)=B_0\exp(-B_1T) \qquad (2.18)$$

where B_0, B_1 and C are the three adjustable Tait parameters. The value of constant C was estimated to be similar for many hydrocarbons. Furthermore, the Tait relation was found to be valid for high pressure in the glassy state and also for semicrystalline polyethylene. Nowadays, this equation is commonly used to describe the PVT behavior of a large variety of polymers, with a "universal" value of C, C=0.0894. However, Beret and Prausntiz[61] have reported that the three-parameter Tait equation represents the PVT data with appreciably better accuracy than the two-parameter Tait equation (where C is equal to the universal value of 0.0894) especially for polyethylene.

The volume at atmospheric pressure is calculated by extrapolation. $V(0,T)$ can be fitted by a polynomial of the form:

$$V(0,T) = A_0 + A_1 T + A_2 T^2 + A_3 T^3 + \ldots \qquad \text{for } T<T_m \qquad (2.19)$$

And by an exponential of the form:

$$V(0,T) = V_0 \exp(\alpha T) \qquad \text{for } T>T_m \qquad (2.20)$$

with α, V_0 constant thermal expansion coefficient.

2.3.2.2) The Inverse-Volume Equation

This equation is based on the observations that, in most polymers, the inverse volume vs. temperature curve at constant pressure, $(\partial\rho/\partial P)_T$ vs. pressure at constant temperature, and the thermal expansion coefficient α vs. temperature can all be approximated by straight lines. Kamal and Levan[59] proposed the following inverse-volume equation of state with six adjustable parameters ρ_∞, $\left(\frac{\partial\rho}{\partial P}\right)_{P=0}$, a, b, c, and d:

$$\rho = \rho_{\infty} + \left(\frac{\partial \rho}{\partial T}\right)_{P=0} \times T + (a + bT)P + \frac{1}{2}(c + dT)P^2 \qquad (2.21)$$

where $\rho(T,P)$ is the density at pressure P and temperature T, and ρ_{∞} is the density at zero pressure and 0°K. The authors found this equation to fit available experimental PVT data of polymers very well. In addition, they made a comparison among various equations of state. It was found that only the inverse-volume equation was observed to predict correctly an increase in thermal expansion with increasing temperature.

2.3.3) Compressibility and Thermal Expansion Coefficient

It is common to express certain properties of the equation of state in the form of derivatives to represent the solid-state and the melt behavior of polymers. The isothermal compressibility K(P,T) is defined as:

$$K(P,T) = \frac{-1}{V(P,T)}\left(\frac{\partial V(P,T)}{\partial P}\right)_T \qquad (2.22)$$

and the coefficient of volume thermal expansion α(P,T) as

$$\alpha(P,T) = \frac{1}{V(P,T)}\left(\frac{\partial V(P,T)}{\partial T}\right)_P \qquad (2.23)$$

The two empirical equations discussed in this paper yield the forms for compressibility and thermal expansion coefficient shown Table 2.1.

For polyethylene, Galeski et al.[20] measured the bulk thermal expansion coefficient of the melt at atmospheric pressure, $\alpha = 8.55\times10^{-4}°K^{-1}$, and in the solid state, α was equal to 3.0×10^{-4} °K^{-1}. Compressibility of polymers has generally the following values: for the solid state, from 1×10^{-4} to 3×10^{-4} MPa^{-1}, and from 3×10^{-4} to 25×10^{-4} MPa^{-1} for the melt[62].

Table 2.1:Expressions of Compressibility and Thermal Expansion Coefficient for the Tait and the Inverse-Volume Equations.

Equation	α ($^{\circ}C^{-1}$)	K (Pa^{-1})
Tait	$\alpha_0 - KPB_1$	$\frac{1}{(P+B)\left[\frac{1}{c} - ln\left(1+\frac{P}{B_0 exp(-B_1 T)}\right)\right]}$
Inverse-Volume	$-V\left[\left(\frac{\partial P}{\partial T}\right)_{P=0} + bP + \frac{dP^2}{2}\right]$	$V[a+cP+T(b+dP)]$

2.3.4) Literature Review for Various Polyethylenes

Many studies investigated the PVT properties of polyethylene, and experimental data were predominantly fitted to the empirical Tait equation. Since polyethylene resins can easily vary from one type to another, the different literature values of the Tait equation parameters should not be compared. However, Table 2.2 presents a range in which those parameters were found. The literature values reported below were calculated using the universal value of the constant C of 0.0894. For the melt, the different Tait parameters exhibit in the values reported Table2.2:

Table 2.2: Value range for the fitting parameters of the Tait Equation in the melt for polyethylene

Polymer Type	Density (g/cm^3)	V_0 (cm^3/g)	α ($^{\circ}C^{-1}$)	B_0 (MPa)	B_1 ($^{\circ}C^{-1}$)
Low density	0.9190	1.148	6.95	192.9	4.70
Branched	0.9320	0.940	7.34	177.1	4.63
Linear	0.9794	0.971	7.81	176.7	4.66

Note: the values of this table were obtained from the Polymer Handbook (Ref. 55)

Among the large amount of literature concerning PVT properties of polymers, few studies compared PVT behavior of similar polymeric materials. Nevertheless,

Zoller[63] investigated the PVT behavior of three identical low-density polyethylenes, which had equal density and identical number-average molecular weight, but differed in weight-average molecular weight and in vinyl groups. These three resins were found to exhibit similar PVT properties in the melt, i.e. comparable Tait parameters. However, variations in the zero-pressure compressibility were reported.

References

1 L. Mandelkern, *Crystallization of Polymers*, McGraw-Hill, New York, 1964.
2 F. Khoury and E. Passaglia, *Treatise on Solid State Chemistry*, vol. 3, N. B. Hanny, Ed., Plenum Press, New York, 1976.
3 J. D. Hoffman, G. T. Davis, and J. L. Lauritzen, *Treatise on Solid State Chemistry*, vol. 3, N. B. Hanny, Ed., Plenum Press, New York, 1976.
4 J. H. Magill, *Properties of solid polymeric materials, Part A*, Treatise on Materials Science and Technology, 10, (J.M. Schultz Ed.), Academic Press, New York, 1977.
5 B. Wunderlich, *Crystal Structure, Morphology, Defects*, Macromolecular Physics, vol. 1, Academic Press, New York, 1973.
6 B. Wunderlich, *Crystal Nucleation, Growth, Annealing*, Macromolecular Physics, vol. 2, Academic Press, New York, 1976.
7 B. Wunderlich, *Crystal Melting*, Macromolecular Physics, vol. 3, Academic Press, New York, 1980.
8 E. Chu, Master of Engineering, McGill University
9 L. Mandelkern, Physical properties of Polymers, 2nd ed., ACS Professional Ref Book, ACS, Washington, 1993.
10 G. R. Strobl, *Concepts for understanding their structures and behavior*, The Physics of Polymers, Springer Ed., Berlin, 1996.
11 D. C. Bassett, B. Turner, *On Chain-extended and chain-folded crystallization of Polyethylene*, Phil. Mag., 29, 285 (1974).
12 K. H. Storks, *An Electron-Diffraction Examination of Some Linear High Polymers*, J. Am. Chem. Soc., 60, 1753 (1938)
13 A., Keller, Phil. Mag., 2 1171 (1957)
14 E. W. Fischer, Z. Naturforsh, 12A, 753 (1957)
15 P. H., Jr. Till, J. Polym. Sci., 24, 301 (1957)
16 T. Davidson, B. Wunderlich, *Differential Analysis of Polyethylene under High Pressure*, J. Polym. Sci., Part A2, 7, 377 (1969)
17 Y. Maeda, H. Kanetsuna, K, Tagashira, and T. Takemura, J. Polym. Sci. Polym. Phys. Ed., 19,1313 (1981)
18 J. A. Parker, D.C. Bassett, R. H. Olley, and P. Jaaskelainen, *On high pressure crystallization and the characterization of linear low-density polyethylenes*, Polymer, 35, 4140, (1994)
19 T. Hatakeyama, H. Kanetsuna, H. Kaneda, and T. Hashimoto, *Effect of Pressure on the Crystallization Kinetics of Polyethylene*, J. Macromol. Sci. Phys., B10(2), 359 (1974)
20 T. Kowalewski and A. Galeski, *Crystalization of Linear Polyethylene from Melt in Isothermal Compression*, J. Appl. Polym. Sci., 44, 95 (1992).
21 D, Turnbull and J.C. Fisher, *Rate of Nucleation in Condensed Systems*, J. Chem. Phys., 17, 71 (1949)
22 F. P. Price, *Nucleation in Polymer Crystallization*, in "Nucleation" (A. C. Zettlemoyer, ed.), pp. 405-488 Marcel Dekker, New York (1969)
23 F. P. Price, *Kinetics of Spherulite Formation*, J. Polym. Sci., C, 3, 117 (1963).
24 M. Kyotani and H. Kanetsuna, *Crystallization Kinetics of Polyethylene under Pressure*, J. Polym. Sci. Polyms. Phys., Ed., 12, 2331 (1974).

25 S. Sawada and T. T. Nose, *Crystallization Kinetics of Fractionated Polyethylenes at high pressures by a DTA method*, Polym. J., 11, 477, (1979).
26 D. R. Brown and J. Jonas, *NMR Study of Polyethylene Crystallization Kinetics under High Pressure*, J. Polym. Sci. Polym. Phys. Ed., 22, 655 (1984).

27 H. D. Keith, and F.J., Jr., Padden, Spherulitic *Crystallization from the melt. II. Influence of Fractionation and Impurity Segregation on the Kinetics of Crystallization*, J. Appl. Phys., 35, 1270 (1964).
28 D. W. van Krevelen, *Crystallinity of polymers and the means to influence the crystallization process*, Chimia, 32, 279 (1978).
29 Y. K. Godovsky and G. L. *Slonimsky, Kinetics of Crystallization from the Melt (Calorimetry Approach)*, J. Polym. Sci. Polym. Phys., Ed., 12, 1053 (1974).
30 B. C. Edwards and P. J. Phillips, *High-Pressure Phases in Polymers II...* J. Polym. Sci.: Polym. Phys. Ed., 13, 2117 (1975).
31 J. M. Schultz, J. S. Lin, and R. W. Hendricks, *A dynamic Study of the Crystallization of Polyethylene from the melt*, J. Appl. Cryt., 11, 551 (1978).
32 . Matsuoka, *Pressure-induced Crystallization in Polyethylene*, J. Polym. Sci., 42, 511 (1960).
33 G. M Martin and L. Mandelkern, J. Appl. Phys, 34, 2312 (1963).
34 H. H. Hoehn, R. C. Fergurson, and R. R. Herbert, *Effect of Molecular weight on high pressure crystallization of linear polyethylene. I kinetics and gross morphology*, Polym. Eng. Sci., 18, 457 (1978).
35 P. D. Calvert and D. R. Uhlmann, *Crystallization of polyethylene at high pressures: A kinetic view*, J. Polym. Sci. A-2, 10, 1811 (1972).
36 R. Eckel, M. Buback, and G. R. Strobl, Colloid Polym. Sci., 259, 326 (1981).
37 B. J. Bridges, A. Charlesby, and R. Folland, Proc. R. Soc. Lodon Ser. A, 367, 343 (1979).
38 M.C. Tobin, *The Theory of Phase Transition Kinetics with Growth Site Impingement. II. Heterogeneous Nucleation*, J. Polym. Sci.: Polym. Phys. Ed., 14, 2253 (1976).
39 W. Dietz, *Sphärolithwachstum in Polymeren*, Coll. Polym. Sci., 259, 413 (1981).
40 Y. A. Malkin, V. P. Beghishev, I. A. Keapin, and Bolgov S. A., *General treatment of polymer crystallization kinetics--Part1. A new macrokinetic equation and its experimental verification*, Polym. Eng. Sci., 24, 1396 (1984).
41 S. P. Kim and S. C. Kim, *Crystallization of Polyethylene Terephthalate. Part I: Kinetic Equation with Variable Growth Rate*, Polym. Eng. Sci., 31, 110 (1991).
42 K. Nakamura, T. Watanabee, and K. Katayama, J. Appl. Polym. Sci., 16, 1077 (1972).
43 M. R. Kamal and E. Chu, *Isothermal and Non-isothermal Crystallization of Polytehylene*, Polym. Eng. Sci., 23, 27 (1983).
44 M. Avrami, J. Chem. Phys., 7, 1103 (1939).
45 M. Avrami, J. Chem. Phys., 8, 212 (1940).
46 L. Mandelkern, J. Appl. Phys. 26, 443 (1955).
47 I. H. Hiller, J. Plym. Sci., A, 3, 3069 (1965).
48 B. B. Burnett, and W. F. McDevit, J. Appl. Phys., 28, 1101 (1957).
49 A. Ziabicki, Colloid Polym. Sci., 252, 207 (1974)

50 S. Saeki, S. Taeki, Y. Ookubo, M. Tsubokawa, T. Yamaguchi, and T. Kikegawa, *Pressure dependence of melting temperatures in branched polyethylene up to 2 GPa*, Polymer, **39**, 4267 (1998).
51 K. Takamizawa, A. Ohno, and Y. Urabe, *Effect of Pressure on Melting Temperatures of Polyethylene Fractions*, Polym. J., **7**, 342 (1975)
52 Von F. Simon and G. Glatzel, *Bemerkungen zur Schemelzdruckkurve*, Z. Anorg. Allg. Chem., **178**, 309 (1929).
53 C. P. Chiu, K. A. Liu, and J. H. Wei, *A Method for Measuring PVT Relationships of Thermoplastics Using an Injection Molding Machine*, Polym. Eng. Sci., **35**, 1505 (1995).
54 Y. A. Fakhreddine and P. Zoller, *Pressure-Volume-Temperature Studies: A Versatile Analytical Tool for Polymers*, ANTEC. Conference Proceedings. 1991. Soc. of Plastics Engineers, Brookfield, CT, USA., 1642 (1991).
55 P. Zoller, "Polymeric Equations of State," *Polymer Handbook*, 3rd Edition, J. Brandup and E. H. Immergut, Editors: Wiley & Sons, (1989).
56 S. K. Bhateja and K. D. Pae, *J. Macromol. Sci. Revs. Macromol. Chem.*, **13**, 77 (1975).
57 R. Simha and T. Somcynsky, *Macromolecules*, **2**, 342 (1969).
58 R. Simha and R. K. Jain, *J. Polym. Sci. Polym. Phys. Ed.*, **16**, p1471-89 (1978).
59 M. R. Kamal and N. T. Levan, *Polym. Eng. Sci.*, **13**, p131-138 (1973).
60 P. G. Tait, "*Physics and chemistry of the voyage of H. M. S. challenger*," **2**, Pt.4, University Press, Cambridge, p1900 (1888).
61 S. Beret and J. M. Prausnitz, *Densities of Liquid Polymers at High Pressure. Pressure-Volume-Temperature Measurements for Polyethylene, Polyisobutylene, Poly(vinyl acetate) and Poly(dimethylsiloxane) to 1kbar*, Macromolecules, **8**, 536 (1975).
62 *Dilatometry*, Encyclopedia of Polymer Science and Engineering, 2nd Edition, H. Mark, N. Bikales, Ch. Overberger, Ed.; Wiley & Sons, New York, 1986.
63 P. Zoller, *The pressure-volume-temperature properties of three well-characterized low-density polyethylenes*, J. Appl. Polym. Sci., **23**, 1051 (1979).

CHAPTER 3

OBJECTIVES

The present work is part of a more general research program, currently in progress in this laboratory, to study the effect of processing conditions, such as pressure, temperature, stress, and deformation history, on morphology and crystallinity, and, subsequently, on the optical and mechanical properties of the final product. Using a pressure-volume-temperature apparatus, the present research project attempts to study and compare the PVT behavior and the effect of pressure on crystallization kinetics of various grades of polyethylene resins.

The main specific objectives of the present study are outlined as follows:

(1) To carry out PVT measurements up to 200 MPa for the 13 resins in the isothermal and isobaric modes of investigation.

(2) To perform isothermal crystallization studies under various pressures for the resins.

(3) To obtain the equations of state of the PVT melt behavior of the resins using the isothermal experiment data.

(4) To assess the melting and crystallization temperatures up to 200 MPa and their dependence on pressure.

(5) To fit kinetic data with the Avrami equation and compare the crystallization kinetics of the various grades of polyethylene resins.

(6) To evaluate the influences of the polymerization process parameters and the structural parameters of the polymer on the crystallization behavior under pressure of polyethylene resins.

Some polymers are known to solidify in a two-step crystallization process, referred to as primary and secondary crystallization. However, the Avrami equation cannot be used to represent the two-step process. Nevertheless, primary crystallization is

the most kinetically important step during solidification. Therefore, the present work has also involved the development of an analytical technique to assess consistently the end of primary crystallization for fitting purpose.

CHAPTER 4

EXPERIMENTAL

This chapter is devoted to describing the physical properties of the materials used in the present study. Detail description of the pressure-volume-temperature apparatus, its principle and the measurement procedure employed in this work are also presented.

4.1) Polyethylene Resin Properties

The 12 LLDPE resins, used in the present study, were provided by Nova Chemicals, as well as the commercial HDPE resin, Sclair 2908. The LLDPE resins are experimental resins that were prepared under different polymerization conditions. The resins were copolymerized in gas phase or solution medium, using Ziegler-Natta or Metallocene catalysts with different comonomer types (butene, hexene or octene). The properties resulting from the various polymerization conditions, as supplied by NOVA, are listed in Table 4.1.

Table 4.1: Proprieties of polyethylene resins.

Code	Comonomer Type	Medium	Catalyst	Density (g/cm^3)	Melt Index (g/10min)	Mn (g/mol)	Mw (g/mol)	Mw/Mn	Comonomer %
HDPE	/	/	/	0,961	7,4	22300	74500	3,3	/
A	Hexene	Gas	ZN	0,9208	0,90	30000	111000	3,7	3,94
B	Butene	Gas	ZN	0,9194	0,94	24200	98700	4,1	4,03
C	Hexene	Solution	Met	0,9234	0,85	36000	111300	3,1	3,77
D	Hexene	Gas	Met	0,9192	1,00	44000	98000	2,2	3,08
E	Hexene	Gas	Met	0,9194	1,03	43000	94000	2,2	2,56
F	LDPE	Gas	/	0,9190	2,30	12000	88000	7,3	/
G	Octene	Solution	ZN	0,9200	1,00	17000	106000	6,2	3,20
H	Butene	Solution	ZN	0,9190	0,75	24900	120000	4,8	3,80
I	Octene	Solution	Met	0,9070	6,50	22000	53000	2,4	5,00
J	Octene	Solution	Met	0,9180	1,80	38000	70000	1,8	3,20
K	LDPE	Gas	/	0,9198	/	/	/	/	/
L	LLDPE	Solution	/	0,9222	/	/	/	/	/

4.2) Pressure-Volume-Temperature Apparatus

A fully automatic GNOMIX high-pressure dilatometer, based on principles described by Zoller[64] was used and is presented in this paragraph. A schematic drawing of the PVT apparatus is given in Figure 4.1.

In this apparatus, the sample is contained in a piezometer cell together with a confining fluid (in this study, mercury), which must not interact with the sample. Volume changes of the sample are calculated by subtracting the known volume change of fluid from the combined volume changes of the sample and the confining fluid.

The apparatus uses the bellows technique. The sample and the confining liquid are enclosed in a rigid sample cell, the piezometer cell, one end of which is closed by a flexible metal bellows. A hydrostatic pressure is applied outside the cell. The hydrostatic pressure of silicone oil (Dow Corning 210H) is produced with a high-pressure motorized (or manual) pump. The pump can produce pressures up to 200 MPa. The pressure is sealed in both ends by the vertical force of a 25-ton hydraulic ram. The pressure is transmitted to the contents by the flexible bellows, which expands until the pressure in the cell equals the applied pressure, except for a small pressure difference resulting from the spring constant of the bellows (amounting to less than 0.1 MPa[65]). The length change of the bellows is a measure for the volume change of the contents, provided the effective cross-sectional area of the bellows is known. The length change is measured by a linear variable differential transformer (LVDT), located beneath the pressure vessel. The highest part of the sample cell contains the polymer sample and is separated from the bellows using a nickel sample cup, which prevents molten polymer from getting into the corrugations of the bellows and maintains a hydrostatic pressure[65].

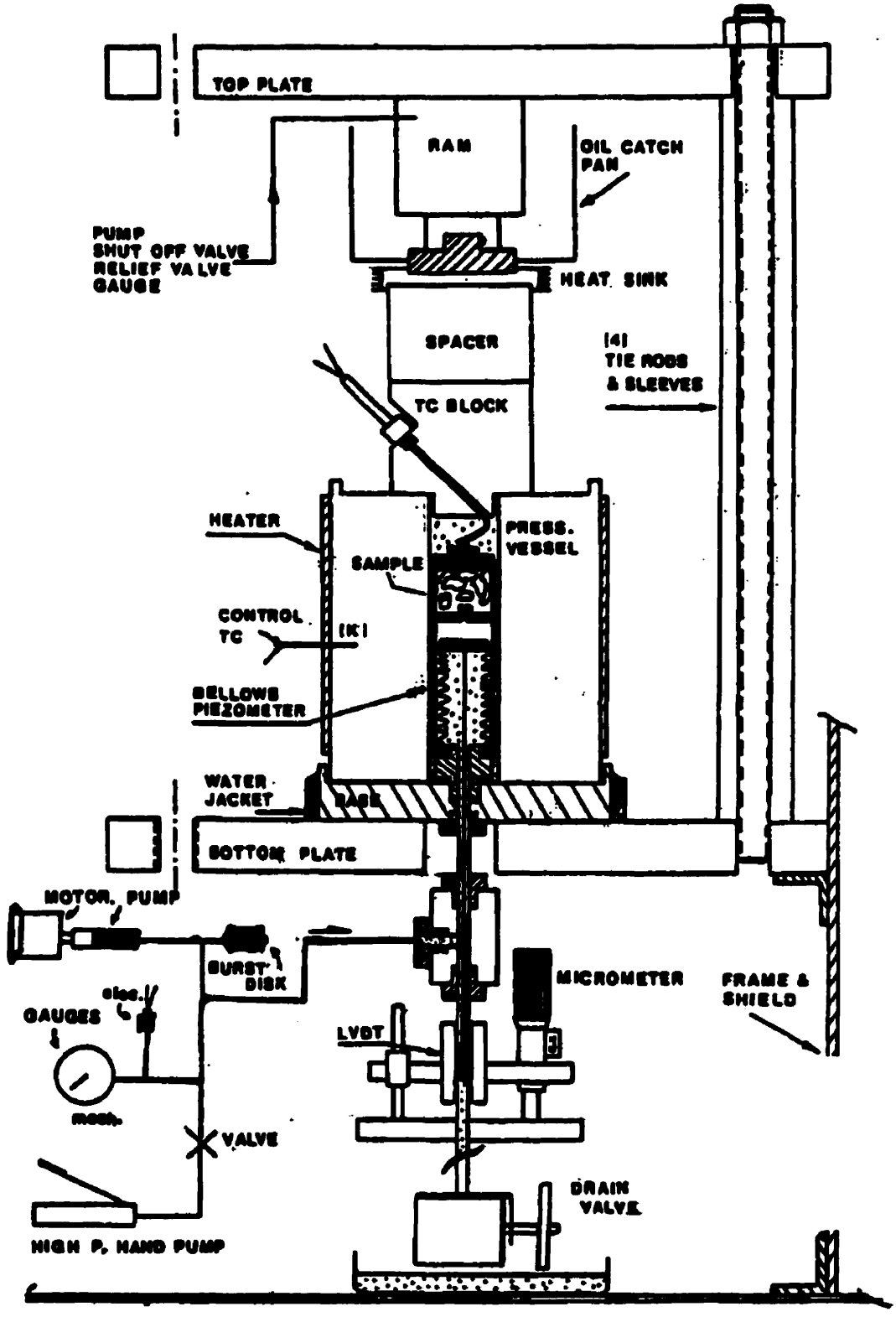

Figure 4.1: Schematic drawing showing the assembly of the PVT apparatus

A high-pressure thermocouple (type K), which has its sheathed end located close to the sample in the cell, measures the sample temperature. A separate thermocouple (type K) is used to control the temperature. It is located in a hole drilled about 1/2 in. into the side of the pressure vessel. A temperature calibration is needed to relate the sample temperature and the controlled temperature. The vessel is equipped with a 1700-1800 watt electrical heater. To prevent excessive heating of the bottom plate, the base of the assembly is water-cooled. A fan provides cooling to the upper part of the assembly.

The measurement data including sample temperature, pressure, and voltage from the LVDT (representing bellows deflection), are read by a data acquisition board, located in the MS-DOS computer. The computer also guides the user through the proper operation of the equipment.

4.3) PVT Measurement Techniques

There are three main modes of operating the PVT apparatus: isothermal, isobaric, and isothermal/isobaric. In the isothermal mode, the sample is heated and then maintained at a constant temperature. Subsequently, the pressure is increased, with specific volume recorded at pressure intervals set by the operator. The second mode of operation is the isobaric mode, in which the pressure is maintained at a certain value, while the temperature is changing at a certain heating or cooling rate, with volumes recorded in selectable time intervals. The last mode of operation is the isothermal/isobaric crystallization mode. In this mode, specific volume is recorded as a function of time at constant pressure and temperature.

4.3.1) Sample Preparation

PVT experiments permit the study of various shapes of polymer samples such as pellets, pieces of moldings, and liquids. The use of fine powders and fibers are, however, not strongly recommended since some problems might be encountered during the filling of the cell with a confining fluid. Considering the volume of the cell and the limited

bellows deflections, the suitable amount of polymer is about 1.5 cm^3 for semicrystalline samples and 2 cm^3 for amorphous materials. Consequently, the sample masses employed in this study were in the range from 1.15 to 1.30 grams. Samples were used in form of pellets, as provided by the company. The complete sample preparation procedure can be found in Appendix I.

4.3.2) Calibration

A calibration run is required for each measurement, if the bellows, one piece of the cell, or the confining fluid is replaced. The volume changes measured with the PVT apparatus depend on the relative position of the core and the coil of the LVDT. This position is not solely influenced by the volume change of the polymer. Therefore, a calibration run consists of measuring the volume changes due to the confining fluid in the cell, the bellows, the vessel and all the other parts of the apparatus that can be influenced by temperature and pressure increases. All these parameters are accounted for by the correction function $d_1(P,T)$ that is obtained in a separate experiment carried out with the cell filled with the confining fluid only. Calibration points are taken from room temperature upto 400°C along isotherms every 15°C and for pressure between 0 and 200 MPa every 10 MPa. These data are fitted to the correction function with the following relation,

$$d_1(P,T) = a_0 + a_1P + (a_2 + a_3T)P \qquad (3.1)$$

which is subtracted from the reading during a sample run. A calibration run is carried out by following the same methodology as with a sample run, except that the cell is filled with the confining fluid only. A detailed procedure of a sample run is described in Appendix I.

4.3.3) Experiment Description

Due to the specifications of the PVT apparatus, the highest temperature is limited to 405°C and the pressure maximum is 200 MPa. However, the temperature range that

was chosen for PVT experiments was mainly determined by the degradability of materials studied. Thermal-oxidation of polyethylene was reported to occur over 250°C, at atmospheric pressure[66]. In this study, polyethylene samples were immerged in mercury and under pressure of, at least, 10 MPa. A maximum temperature of 240°C was therefore a reasonable choice to avoid any degradation.

4.3.3.1) Isothermal measurements

An isothermal PVT measurement consisted of recording volumes along isotherms with increasing pressure from 10 MPa to 200 MPa by increments of 10 MPa. All the parameters of isothermal experiments, such as pressure increment, isotherm spacing, holding time and pressure and temperature range, were set before each experiment.

In this work, isotherms were carried out from 30 to 220°C in order to observe the polyethylene sample behavior, up to 200 MPa, in the semicrystalline, the transition and the melt regions. Isotherms were spaced by 10°C from 30 to 90°C, by 5°C from 95 to 175°C, and by 10°C from 180 to 220°C. Isotherms were spaced by 5°C in the transition region due to the large volume changes induced by melting or crystallization.

A typical isothermal experiment started at room temperature under 10 MPa, the sample was first heated to the desired isotherm under 10 MPa, and, after temperature stabilization, pressure was next increased up to 200 MPa, by increments of 10 MPa. The holding time, which is the time that the program will pause at each of the pressure points requested, was set at a compromised value of 20 seconds, taking into account accuracy and residence time (degradation). This holding time was also recommended in the PVT apparatus manual. After having reached 200 MPa, pressure was then released and the sample was heated to the next isotherm. The program could not control the heating rate. One cycle, from one isotherm to another, lasted approximately 20 to 30 minutes. After a full isothermal run, the sample had to be replaced since it could be degraded.

Each isotherm was saved as a separate ASCII file. It was essential to record several isotherms around room temperature. Indeed, these data were utilized to calculate

the additional volume of the sample, which allowed the determination of the exact sample specific volume, at the initialization temperature and zero pressure (cf. Section 5.1)).

4.3.3.2) Isobaric measurements

Isobaric experiments consisted of recording volume in selected time intervals while heating or cooling the sample at a constant, preset rate and pressure. The best compromise, between speed and accuracy, was obtained for a rate of 2.5°C/min. The melting and crystallization curves were obtained for each resin at 2.5°C/min under the pressures of 10, 50, 100, and 200 MPa. Specific volume change data were recorded every 10 seconds, and saved in a separate file for each melting and crystallization curve.

Prior to each melting experiment, the sample was first heated at 4°C/min under a pressure of 10 MPa to 200°C, at which it was maintained for 20 minutes. The sample was next cooled to room temperature at 2.5°C/min under 10 MPa. This method allowed the reuse of the same sample for different isobaric runs as long as each cooling experiment at 10 MPa, between the runs at higher pressure, revealed the same crystallization behavior as that of a fresh sample. This method also produced an identical thermal history of the sample prior to each new pressure experiment.

4.3.3.3) Isothermal/Isobaric Measurements

In the isothermal/isobaric experiments, volume changes were recorded as a function of time at constant pressure and temperature. In this mode, pressure and temperature were controlled by the operator through the software.

a) General Procedure.

This procedure was based on the one developed by Samara[67] for his study on crystallization kinetics under pressure of the same HDPE resin. In this procedure, the sample was first heated at 4°C/min to 200°C under 10 MPa. After 20 minutes, which is the time necessary to stabilize the volume of the melt (indicating complete melting), the

sample was then cooled under 10 MPa to the desired crystallization temperature. The cooling rate was approximately 5-6°C/min, which corresponded to the maximum rate provided by the apparatus. The sample was maintained at this specific temperature for another 20 minutes to allow stabilization of the temperature.

Prior to pressurization, data acquisition was set to record volume, temperature, and pressure at minimum intervals of 10s, which is the shortest interval of time allowed by the software. This limitation is probably due to the time needed to obtain a representative signal from the hardware. Next, the pressure was increased manually from 10 MPa to the desired crystallization pressure. Manual compression was preferred to the computer-controlled pressurization because pressure could be raised considerably faster. For instance, pressurization from 10 to 200 MPa lasted about six minutes when it was computer controlled, and about 30 seconds for manual compression. This becomes of major importance for low crystallization temperatures, i.e. high degree of supercooling, for which crystallization is likely to occur during slow pressurization.

It was convenient to employ the online plotter to follow the progress of the crystallization. At the end of the crystallization kinetic experiment, data acquisition was stopped and pressure was brought down manually to 10 MPa. If the same sample was reused, the temperature was then raised back to 200°C, and another isothermal could be performed. If the sample was degraded, the temperature was then decreased to 20°C, the pressure to atmospheric pressure, and the cell was cleaned and a new sample was prepared.

At least three different crystallization temperatures were employed at each of the following pressures 50, 100, 150, and 200 MPa. Due to the rather slow maximum cooling rate, experiments at 10 MPa could not be carried out, since crystallization would probably occur during cooling.

b) Choosing the Crystallization Conditions: Temperature and Pressure

At atmospheric pressure, the true supercooling is theoretically defined as: $\Delta T = T_m^0 - T_{exp}$, where T_m^0 is the equilibrium melting point and T_{exp} is the crystallization temperature of the experiment. However, values of the equilibrium melting point under pressure have not been reported in the literature; therefore, in this work, the

supercooling was defined as follows: $\Delta T = T_m^P - T_{exp}$, where T_m^P is the melting point obtained from the isobaric experiments at the experimental pressure, and T_{exp} is the experimental crystallization temperature. This method has been successfully used by other workers[16,19].

At each different pressure, crystallization kinetics experiments were performed in the same range of degree of supercooling, in order to compare experiments at distinct pressures and for various resins. In addition, because of the fast crystallization of polyethylene, the set of experiments was conducted in a limited supercooling range. The supercooling was typically in the range from 2 to 10°C. Under these conditions, crystallization was rather slow, it took about 20 minutes to 24 hours to be completed. The supercooling range was also chosen to generate an induction time larger than 80 seconds. This interval time was necessary for better accuracy in detecting the beginning of crystallization (cf. section 5.3.2).

Under very low supercooling, ΔT<2°C, the volume change due to crystallization was of the same order of magnitude as the sensitivity of the apparatus, resulting in large error in the results. Under high supercooling, ΔT>10°C, crystallization was so fast that some phase transformation occurred during pressurization, and the analysis of these experiments was therefore complex and error sensitive.

Crystallization temperatures were thus selected to give a certain degree of supercooling. The compression heating effect had to be considered in the estimation of crystallization temperatures. For instance, for an experiment under 100 MPa, the crystallization temperature set in the software was:

$$T_{isotherm} = T_m^{P=100} - \Delta T - \Delta T_{compression} \qquad (4.1)$$

where $\Delta T_{compression}$ is the approximate expected increase of temperature due compression and ΔT is the desired supercooling. With this method, the supercooling was predicted within 1°C.

c) Compression heating

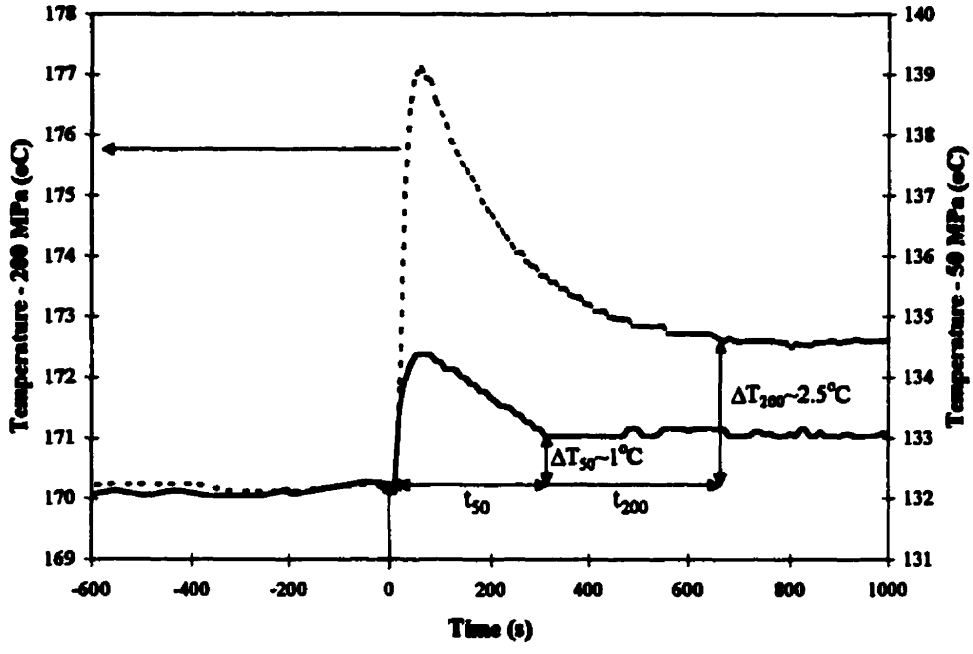

Figure 4.2: Temperature versus Time during rapid compression. The solid line is for an increase of pressure from 10 to 50 MPa, and the dashed-line from 10 to 200 MPa.

The rapid manual pressurization caused a temperature increase (and thus, instability of temperature), which was predictably dependent on the pressure increase, as illustrated in Figure 4.2. The temperature increased by 2 to 7°C during the first minute and then decreased and stabilized in 5 to 10 minutes depending on pressure. It was noticed that the temperature stabilized at a value higher than the temperature of the isotherm before pressurization. An augmentation of ~1°C was observed for an experiment at 50 MPa, and of ~2.5°C for one at 200 MPa.

64 P. Zoller, P. Bolli, V. Pahud, and H. Ackerman, *Apparatus for measuring pressure-volume-temperature relationships of polymers to 350(C and 2200 kg/cm2*, Rev. Sci. Instrum., 47, 948 (1976).
65 J. He, Y. A. Fakhreddine, and P. Zoller, J. Appl. Polym. Sci., 45, 45 (1992).
66 *Linear Low Density Polyethylene*, Encyclopedia of Polymer Science and Engineering, 2nd Edition, H. Mark, N. Bikales, Ch. Overberger, Ed.; Wiley & Sons, New York, vol. 17, 756, 1986.
67 M. Samara, PhD's Thesis, McGill University, in print.

CHAPTER 5

DATA ANALYSIS

This chapter is devoted to describing the analysis of the experimental data files. The procedure to obtain the parameters of the equations of state from isothermal experiments is first presented. The evaluation of the melting points and the crystallization temperatures from isobaric experiments is next explained. Finally, a detailed description of the method used to extract the crystallization kinetics data from isothermal/isobaric experiments is discussed.

5.1) ISOTHERMAL MEASUREMENTS

This paragraph is dedicated to explaining how to relate the recorded volume changes to the true specific volumes, and how to fit these adjusted volumes to the Tait equation and the Inverse-Volume equation.

5.1.1) Determination of the Additional Volume

The additional volume is added to the volume change data to yield the true specific volume values. The additional volume was calculated from isothermal run data and the value of the specific volume (inverse of density) at 23°C and zero pressure. The zero pressure volume changes were plotted versus temperature (from 30°C to 100°C). The additional volume of the sample was obtained by extrapolating the zero pressure data to the temperature at which the exact specific volume of the sample was known and by using the following equation:

$$V_{additional} = V_{exact} - V_{extrapolated} \qquad (5.1)$$

5.1.2) Determination of the Melt and Solid State Regions

The first step of the analysis was to identify the temperature range in which the transition takes place. This transition region can be easily observed by plotting specific volume data versus pressure for each isotherm, as shown in figure 5.1.

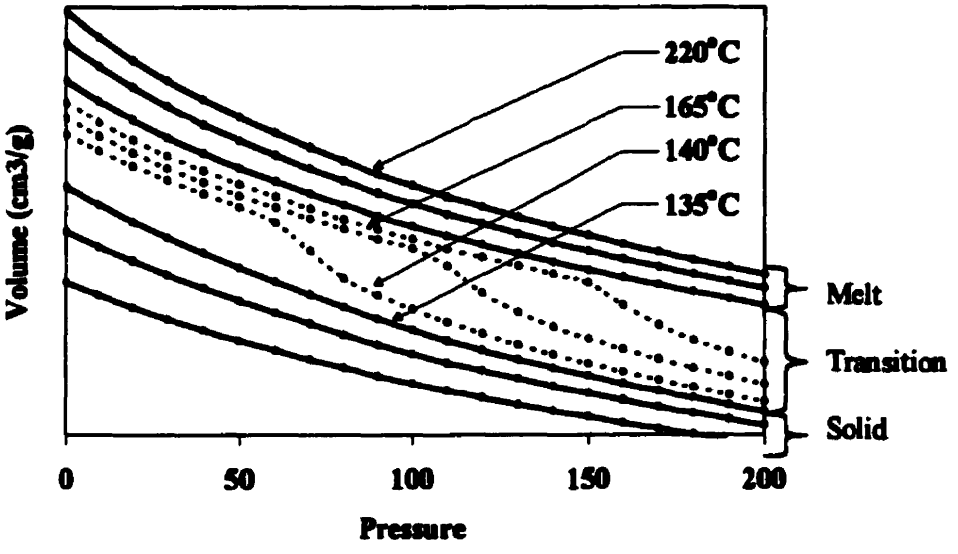

Figure 5.1: Plot of Specific Volume versus Pressure for different isotherms.

This figure suggests that the isotherms between 140°C and 165°C should be omitted from PVT relations for the liquid and melt phases for the pressure range up to 200 MPa. Indeed, these isotherms exhibit a volume drop along the curve that corresponds to the occurrence of crystallization during pressurization. The PVT melt data, which were obtained for a chosen pressure range, were then fitted to an equation of state. Data for the solid state region could also be used to evaluate thermal expansion coefficient and isothermal compressibility of the semicrystalline phase.

5.1.3) Determination of the Parameters of the Tait Equation

Two techniques were tested to fit experimental data to the empirical Tait equation, eq. (2.17). In both cases, it was found that the universal value of 0.894 for the constant C yielded results with a comparable accuracy to those obtained with C as

variable. The first fitting technique was composed of three steps, whereas the second one had only one step.

For a better understanding of the Tait equation, a three step non-linear regression was first used to determine the four parameters of the Tait equation: V_0, α, B_0 and B_1. The experimental specific volumes were first fitted to the following equation:

$$V(P,T) = V(0,T) \times \left\{ 1 - C \times \ln\left[1 - \left(\frac{P}{B} \right) \right] \right\} \qquad (5.2)$$

with C equal to the standard value of 0.0894. For each isotherm, a value of the Tait parameter B was then obtained. $B(T)$ was next fitted by a non-linear regression to an exponential function, as follows:

$$B(T) = B_0 \exp(-B_1 T) \qquad (5.3)$$

In addition, the specific volume at atmospheric pressure was fitted by the same method to the following equation:

$$V(0,T) = V_0 \exp(\alpha T) \qquad (5.4)$$

Although this three-step method yields a precise representation of the experimental data, and a good overview of the Tait equation, it is time consuming.

On the other hand, the second method used to analyze the PVT data was less time demanding. Indeed, the specific volume data were fitted directly to the Tait equation, as follows:

$$V(P,T) = [V_0 \exp(\alpha T)] \times \left[1 - 0.0894 \ln\left(1 + \frac{P}{B_0 \exp(-B_1 T)} \right) \right] \qquad (5.5)$$

The four parameters, V_0, α, B_0 and B_1, were thus obtained in one non-linear regression. This method yielded a slightly better fitting than the three-step regression described earlier. The following standard deviations were obtained for the fittings of the PVT melt behavior of a LLDPE resin:

$\sigma = 0.0003$ cm^3/g for the three-step method

$\sigma = 0.0002$ cm^3/g for the direct non-linear regression.

Because of its convenience and its accuracy, the second and direct method was used to analyze the PVT melt behavior of all isothermal experiments.

5.1.4) Determination of the Parameters of the Inverse-Volume Equation

The melt region was first obtained using the same method described in the previous section. The Inverse-Volume equation was also fitted using two different methods, a two-step and a direct nonlinear regression. The two-step procedure was applied as defined by Levan[68]. The experimental densities (the inverse of the specific volumes) were first fitted by a linear regression for each isobar as follows:

$$\rho(P,T) = Q_1 + Q_2 T \tag{5.6}$$

The second observation made by Levan is that the density can be represented at constant temperature by a second order polynomial. Consequently, Q_1 and Q_2 were fitted to the two following equations:

$$Q_1 = \rho_\infty + aP + cP^2 \tag{5.7}$$

$$Q_2 = \left(\frac{\partial \rho}{\partial T}\right)_{P=0} + bP + dP^2 \tag{5.8}$$

This procedure yielded the six parameters of the Inverse-Volume equation, which are ρ_∞, $\left(\frac{\partial \rho}{\partial T}\right)_{P=0}$, a, b, c, and d. However, it was possible to obtain these parameters using a non-linear regression by directly fitting data to one equation, as follows:

$$\rho = \rho_\infty + \left(\frac{\partial \rho}{\partial T}\right)_{P=0} \times T + (a + bT)P + (c + dT)P^2 \tag{5.9}$$

Similarly as for the Tait equation fitting, the direct estimation gave a slightly better fit than that of the non-direct calculation. Therefore, this technique was used to evaluate the parameters of the inverse-volume equation.

5.1.5) Isothermal Measurement Limitations

In the transition region, melting and crystallization occur during isothermal experiments. At the onset of certain isotherms under 10 MPa, the sample is in the melt, but, with increasing pressure, the sample starts crystallizing due to change in the

thermodynamic equilibrium (see isotherm at 140°C in Figure 5.1). At 200 MPa, the sample might be partly or completely solidified depending on the isotherm temperature. A partly solidified sample implies that crystallization was already in progress when the volume value was recorded, which is probably a first source of error.

Crystallization during pressurization can influence the specific volume values recorded at pressure increments after crystallization. For instance, in Figure 5.2, the HDPE resin investigated in this work seems to possess a negative thermal expansion coefficient at certain pressure. This effect is due to the measurement technique and will be discussed in more details in Chapter 6.

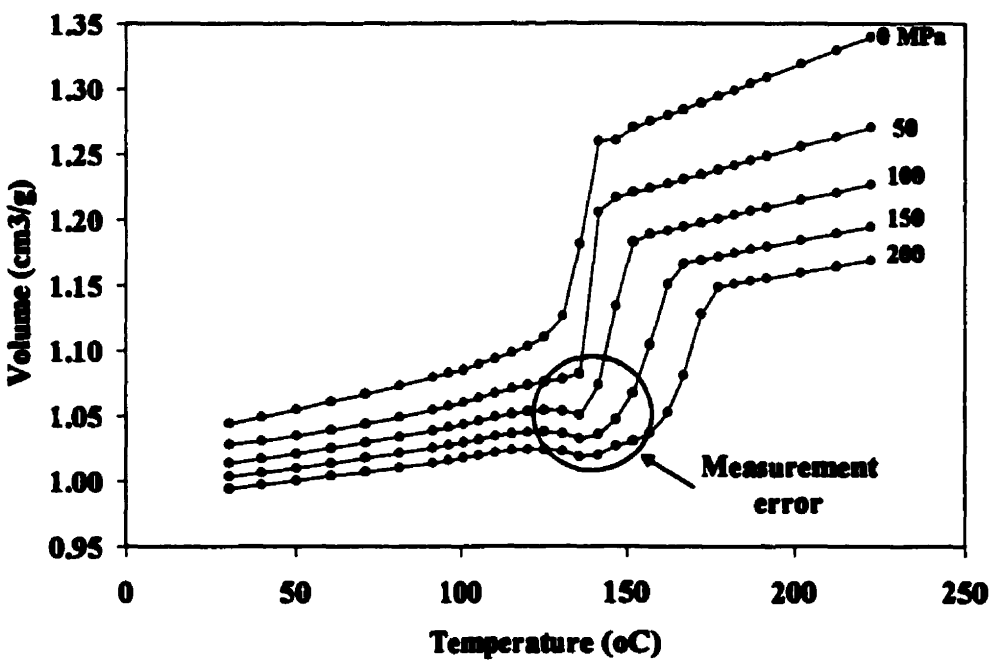

Figure 5.2: Cross-plotted isothermal data for Sclair 2908 exhibiting a decrease of volume with increasing temperature due to measurement error.

5.2) ISOBARIC MEASUREMENTS

A typical isobaric experiment is shown in Figure 5.3. From this plot, it is possible to estimate the temperatures corresponding to the onset, $T_{o,m}$, and the end, $T_{e,m}$, of melting, in heating runs.

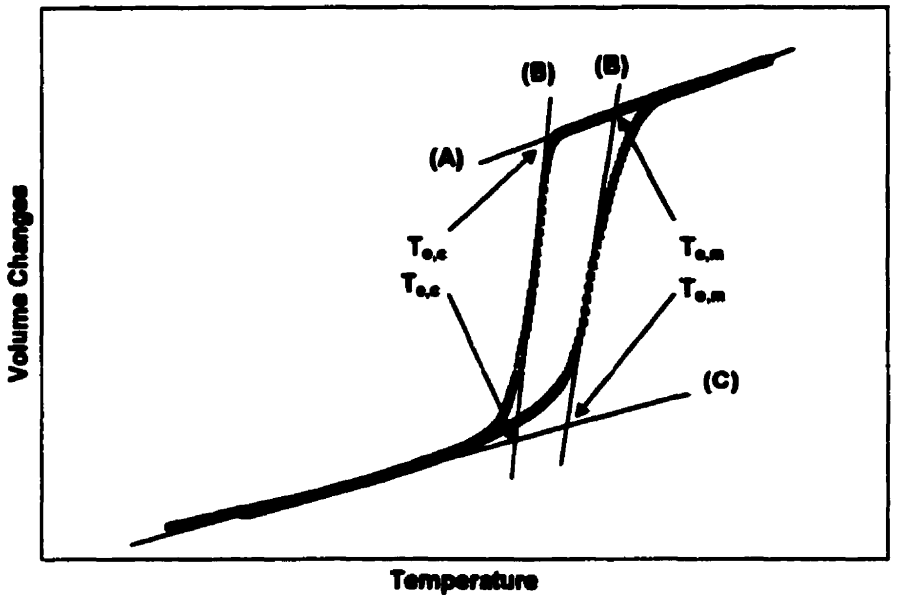

Figure 5.3: Illustration of the graphical determination of the end of the melting and the onset of crystallization from isobaric experiments of HDPE under 100 MPa at 2.5 °C/min.

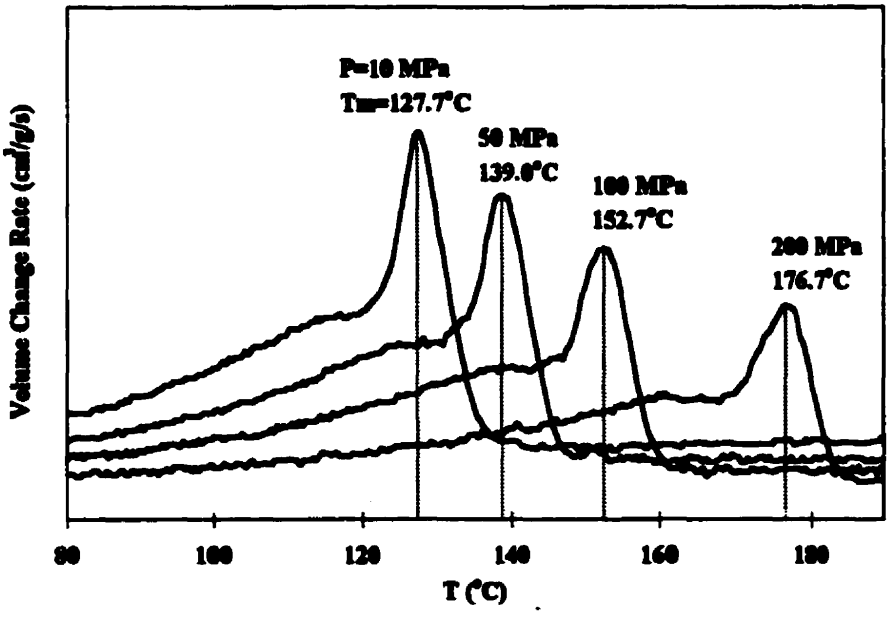

Figure 5.4: Volume Change Rate versus Temperature from the melting curves at 2.5 °C/min of LLDPE-B

Similarly, it is possible to estimate the temperatures corresponding to the beginning, $T_{o,c}$, and the end, $T_{e,c}$, of crystallization, in cooling runs. These temperatures are graphically acquired from the heating and cooling runs, as illustrated in Figure 5.3. The (A) line is the tangent of the curve in the melt region, the (B) lines are the tangents at the inflexion point of the curves in the transition region, and the (C) line is the tangent of the curve representing the solid state behavior.

The melting points and crystallization temperatures were defined as the temperature at which the maximum volume change rate was observed during melting and crystallization, respectively. Figure 5.4 shows typical melting curves of the volume change rate versus temperature for a LLDPE resin. These curves were also useful for comparing the differences in crystallization or melting behavior of the various grades of polyethylene resins.

5.3) Isothermal/Isobaric Measurements

A methodological analysis of the isobaric/isothermal experimental data had to be developed. Indeed, the temperature of the experiment, the occurrence of crystallization during pressurization, the induction time, and the beginning and end of crystallization are quite sensitive to error during analysis. In order to obtain crystallization data that could be fit to kinetic equations, all the above mentioned quantities had to be known.

The three main parts of a kinetics experiment are cooling, pressurization, and crystallization. These segments are easily determined, and they can be observed by plotting volume changes versus time, as shown in Figure 5.5.

5.3.1) Crystallization during Pressurization

It is of primary importance to determine when crystallization starts, especially for low crystallization temperature. Indeed, crystallization is likely to occur during pressurization at high supercooling. When no induction period was observed, two methods were used for verifying the occurrence of crystallization

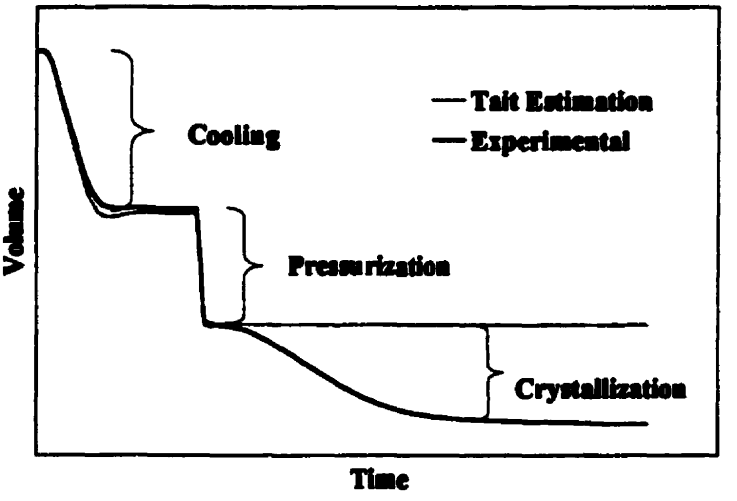

Figure 5.5: Schematic plot of an isothermal/isobaric crystallization experiment

Firstly, using the PVT melt data from the isothermal experiments, the volume values of the melt were extrapolated to the temperatures and pressures considered in the kinetics experiment. Figure 5.5 presents a run in which the Tait equation was employed to estimate the different volume changes. Deviation from the curve representing the Tait estimation will indicate crystallization, as shown in the last part of the plot in this figure.

A second complementary method consisted of comparing the volume change due to the increase of pressure with other experiments carried out at higher temperatures, which exhibit an incubation period. In fact, the presence of an induction period implied that no crystallization had occurred during pressurization. The slight temperature dependence of the compression volume change was negligible.

When crystallization was detected during pressurization, experimental data were analyzed, but the error generated by the analysis was large. In such cases, a trial and error approach was used, employing extrapolation of an Avrami type function.

In this work, crystallization temperatures were generally chosen to ensure that no crystallization would occur before the end of pressurization, and that the experiments would exhibit an induction time larger than 80 seconds. The incubation period of 80 s was determined to ensure that crystallization would start after the volume stabilization due to rapid compression was over, as explained below.

5.3.2) Induction Time and Beginning of Crystallization

The beginning of crystallization, which corresponds to the end of the induction time, was defined at the point at which the curve deviates from the straight line observed during the induction time, as shown in Figure 5.6.

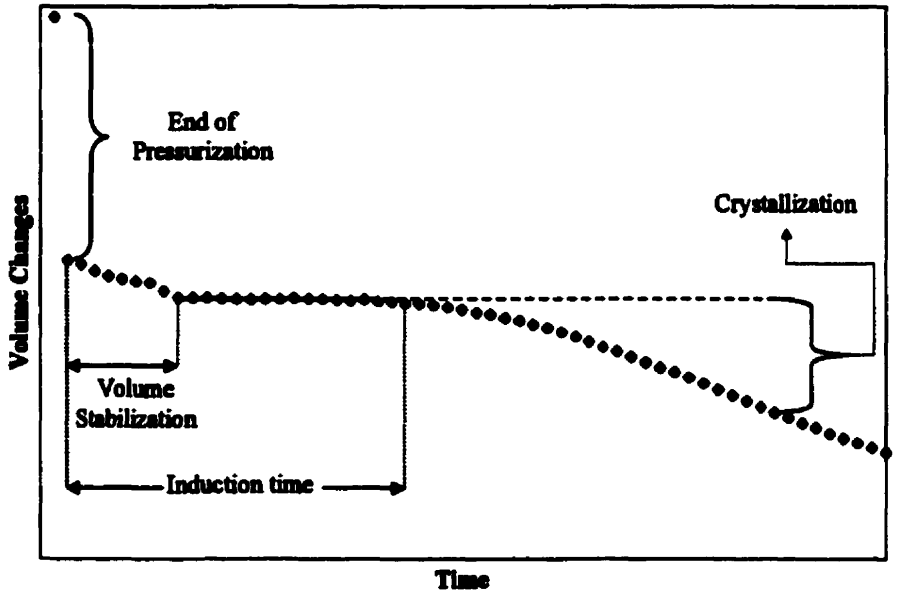

Figure 5.6: Schematic diagram of a typical crystallization kinetic experiment.

This figure also illustrates the changes observed during the induction time. The volume decrease, referred as volume stabilization, was observed during the first 80 seconds (average value) of the induction time. The decrease in volume is probably due to a combination of several factors such as the viscoelastic relaxation of the silicon oil, pressure stabilization, and the bellows response. This decrease is certainly not attributed to any crystallization since it was also observed when a polymer melt was pressurized to a pressure under which the sample remains in the melt. This volume decrease was in the range from 1.0 to 1.5mm^3 for pressurization to 50 MPa, and from 4.0 to 4.5mm^3 for pressurization to 200 MPa. In addition, slight variations were observed for long induction periods due to temperature fluctuations.

5.3.3) End of Crystallization

Crystallization kinetics experimental results are usually represented by the relative crystallinity versus time. In dilatometric studies, the relative crystallinity, X, is defined as:

$$X = \frac{V_t - V_0}{V_\infty - V_0} \tag{5.10}$$

The value V_0 is the volume at which crystallization begins, corresponding to the end of the induction time, as defined earlier, and the value V_∞ is defined as the end of crystallization. In theory, the end of crystallization does not seem difficult to evaluate. However, certain polymeric materials such as, for example, polyethylene terephthalate and linear low-density polyethylene exhibit secondary crystallization, which is a very slow process that can last days to be completed under certain conditions.

Since the objective of this work was to compare crystallization kinetics of various grades of polyethylene resins, the development of an analytical method that was repeatable and convenient, was of utmost importance. The method developed by Samara[67] for his study on crystallization under pressure of HDPE, which was based on the assumption that, at constant pressure, the maximum volume change - due to complete crystallization - was not dependent on temperature, was not applicable to LLDPE resins for two reasons. Firstly, secondary crystallization was extremely slow, and its completion had never been reached, even after 24 hours. Secondly, the maximum volume change was dependent on crystallization temperature. These two observations are discussed and illustrated in section 6.3.1).

The main idea of this method was to exclude the data corresponding to secondary crystallization since the completion of crystallization could not be observed in reasonable time, and since the Avrami equation only fit accurately primary crystallization. The value of V_∞, which thus corresponds to the end of primary crystallization, was determined by a methodology based on a principle that was first indicated by Avrami[44]. He suggested that it was possible to shift isothermal kinetics data to a single master curve with respect to an arbitrarily chosen reference temperature. Kinetics data of all experiments (at different pressures and temperatures and for all resins) were shifted to one single master curve by

varying the value of V_∞. This was achieved using a program that compared the Avrami fitted values of the reference experiment to the run under analysis. The reference experiment was chosen to represent 80% of crystallinity and yielded a good linear correlation coefficient (R^2>0.99) of the Avrami equation fit. Using the estimated value of the end of primary crystallization, the relative crystallinity was calculated, and data were then fitted to the Avrami equation by a non-linear regression.

5.3.4) Crystallization Temperature of the Experiment

The temperature at the isotherm before pressurization, the maximum temperature at the peak due to compression heating, the temperature at the beginning of crystallization or the average temperature during crystallization were all the possible values that could have been used to represent the crystallization temperature of an experiment. However, the use of the temperature at the isotherm would have neglected the temperature rise due to compression heating. The value at the peak would have been irrelevant for slow experiments in which crystallization occurs after temperature stabilization. The temperature at the onset of crystallization would have not represented accurately fast experiments during which temperature was importantly varying. Finally, the temperature of the experiment was defined as the average value of the temperatures recorded during crystallization from V_0 until V_∞.

CHAPTER 6

RESULTS & DISCUSSION

The results for the resins investigated in this study are presented in three sections, corresponding to the three types of PVT experiments carried out. In each section, a comparative presentation of the results for the various resins is reported and then discussed. The PVT properties for the melt and the solid states, as fitted by the Tait and Inverse-Volume equations, are given in the first part. The dependence on pressure of the crystallization and melting processes, characterized by the melting points and crystallization temperatures are then presented. The final section presents a discussion of the results of the crystallization kinetics experiments under pressure.

6.1) PVT PROPERTIES

This part is devoted to presenting the differences in PVT behavior of all the resins in the temperature and pressure range under investigation in the isothermal experiments. The PVT melt behavior and its representation by the Tait and Inverse-Volume equations is also discussed. The empirical Tait equation was chosen because it is the most commonly used equation of state in polymer processing computer simulations. In addition, the inverse volume equation was employed to compare its predictions of the thermodynamic parameters, such as the isothermal compressibility and thermal expansion coefficient, with the estimates of the Tait equation.

6.1.1) General PVT Behavior

Isothermal experiments are commonly presented in the form of cross-plotted isobars, as shown in Figures 6.1 to 6.4. Figure 6.1 illustrates the PVT behavior of typical HDPE and LLDPE resins up to 200 MPa. Each cross-plotted isobar curve can be divided into three regions. The high temperature region, in which the specific volume is linearly dependent on temperature, corresponds to the behavior of the melt state. The low temperature region is referred to as the semicrystalline region. Between both sections, there is the transition region in which large volume changes are observed due to crystallization along the isotherm during pressurization. The large specific volume difference in the solid state region in Figure 6.1 is due to the density difference between the A and HDPE resins. In contrast, no obvious distinctions can be noticed in the semicrystalline state region in figures 6.2-6.4 because of the similar densities of the LLDPE resins. In addition, it is interesting to note that these figures indicate an almost identical PVT behavior of the melt state for all the resins, including HDPE. This indicates that the polymer chain structure, such as branching size, branching distribution, molecular weight, and polydispersity, does not affect strongly the PVT behavior of the melt state. The major differences in comportment are observed in the region where crystallization occurs. For instance, the HDPE resin has a narrow transition region, similar to a first-order transition, whereas the LLDPE resins have tendency to exhibit a broader transition region. Moreover, some distinctions can be reported between LLDPE resins. Resins F, and I have certainly distinct behaviors, which are related to their density and molecular structure. The resin F is a low density polyethylene, and the resin I is a very low density polyethylene. The uncertainty (cf. Appendix II) and the reproducibility of the results are 0.003 and 0.002 cm^3/g, respectively.

The apparent decrease of the volume observed for the HDPE resin in Figure 6.1 is merely due to the measurement procedure. At certain isotherms, crystallization occurs during pressurization yielding a denser sample. This was confirmed by the fact that a run carried out with a sample prepared by crystallization under 200 MPa did not exhibit such a behavior.

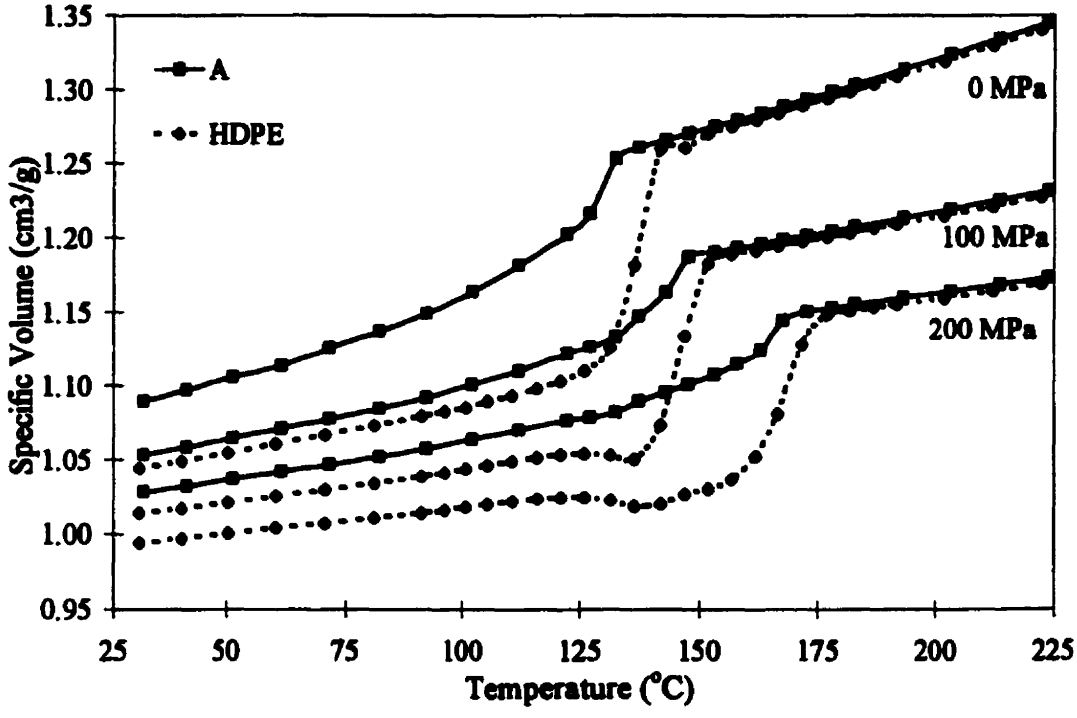

Figure 6.1: Cross-plotted isothermal experiments of resins A and HDPE.

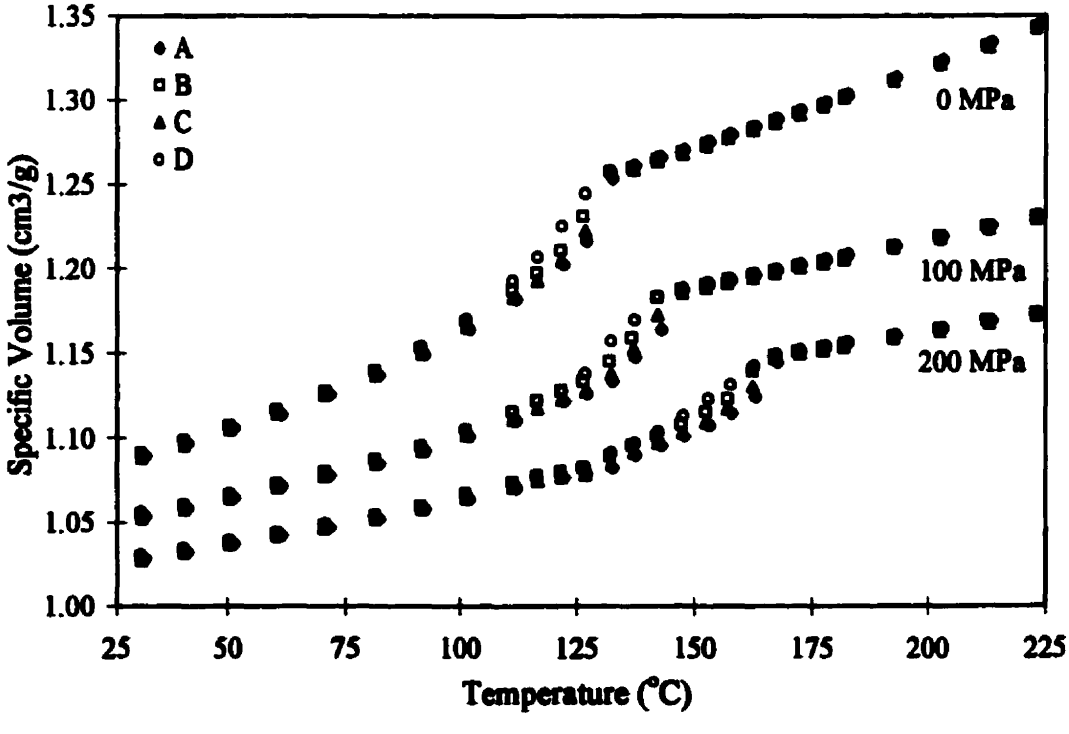

Figure 6.2: Cross-plotted isothermal experiments of resins A, B, C, and D.

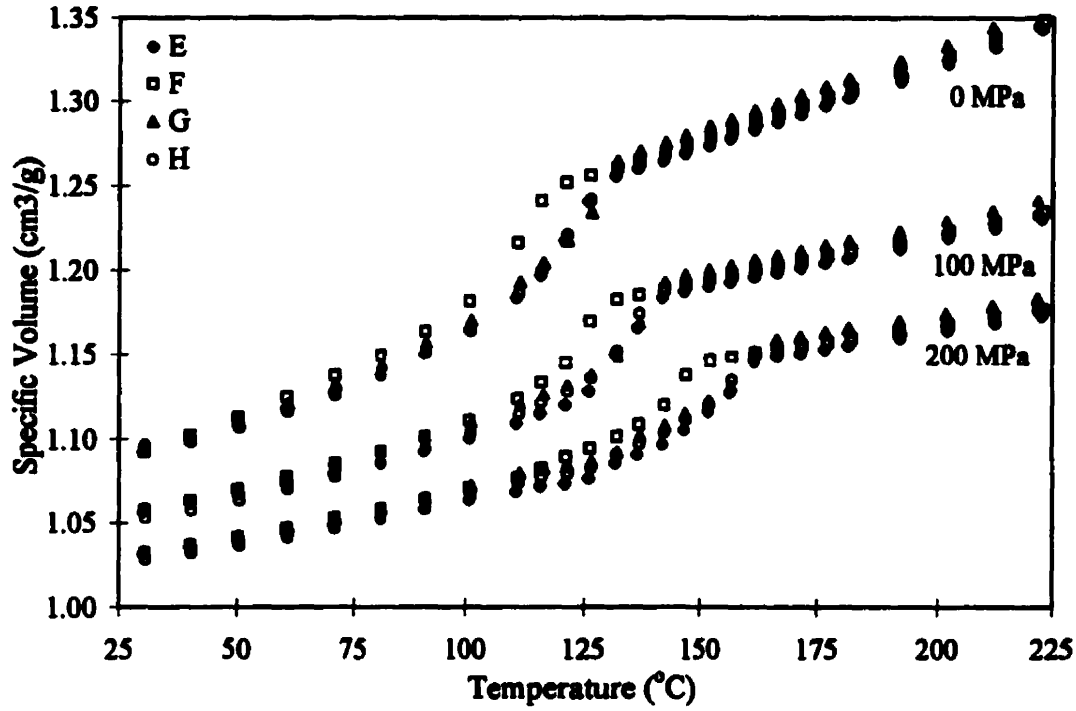

Figure 6.3: Cross-plotted isothermal experiments of resins E, F, G, and H.

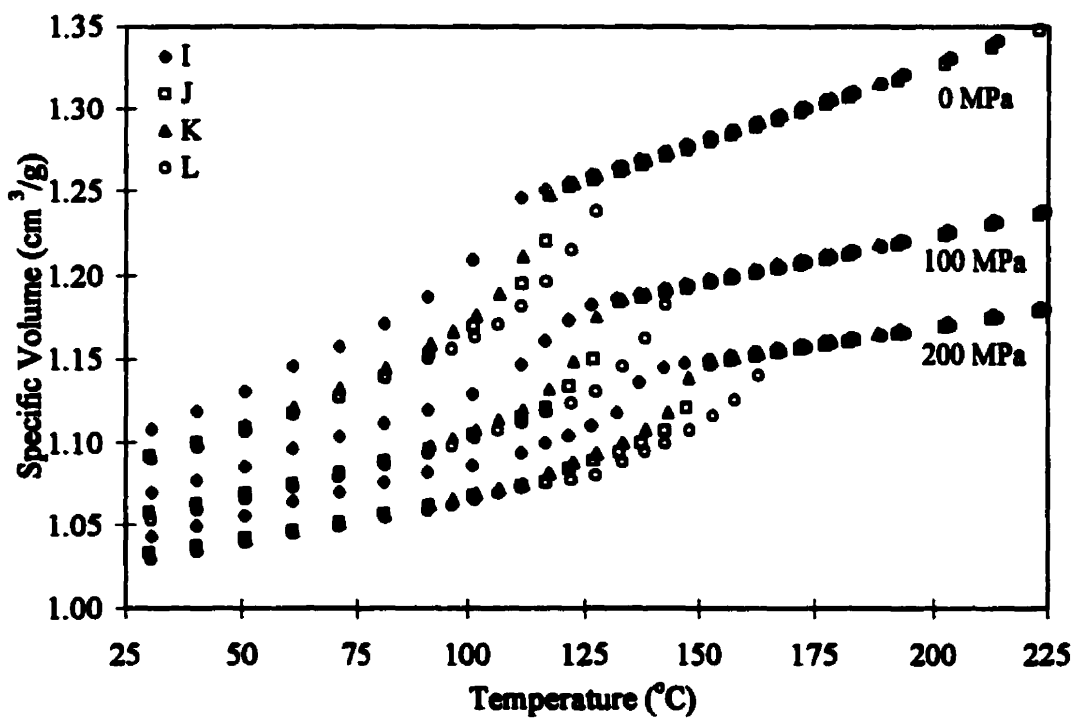

Figure 6.4: Cross-plotted isothermal experiments of resins I, J, K, and L.

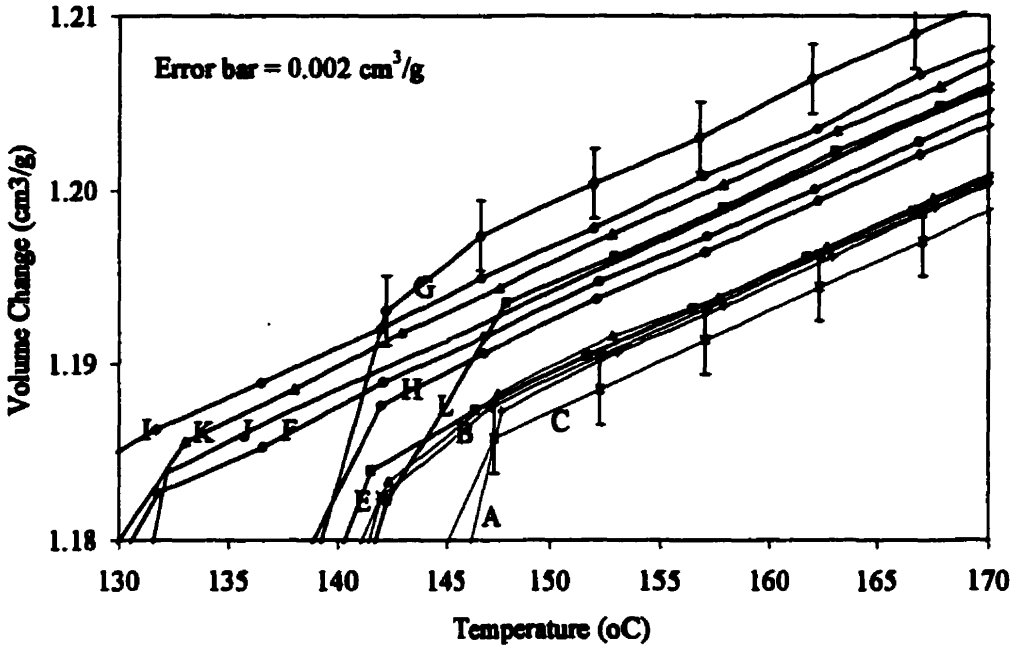

Figure 6.5: Cross-plotted isothermal experiments of all LLDPE resins; Behavior in the Melt state under 100 MPa.

6.1.2) PVT Melt Behavior

The PVT melt behavior of the isothermal experiments was defined for the pressure range up to 200 MPa, and subsequently for a certain range of temperature. At 200 MPa, the onset of the melt state region for the resins was found to lie between 142°C and 177°C, as shown Table 6.1. Figure 6.5 illustrates these differences in the onset of the melt region of all LLDPE resins under 100 MPa. It can be observed that resin I exhibits the lowest onset temperature, followed, at slightly higher temperatures, by the group of resins F, J, and K, and finally, all the others LLDPE resins show a similar high onset temperature. This is mainly explained by the differences in density. Indeed, it is well known that the melting of polyethylene resins occurs at higher temperature for higher density. The melt region defined up to 200 MPa was then fitted by two equations of state: the Tait and Inverse-Volume equations.

Table 6.1: Onset temperatures of the melt state at various pressures.

P (Mpa)	A	B	C	D	E	F	G	H	I	J	K	L	HDP
0	138	132	132	132	131	121	137	132	112	127	123	133	142
100	148	142	147	142	142	137	142	142	126	127	133	148	162
200	173	167	167	168	162	152	167	162	142	152	153	168	177

6.1.2.1) Tait Equation

Using the fitting method described in Chapter 5, the PVT melt data for all the resins were fitted to the empirical Tait equation:

$$V(P,T) = V_0 \exp(\alpha_0 T) \times \{1 - C \ln[1 + \frac{P}{B_0 \exp(-B_1 T)}]\} \qquad (6.1)$$

In this study, the "universal" value of C (C=0.0894) was employed to fit the experimental data. The fitting results for the four parameters of the Tait equation for the various grades under study are given in Table 6.2.

The results for the exponential parameter V_0 and the thermal expansion coefficient α_0 are in good agreement with the values found in the literature, as shown in section 2.3.4). However, the values of B_0 and B_1, which represent the pressure dependence of the specific volume, are slightly higher than the literature data. This small difference produces higher values for the specific volume of the same order of magnitude of the uncertainty in the results. Moreover, the results are slightly dependent on the measurement technique, the fitting method, and the resin grade. Therefore, these results are considered consistent with the values in the literature. In Table 6.2, the symbol σ represents the standard deviation of the difference between experimental and estimated values, and it indicates a remarkably good reproducibility of the experimental data by the Tait equation. The parameters of the Tait equation confirmed that these polyethylene resins have an almost identical PVT behavior in the melt state. Actually, all the parameters only differ one from the other by a maximum of 6%. Table 6.2 lists densities of the resins by descending value. It can be seen that, although they behave similarly, there exists a tendency in the dependence of the parameters on density. The coefficient α

Table 6.2: Fitting results of the Tait equation parameters.

Code	Density (g/cm^3)	V_0 (cm^3/g)	α_0 ($*10^4$)	B_0 (MPa)	B_1 ($*10^3$)	σ (cm^3/g)
HDPE	0.9620	1.130	7.68	197.1	5.11	0.0003
C	0.9234	1.134	7.54	198.7	5.08	0.0002
L	0.9222	1.140	7.56	203.7	5.21	0.0003
A	0.9208	1.136	7.52	194.5	4.99	0.0004
G	0.9200	1.145	7.55	198.3	5.04	0.0003
K	0.9198	1.143	7.53	198.0	5.05	0.0002
E	0.9194	1.138	7.44	196.3	4.99	0.0002
B	0.9194	1.137	7.46	194.4	4.93	0.0002
D	0.9192	1.138	7.42	199.5	5.08	0.0002
H	0.9190	1.141	7.39	199.8	5.01	0.0002
F	0.9190	1.143	7.40	197.0	5.03	0.0002
J	0.9180	1.144	7.35	195.2	4.91	0.0002
I	0.9070	1.148	7.26	194.1	4.91	0.0002

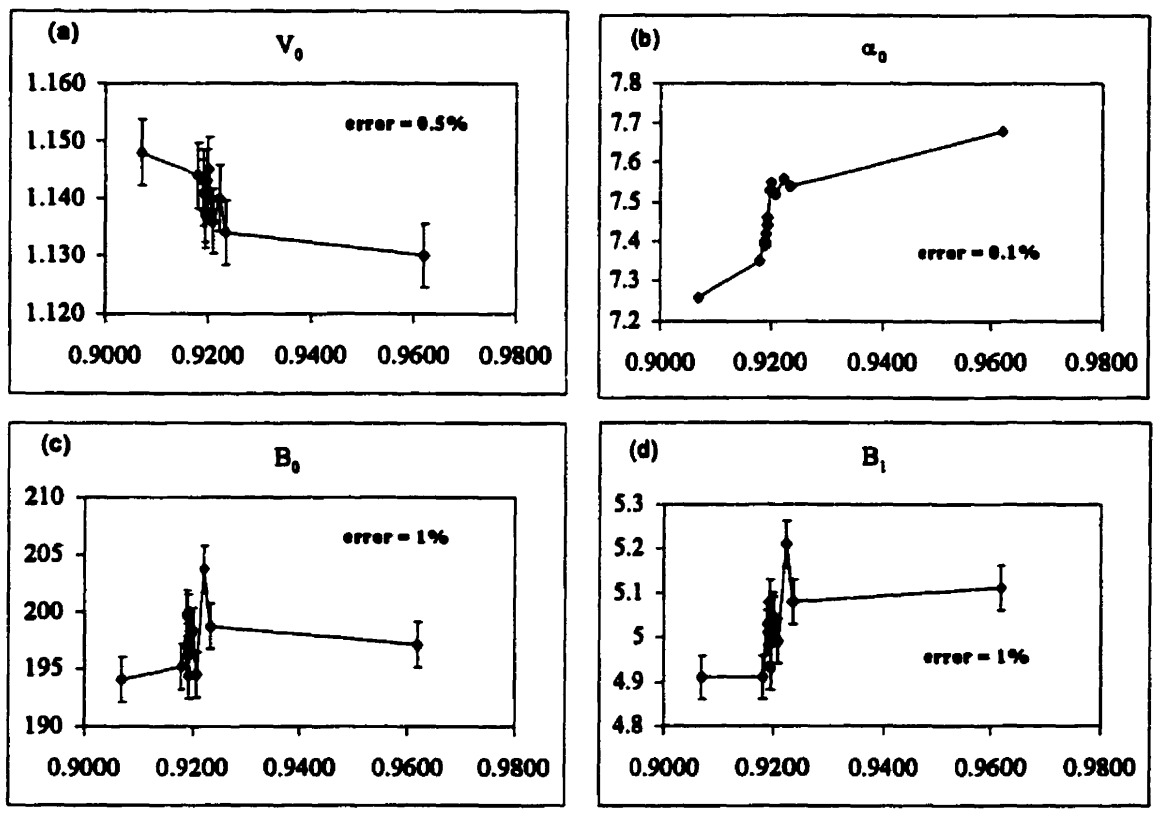

Figure 6.6: *Tait equation parameters vs. density; each data point represents a resin.*

seems to increase with increasing density, as illustrated in Figure 6.6 (b). This is in agreement with the observation of Zoller[54].

Figure 6.6 (c) and (d) show that the Tait parameters, B_0 and B_1, are not clearly dependent on density. Furthermore, from these figures, it can be noticed that resin L exhibits a singular behavior, (the highest value of B_0 and B_1), which indicates that resin L probably possesses a slightly different response to pressure. No further conclusions on chemical structure can be drawn because of the variety in molecular weight and molecular weight distribution of the resins.

6.1.2.2) Inverse-Volume Equation

The experimental data were also fitted to the Inverse-volume equation, which is defined as:

$$\rho = \rho_\infty + \left(\frac{\partial \rho}{\partial T}\right)_{P=0} \times T + (a + bT)P + \frac{1}{2}(c + dT)P^2 \qquad (6.2)$$

where ρ_∞, $\left(\frac{\partial \rho}{\partial T}\right)_{P=0}$, a, b, c, and d are the six parameters that are obtained by fitting, as explained in section 5.1.4. The fitting results of the Inverse-Volume equation are summarized in Table 6.3. As for the Tait equation fitting, the parameters are almost identical with some variations depending on density, as shown in Figure 6.7. For instance, the thermal density expansion, $\left(\frac{\partial \rho}{\partial T}\right)_{P=0}$, plotted in Figure 6.7 (iv) exhibits a similar behavior as the thermal expansion coefficient. However, a singular behavior is also observed in Figure 6.7 (iii), (v), and (vi) for the resin A. The parameters tend to be similar to the ones for the HDPE resin. No theoretical explanation can be given for this observation on the basis of the available data.

Table 6.3: Fitting results of the Inverse-Volume equation parameters

Resin	Density (g/cm^3)	ρ_{ref} (g/cm^3)	a ($g.cm^{-3}.MPa^{-1}$)	c [a].$°C^{-1}$	$d\rho/dT$ ($g.cm^{-3}.°C^{-1}$)	b ($g.cm^{-3}.MPa^{-2}$)	d [b].$°C^{-1}$	σ (g/cm^3)
HDPE	0.9620	0.875	2.65E-04	5.87E-08	-5.67E-04	2.43E-06	-6.6E-09	0.0009
C	0.9234	0.872	2.94E-04	-1.13E-07	-5.56E-04	2.26E-06	-5.8E-09	0.0009
L	0.9222	0.867	2.81E-04	-9.51E-08	-5.53E-04	2.31E-06	-5.8E-09	0.0007
A	0.9208	0.871	2.72E-04	4.17E-08	-5.57E-04	2.38E-06	-6.6E-09	0.0007
G	0.9200	0.864	2.91E-04	-1.09E-07	-5.53E-04	2.22E-06	-5.6E-09	0.0007
K	0.9198	0.866	2.95E-04	-1.15E-07	-5.56E-04	2.23E-06	-5.7E-09	0.0008
B	0.9194	0.870	2.98E-04	-9.97E-08	-5.51E-04	2.21E-06	-5.7E-09	0.0008
E	0.9194	0.870	2.91E-04	-7.61E-08	-5.51E-04	2.26E-06	-5.9E-09	0.0007
D	0.9192	0.869	2.82E-04	-5.92E-08	-5.47E-04	2.31E-06	-6.0E-09	0.0008
H	0.9190	0.868	2.80E-04	-4.81E-08	-5.48E-04	2.28E-06	-6.0E-09	0.0009
F	0.9190	0.867	2.98E-04	-1.32E-07	-5.48E-04	2.23E-06	-5.6E-09	0.0009
J	0.9180	0.866	3.02E-04	-1.34E-07	-5.45E-04	2.17E-06	-5.5E-09	0.0009
I	0.9070	0.863	3.11E-04	-1.76E-07	-5.39E-04	2.14E-06	-5.4E-09	0.0010

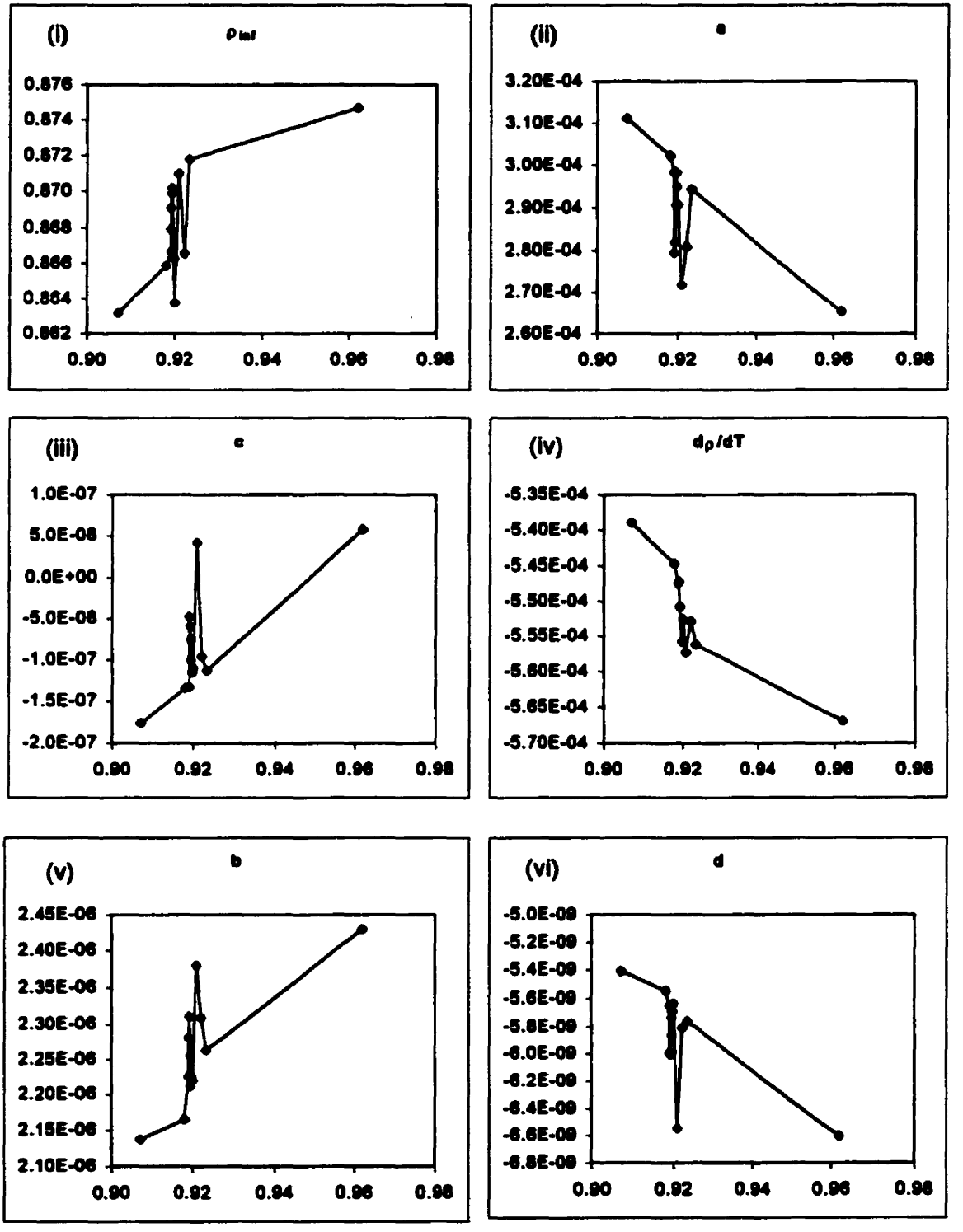

Figure 6.7: Inverse-Volume Parameters vs. density; each data point represent a resin.

6.1.3) Isothermal Compressibility and Thermal Expansion Coefficient

The isothermal compressibility, K, and thermal expansion coefficient, α, are the derivatives of the equation of state $V(P,T)$. They are important in the computer simulation of various polymer processing operations. The PVT data were differentiated numerically to obtain the values of α and K. The numerical differentiation consisted of fitting polynomials to isotherms, and exponentials to isobars followed by differentiation of the polynomials and exponentials. The results are presented for three representative resins: A, I, and HDPE. The resin I has the lowest density, whereas HDPE has the highest, and A represents the typical behavior of the other LLDPE resins. Indeed, a similar behavior was observed for all the resins. In addition, experimental data are compared to the Tait and Inverse-Volume predictions.

6.1.3.1) Isothermal Compressibility

The formulas of the derivative for both equations of state, which are given in Table 2.1, were used to calculate the predictions of experimental isothermal compressibility, K. Table 6.4 presents some values of K at different temperatures and pressures for the three resins considered in this section. At first, these values are consistent with the ones found in the literature (cf. section 2.3.4). The compressibility was logically found to increase with temperature and to decrease with rising pressure. However, the values calculated from experimental data showed a decrease of K with increasing temperature at 200 MPa, which can also be observed in Figure 6.8. This effect is merely due to the use of a second-degree polynomial equation to fit the isothermal data, which induces larger error at high pressure. Finally, it can be seen that the isothermal compressibility of these three different polyethylene resins is almost identical. This isothermal compressibility is therefore not strongly influenced by the chain structure of polyethylene resins.

Table 6.4: Experimental Isothermal Compressibility of the melt state for resins A, I, and HDPE; Average stands for the average value of the temperature interval.

$(MPa^{-1})*10^4$		0	100	200
A	173	8.47	5.70	2.39
	Average	9.25	6.13	2.33
	224	10.20	6.59	2.21
HDPE	177	8.56	5.72	2.35
	Average	9.30	6.15	2.27
	223	10.10	6.50	2.17
HDPE	177	8.57	5.80	2.49
	Average	9.26	6.18	2.41
	222	10.10	6.59	2.26

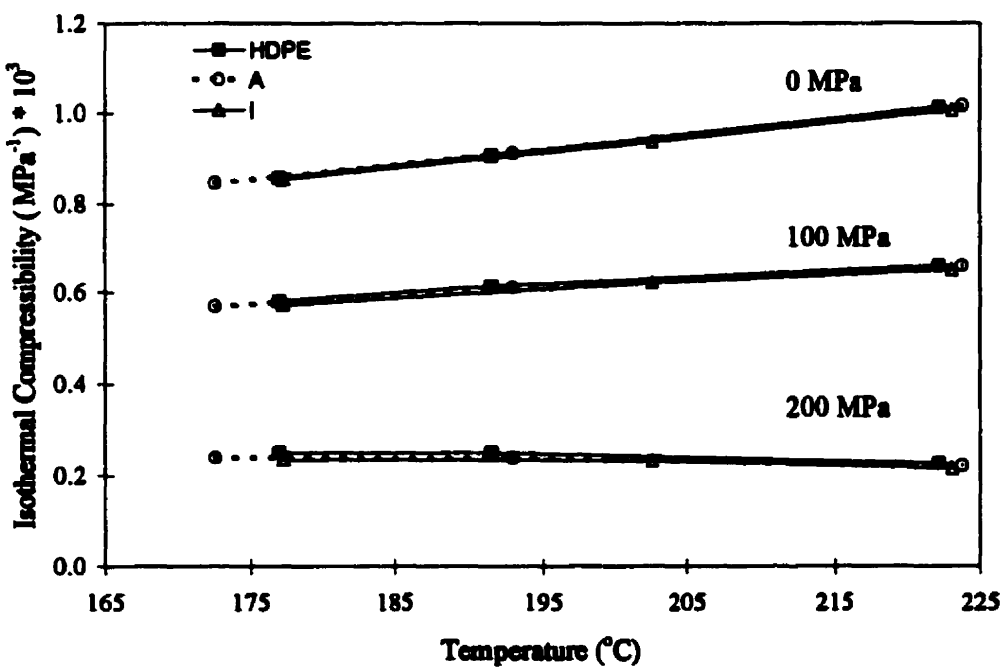

Figure 6.8: Experimental Isothermal Compressibility of the melt state versus temperature for resins A, I, and HDPE.

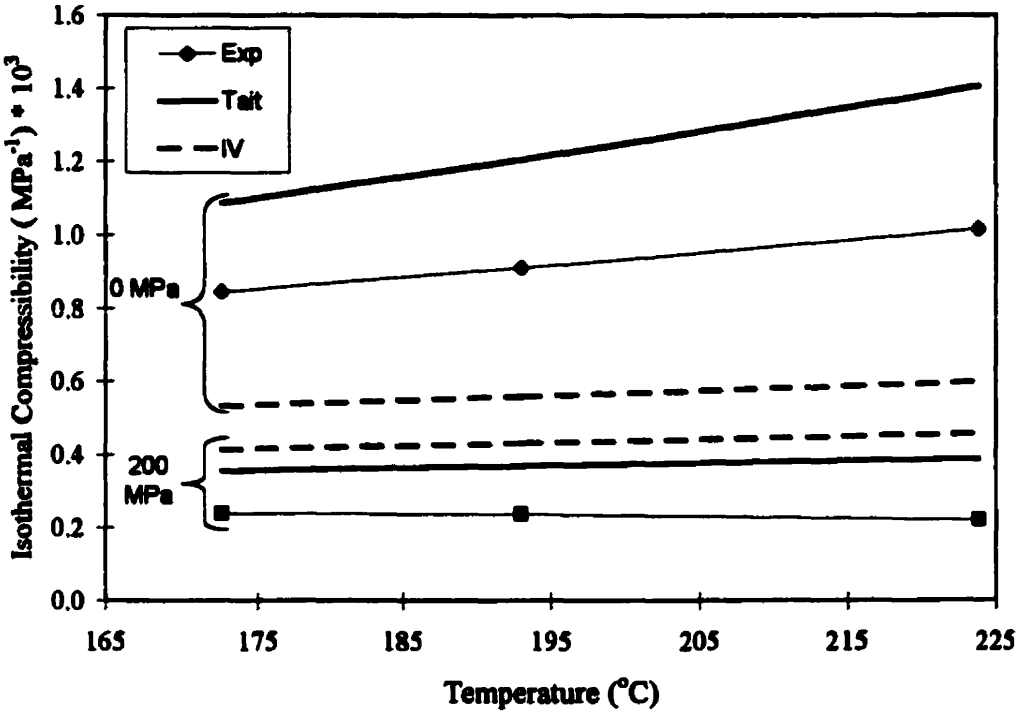

Figure 6.9: Isothermal Compressibility versus Temperature for resin A; Comparison of experimental data (Exp) with Tait equation fitting (Tait) and with Inverse-Volume fitting (IV).

Figure 6.9 illustrates the predictions of isothermal compressibility by the Tait and Inverse-Volume equations for Resin A, which are typical of data for all resins. In this figure, it is apparent that both equations of state yield poor predictions of isothermal compressibility. The average absolute percentage deviation, A_{dev}, defined in Appendix II, was found to be equal to 21% and 35% for the Tait and Inverse-Volume equations, respectively.

6.1.3.2) Thermal Expansion Coefficient

The thermal expansion coefficient, α, is plotted versus temperature at different pressures for resins A, I, and HDPE, in Figure 6.10. Some of these values are also presented in Table 6.5.

Table 6.5: Experimental Thermal Expansion Coefficient of the melt state for resins A, I, and HDPE; Average stands for the average value of the temperature interval.

$(°C^{-1})*10^4$		0	100	200
A	178	9.87	5.73	4.34
	Average	10.0	5.79	4.37
	224	10.2	5.86	4.41
I	177	9.50	5.61	4.32
	Average	9.65	5.67	4.35
	223	9.82	5.73	4.39
HDPE	177	9.95	5.71	4.45
	Average	10.1	5.76	4.48
	222	10.3	5.83	4.53

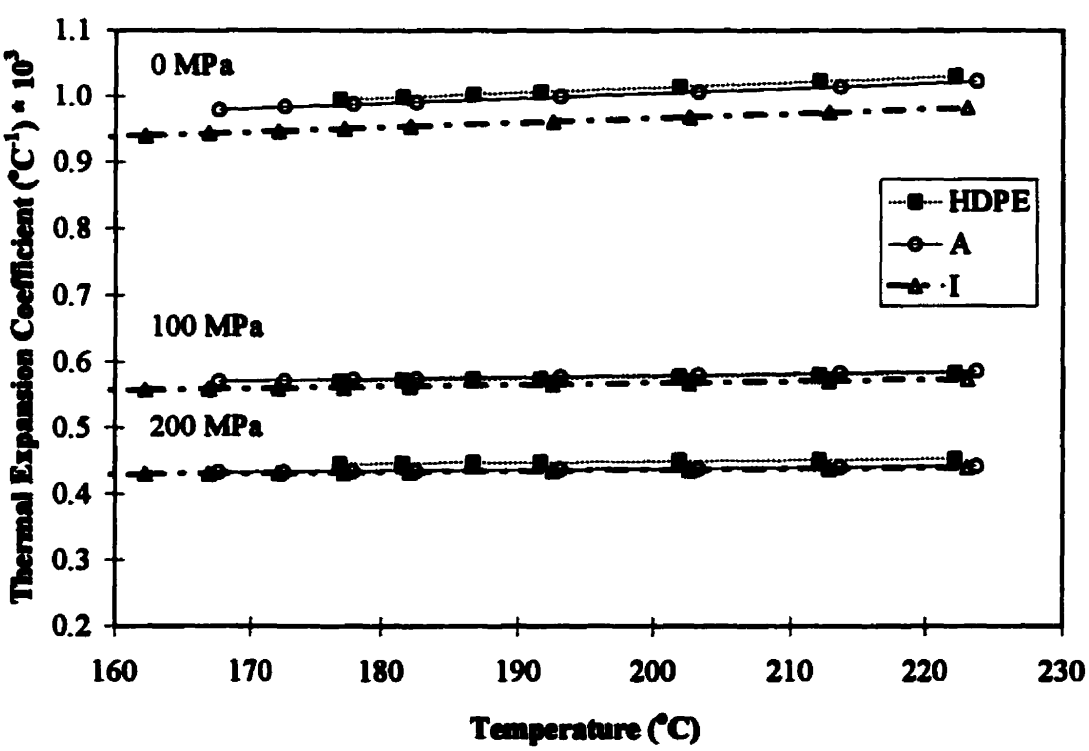

Figure 6.10: Experimental Thermal Expansion Coefficient of the melt state versus temperature for resins A, I, and HDPE.

The thermal expansion coefficient α was found to be similar for all the resins under study. However, some differences were observed, as shown in Figure 6.10 and Table 6.5, in contrast to isothermal compressibility. Resin I, which has the lowest density, exhibited the lowest value of α, whereas the HDPE resin, which has the highest density, showed the highest value of α. These results are consistent with the tendency reported earlier for the estimated Tait equation parameter, α_0. Figure 6.11 shows the predictions of both equations of state for α in the melt region. It is apparent from this figure that both equations of state yield poor predictions of α. The average absolute percentage deviations are 19% and 33% for the Tait and Inverse-Volume equations, respectively. However, it is clear that only the Inverse-Volume equation predicts a positive sign for $d\alpha/dT$, which is in agreement with experimental data.

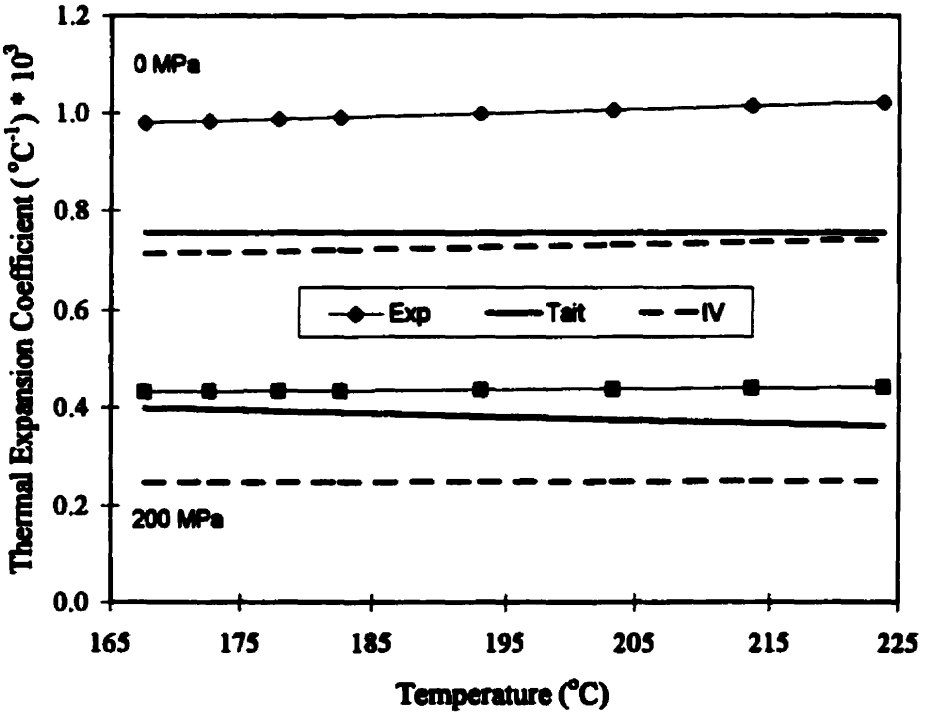

Figure 6.11: Thermal Expansion Coefficient for resin A; Comparison of experimental data to Tait equation (solid lines) and to Inverse-Volume equation (dashed line) predictions under atmospheric pressure and 200 MPa.

6.1.4) Summary

Several conclusions can be drawn from the study of the PVT properties of the polyethylene resins investigated in this work. At first, the PVT experimental data are in good agreement with those reported in the literature, and are reproducible within 0.2%. The general PVT behavior is similar for all grades of LLDPE resins investigated in this project. The HDPE resin differs from the LLDPE resins by its behavior in the solid state region and in the melting/crystallization processes. All the resins had an almost identical PVT melt behavior, including the HDPE resin. It can be therefore concluded that the PVT melt behavior is not strongly affected by the molecular weight, the branching size and their distributions.

These observations were confirmed by the fitting results of the Tait and Inverse-Volume equations. They both predict the experimental data with a better accuracy than the uncertainty in the measurements. From these predictions, the thermal expansion coefficient at atmospheric pressure, α_0, was found to be dependent on density; it increases with density. The same tendency was observed for the thermal expansion coefficient. For the latter and the isothermal compressibility, the predictions by both equations of state were rather poor. However, only, the Inverse-Volume equation could predict the observed tendency for increasing thermal expansion coefficient with temperature.

6.2) PRESSURE DEPENDENCE OF CRYSTALLIZATION AND MELTING

The isobaric experiments, in which the samples were heated and cooled at 2.5°C/min at constant pressure, were employed to study the effect of pressure on the melting and crystallization processes. Characteristic features, such as melting points and crystallization temperatures evaluated.. The pressure dependence of these temperatures, together with their tendencies, are discussed. Then, the curves of the volume change rate versus temperature are presented and compared for all the LLDPE resins.

6.2.1) General Behavior in Isobaric Experiments

Figures 6.12 and 6.13 display a set of isobaric experiments for the HDPE resin and a typical LLDPE resin. Only resin B is presented because all the LLDPE resins exhibit the same curve shape, as shown in Figure 6.14. In contrast, the differences in crystallization and melting behavior between LLDPE and HDPE resins are quite clear from these figures. For instance, the end of crystallization, which is observed when the crystallization curve becomes parallel to the melting curve in the solid state region, is markedly different. HDPE crystallization occurs in a narrow temperature range, whereas LLDPE resins crystallize in a much broader temperature interval, over 50°C. For LLDPE resins, the onset of crystallization is followed by a first rapid diminution of the volume, and then by a slow decrease process. This is the typical behavior of a resin crystallizing in two kinetic steps, referred to as primary and secondary crystallization.

Another characteristic of the HDPE resin is that crystallization under high pressure seems to yield material with higher density. Indeed, the crystallization curve at 200 MPa (in Figure 6.12) is observed to be below the melting curve, after crystallization was complete. On the other hand, the opposite behavior was observed for LLDPE resins, particularly at low pressure, as illustrated in Figure 6.13.

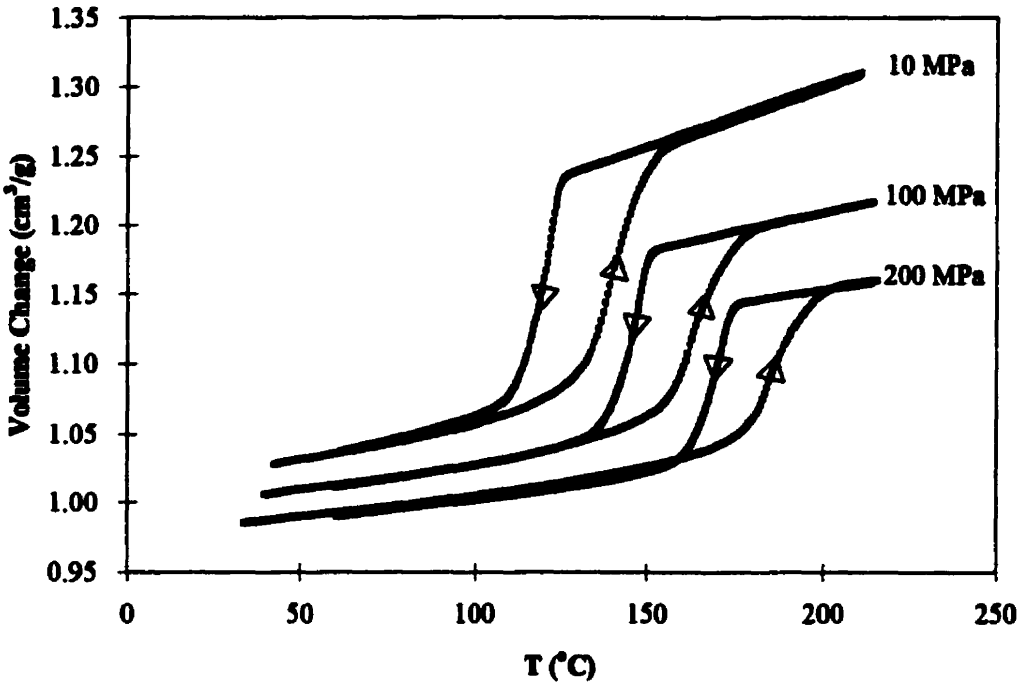

Figure 6.12: Crystallization and melting at 2.5 °C/min under various pressures for the HDPE resin.

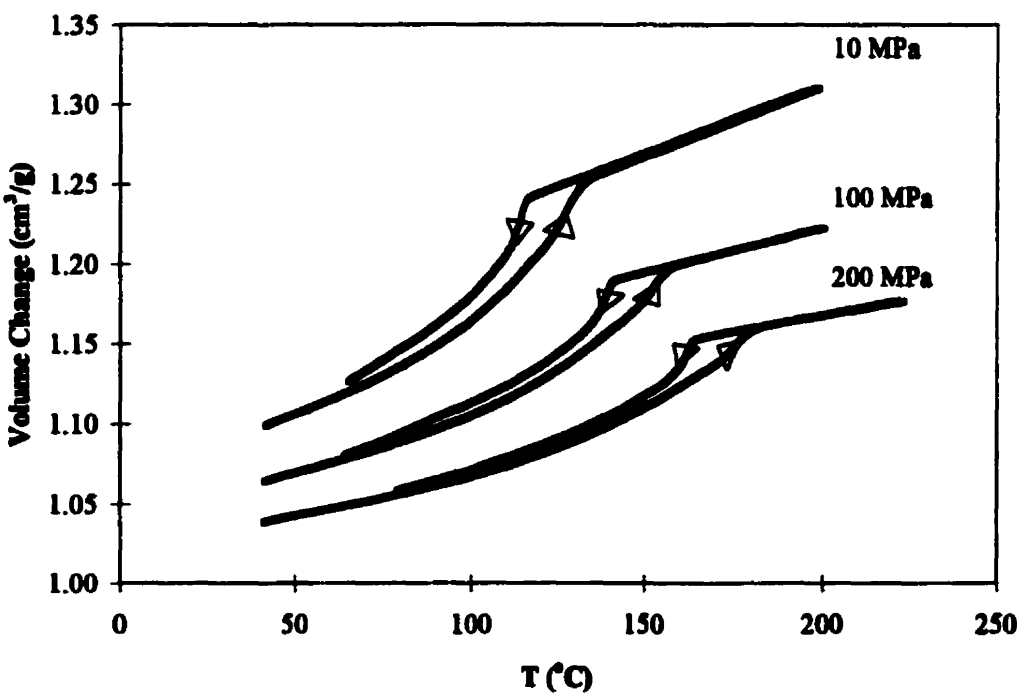

Figure 6.13: Crystallization and melting at 2.5 °C/min under various pressures for resin B.

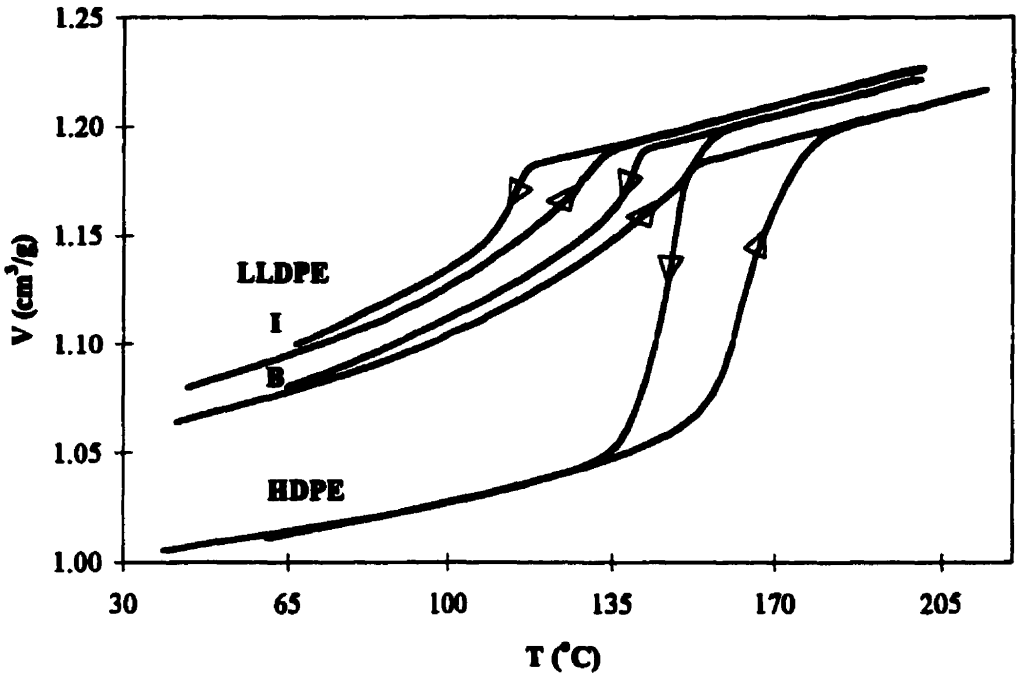

Figure 6.14: Crystallization and melting at 2.5 °C/min under 100 MPa for resins B, I, and HDPE.

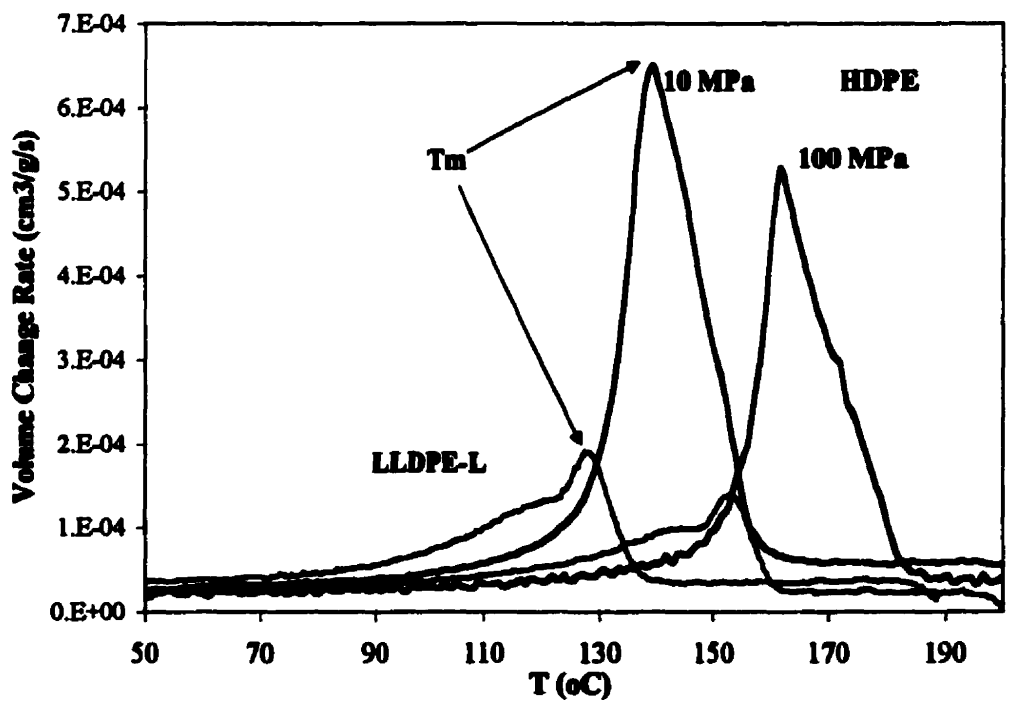

Figure 6.15: Volume Change Rate vs. Temperature representing the melting of resins L and HDPE under 10 and 100 MPa.

6.2.2) Pressure Dependence of T_m and T_c

The melting and crystallization temperatures under pressure were defined as the temperature at which the volume change rate was maximum during melting and crystallization, respectively, under constant pressure, as described in section 5.2. An example of a plot of volume change rate versus temperature showing the pressure dependence of the melting points for resins L and HDPE is presented in Figure 6.15. Melting points and crystallization temperatures under 10, 50, 100, and 200 MPa were determined for each resin. These values are reported in tables in Appendix III.

To evaluate the pressure dependence of T_m and T_c, temperature data were plotted versus pressure, as illustrated in Figure 6.16. From this graph, which is illustrative of the results for all resins, it can be seen that experimental melting and crystallization temperatures are almost linearly dependent on pressure. Data were thus fitted to a linear equation that yielded good fitting results, within 1%. The slope of this line represents a thermodynamic quantity expressed by the Clausius-Clapeyron equation as follows:

$$\frac{dT_m}{dP} = T_m^0 \frac{\Delta V_f^0}{\Delta H_f^0} \tag{6.3}$$

where ΔV_f^0 is the volume change on fusion, ΔH_f^0 is the heat of fusion, and T_m^0 is the equilibrium melting point. However, it has been shown that for large pressure increase, the melting curve of polyethylene decreases in slope with increasing pressure[16,52]. Takamizawa et al.[52] showed that the dependence of the melting point for large pressure increases was best represented by the Simon equation[53]:

$$P - P_0 = a\left[\left(\frac{T_m}{T_{m,0}}\right)^c - 1\right] \tag{6.4}$$

where T_m is the melting temperature at pressure P, and $T_{m,0}$ is the melting temperature at atmospheric pressure; a and c are constants that depend on each substance. Subsequently, data were fitted to the Simon equation. The reproducibility of the temperature data by the

Simon equation was extremely accurate (σ<0.1°C), which is better than the error in the temperature measurements (0.2°C). The results of both correlations are given in Table 6.6. From this table, it can be seen that the fitting parameters are comparable for all the polyethylene resins investigated in this study. The average values of the fitting results are given in Table 6.7. For the pressure range studied, the linear regression yielded a quasi-identical slope for all resins, which was equal to 0.25°C/MPa. This value is in agreement with the ones reported by Wunderlich and Davidson[16], and it is closer to the value they found for folded-chain crystals than that for extended-chain crystals. This was logically expected since no extended-chain crystal formation has been reported for polyethylene below 200 MPa. From Table 6.7, the following parameters of the Simon equation, a=320 and c=4.0, can be used to represent the pressure dependence of T_m and T_c for all resins with an accuracy of 0.8%. These parameters are in agreement with the values reported in the literature[25].

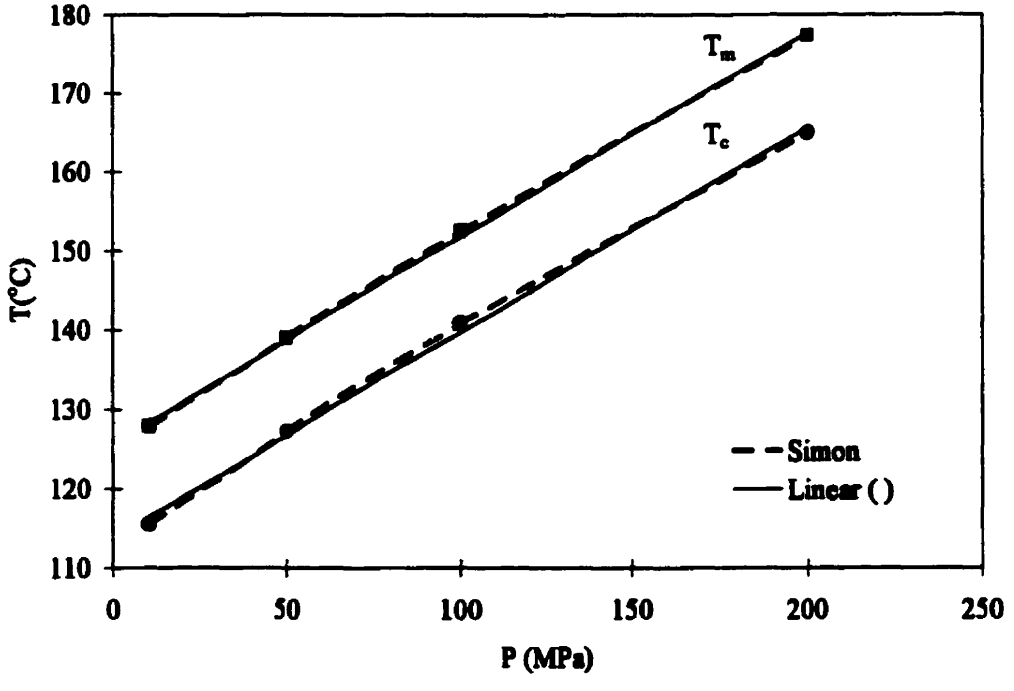

Figure 6.16: Melting points and crystallization temperature versus pressure with the linear and the Simon equation fitting for resin B.

Table 6.6: Fitting Results of the Pressure Dependence of T_m and T_c

Resin	Crystallization Temperature					Melting Point				
	a (MPa)	c	T_0 (°C)	dT/dP (°C/MPa)	T_0 (°C)	a (MPa)	c	T_0 (°C)	dT/dP (°C/MPa)	T_0 (°C)
A	318	3.9	115.0	0.26	116.5	407	3.3	126.9	0.26	128.0
B	277	4.3	111.0	0.25	112.9	386	3.4	124.6	0.26	125.9
C	296	4.1	112.3	0.25	114.0	319	4.0	125.3	0.26	126.9
D	339	3.7	111.4	0.26	112.2	318	4.1	122.7	0.25	123.9
E	260	4.5	109.3	0.25	111.3	202	5.7	120.7	0.24	123.2
F	411	3.4	99.4	0.23	100.5	285	4.5	111.1	0.23	112.8
G	254	4.5	109.9	0.26	111.9	308	4.1	126.1	0.26	127.8
H	222	5.1	106.5	0.25	108.8	458	3.0	124.3	0.25	125.4
I	281	4.5	89.4	0.23	91.1	244	5.2	103.3	0.22	105.2
J	326	3.9	101.6	0.24	102.7	499	2.8	114.8	0.24	115.5
K	331	3.9	99.8	0.24	101.2	583	2.6	113.8	0.23	114.5
L	331	3.7	112.4	0.26	113.9	541	2.5	125.0	0.26	125.8
HDPE	249	4.7	118.5	0.26	120.6	352	4.0	135.4	0.24	136.8

Table 6.7: Average values of the fitting results of Table 6.6.

Simon Equation

	Crystallization		Melting		Both
	Av.	Avdev.	Av.	Avdev.	Tot. Av.
c	4.2	0.4	3.8	0.8	4.0
a	300	40	377	94	338
Fitted with c=4.0					
a	310	8	327	12	319
Linear Equation					
dT/dP	0.25	0.01	0.25	0.01	0.25

6.2.3) Melting and Crystallization curves under Pressure

By plotting the volume change rate versus temperature to assess the transition temperatures, we observed that the melting and crystallization curves varied significantly from one resin to another. Figures 6.17 (a) to (d) present the melting curves under 100 MPa for all LLDPE resins. The crystallization curves under 100 MPa are displayed in Appendix III. The behavior of the HDPE resin is shown in Figure 6.15. Figures 6.17 were plotted by comonomer type, which is equivalent to branching size.

Three typical curve shapes can be observed from these figures. Firstly, the characteristic melting behavior of a resin that possesses a non-uniform branching distribution (Ziegler-Natta catalyzed resins) can be seen for resins B and G. These curves exhibit a peak, between 125 and 128°C, attributed to the melting of the almost linear molecules, and a broad and flat part, corresponding to the melting of the highly branched molecules of various sizes. The metallocene catalyzed resins display the two other types of melting curves. The resins I and J exhibit one simple peak, corresponding to the melting of the uniformly branched molecules. Finally, some other metallocene based resins, such as resins D and E, feature one peak with a shoulder at a lower temperature. This indicates the presence of two dominant molecular structures with a different branching distribution.

Figure 6.17 (a) shows the melting behavior of two butene- ethylene copolymers, which differ mainly by their polymerization process. Resin B, which was manufactured by a gas-phase process, display a more distinctive peak and a higher melting point than that for resin H, which is a solution-polymerized resin. This is consistent with the fact that solution polymerization yields a more uniform branching distribution than that for gas-phase resins[66].

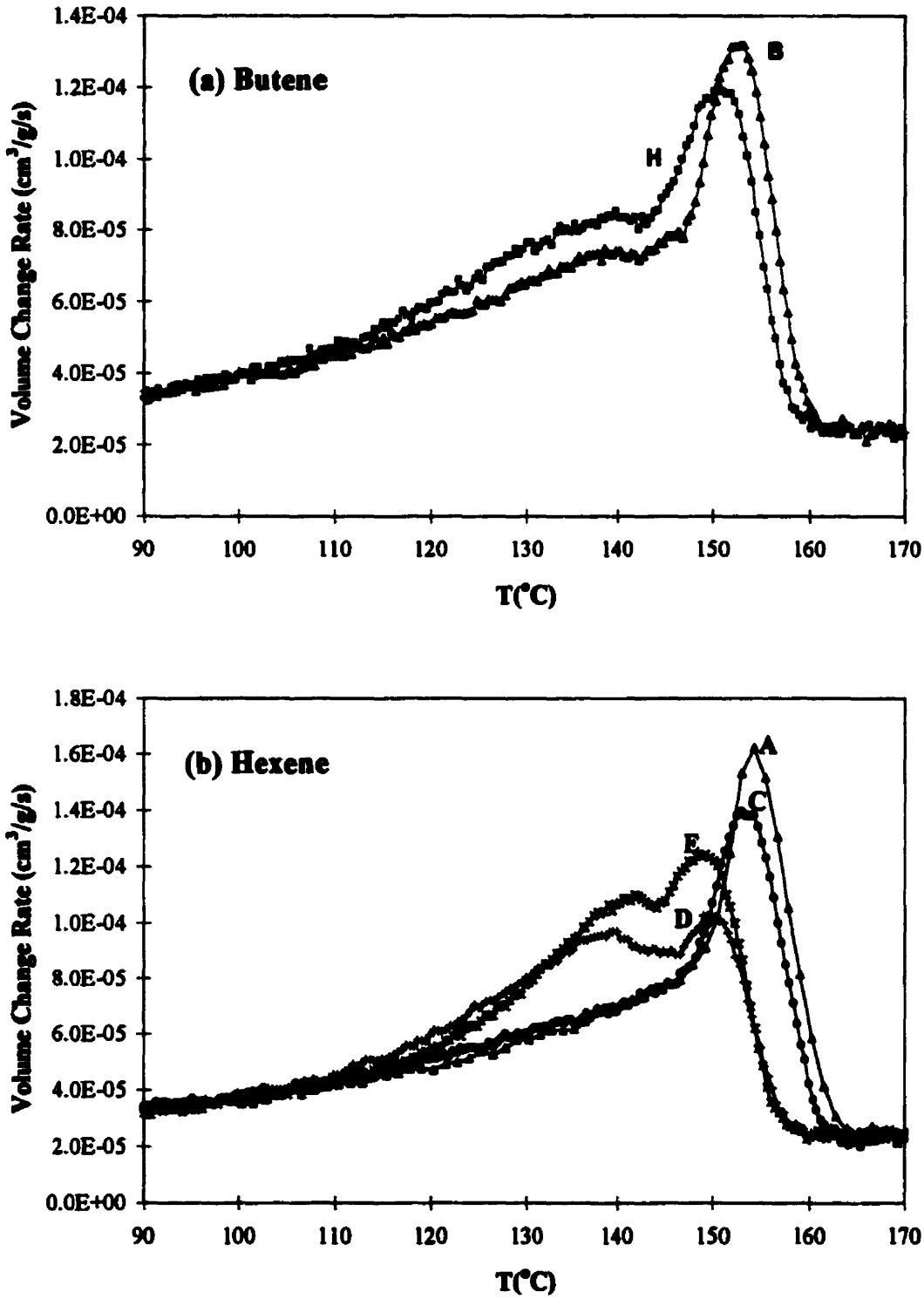

Figure 6.17: Volume Change Rate vs. Temperature for the melting under 100 MPa at 2.5 °C/min of resins with (a) Butene and (b) Hexene comonomers.

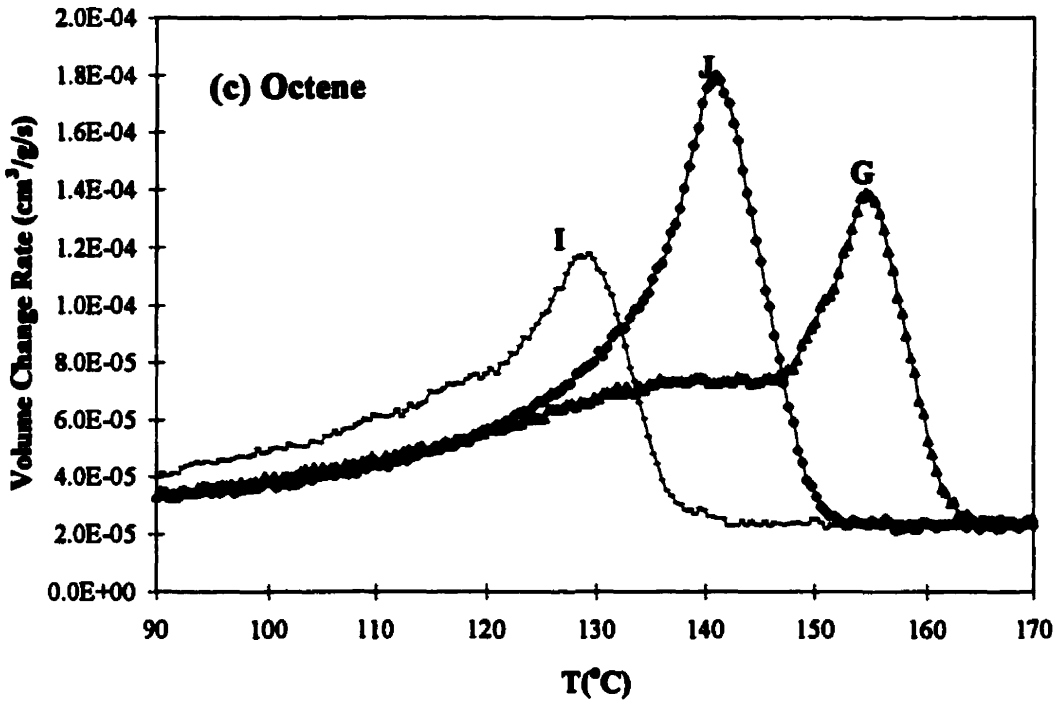

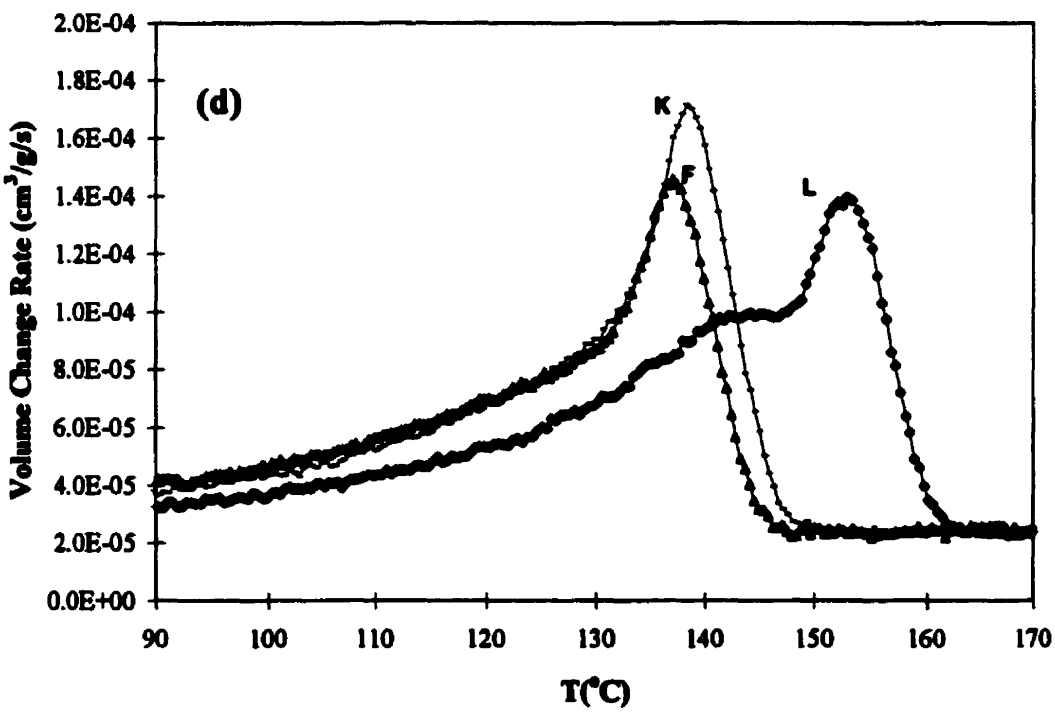

Figure 6.17: Volume Change Rate vs. Temperature for the melting under 100 MPa at 2.5°C/min of resins (c) with Octene comonomers and (d) F, K, and L.

Figure 6.17 (b) presents the melting behavior for the hexene-ethylene copolymers under 100 MPa. The two metallocene catalyzed and gas-phase processed resins, D and E, behave differently in melting than the metallocene catalyzed resin, the resin C, which was solution polymerized. Both resins D and E exhibit a peak with a shoulder indicating the existence of two dominant branching compositions. This confirms that the gas medium seems to induce less uniform branching.

Figure 6.17 (c) shows the melting behavior for the octene-ethylene copolymers. The three polyethylene grades were solution polymerized, but resin G was Ziegler-Natta catalyzed and resins I and J were metallocene catalyzed. From the curves of resins G and J, it is clear that the catalyst type affects the molecular structure, and therefore the melting behavior. The effect of the comonomer content on the melting behavior of metallocene catalyzed resins, i.e. decrease of the melting point with increasing comonomer content, is quite apparent from this figure.

Figure 6.17 (d) illustrates the melting behavior of the LDPE resin F, and resins K and L. The details of the structure of resins F and K are not known, except that they are LDPE resins prepared in the gas phase. Resin L is a solution LLDPE resin. Unfortunately, the composition of this resin is also not known.

6.2.4) Summary

The isobaric experiments yielded important information concerning the melting and crystallization under pressure of polyethylene resins. All the LLDPE resins displayed a secondary crystallization behavior during cooling under pressure. In contrast, the HDPE resin did not exhibit such a behavior, crystallization occured in a narrow temperature range. The melting points and crystallization temperatures of all grades of polyethylene resins investigated in this work were affected similarly by pressure. Up to 200 MPa, T_m and T_c were observed to be linearly dependent on pressure. The pressure dependence of these transition temperatures, dT/dP, was found to be equal to

0.25°C/MPa. Up to 200 MPa, T_m and T_c of all resins can be predicted with an error of 1% by the following linear equation:

$$T^P_{m-or-c} = 0.25 \times P + T_{m,0} \tag{6.4}$$

where $T_{m,0}$ is the melting temperature at atmospheric pressure. However, the Simon equation, which predicted experimental data with a slightly better accuracy than that for a linear fit, should be considered for higher pressure.

Finally, the investigation of the plots of the volume change rate versus temperature clearly demonstrated the differences in melting and crystallization behavior of these various grades of polyethylene resins. The differences in the melting curve shape are attributed to the differences in molecular structure. The differences result from variations in the crystalline packing ability of polyethylene due to the differences in the branching size and distribution. Remarkable variations were observed between polyethylene grades catalyzed by Ziegler-Natta or metallocene catalysts. The effects of the polymerization medium and of the comonomer content on crystallization and melting behavior were also observed from these isobaric experiments.

6.3) CRYSTALLIZATION KINETICS

To study crystallization kinetics, isothermal/isobaric experiments were carried out according to the procedure described in Chapter 4. The sample was pressurized from 10 MPa to the crystallization pressure at constant temperature. Volume data were then recorded as a function of time. Utilizing the procedure detailed in Chapter 5, the induction time and the relative crystallinity were evaluated from experimental data. The relative crystallinity was defined as:

$$X = \frac{V_t - V_0}{V_\infty - V_0} \tag{6.5}$$

The value V_0 was the volume at which crystallization begins, corresponding to the end of the induction time, and the value V_∞ was defined at the end of primary crystallization. Kinetics data were then fitted by the Avrami equation:

$$X = 1 - exp(-kt^n) \tag{6.6}$$

where k and n are the Avrami parameters. The constant, k, represents the overall crystallization rate, and n is an exponent that can be related to the mode of nucleation and growth rate. Even though this work presents solely the kinetics results of the primary crystallization, this section first discusses the secondary crystallization behavior of the LLDPE resins. Crystallization kinetics curves for some polyethylene resins and their representation by the Avrami equation are presented next. Then, the effects of pressure and of polymer type on the Avrami parameters are discussed. The effect of pressure on half-time of crystallization and on induction time at constant supercooling is also considered. Finally, further interpretation of the pressure effect on crystallization rate utilizing the Lauritzen-Hoffman theory is discussed.

6.3.1) Secondary Crystallization

In this work, the completion of crystallization was not observed. The secondary crystallization was still in progress even after more than 20 hours, as shown in Figure 6.18. The linear increase of the degree of crystallinity with the logarithm of time for the secondary crystallization, as reported by Schultz et al.[31], is clearly observed in this figure. In addition, the secondary crystallization rate seemed to be not strongly dependent on temperature at constant pressure. Inaddition, the volume change is dependent on temperature.

Figure 6.19 demonstrates the importance of the end-of-crystallization effect on the Avrami parameters. Figure 6.19 displays the kinetics data for a run that was analyzed in the following ways. The upper data curve corresponds to the case for which crystallinity was calculated with V_∞ being the end of primary crystallization (V_∞ at 20

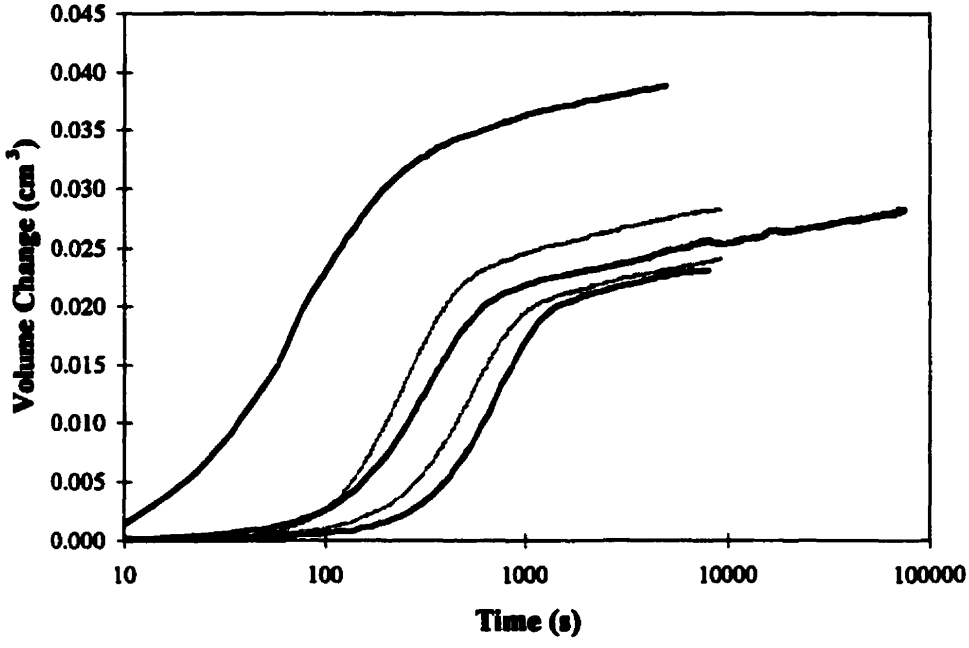

Figure 6.18: Typical LLDPE crystallization experiments at constant pressure for various temperatures, indicating the linear increase of the degree of crystallinity during secondary crystallization.

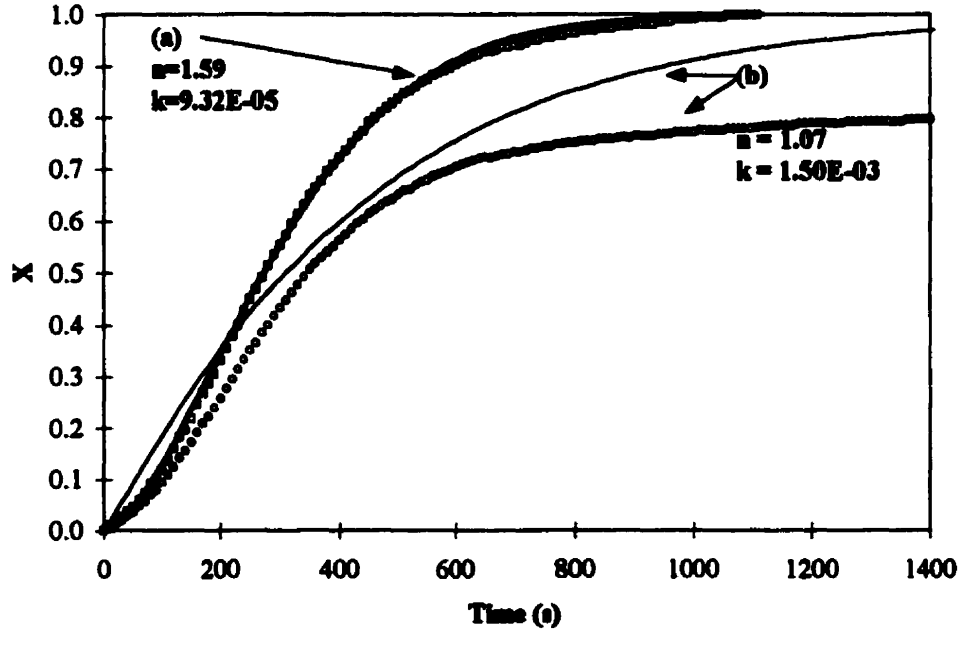

Figure 6.19: Crystallization kinetics experiment for resin B under 100 MPa at 144°C, presenting two different data analyses: (a) V_∞ at end of primary crystallization, and (b) V_∞ at end of secondary crystallization. Symbols are experimental data, solid lines are the Avrami equation fit.

minutes), and the lower curve for the case for which V_∞ is the end of the experiment, (V_∞ at 20 hours). From this figure, it is obvious that the two-step crystallization cannot be represented by the Avrami equation because it affects the Avrami parameters, resulting in a lower value of n, together with a slower crystallization rate. This is in agreement with the observations of other workers[47].

Because of the slowness of secondary crystallization, and the difficulty to represent it by the Avrami equation, the present work has focused on the study of primary crystallization.

6.3.2) Crystallization Kinetic data

Figure 6.20 illustrates the typical curves that were obtained for isothermal/isobaric experiments, and it also shows the end of primary crystallization of each experiment, indicating the curve section that was considered for kinetics analysis.

Volume change data were employed to calculate the relative crystallinity, which was plotted versus time, as shown in Figure 6.21. This figure also shows that the isotherms are superimposable upon shifting the time axis for the same material, with the possible exception of the lowest supercooling. Error is greatest for the lowest supercooling owing to uncertainty in V_∞. The slopes of the curves were almost identical from 50 to 200 MPa for a same material, indicating a consistent mechanism of formation of the crystals. Differences in slopes were observed between materials, as shown in Figure 6.21. This suggests that the polymer chain structure affect the mechanism of crystallization.

Data were next fitted by non-linear regression to the Avrami equation. All the results of the Avrami equation fitting, the values of n, k, induction time t_i, $k_{1.5}$, and half-time of crystallization $t_{1/2}$, may be obtained from Professor M. R. Kamal. The Avrami constant $k_{1.5}$ was obtained from the Avrami fitting with n equal to 1.5. The choice of the value of 1.5 is explained below. Figure 6.22 presents an example of the Avrami fitting of

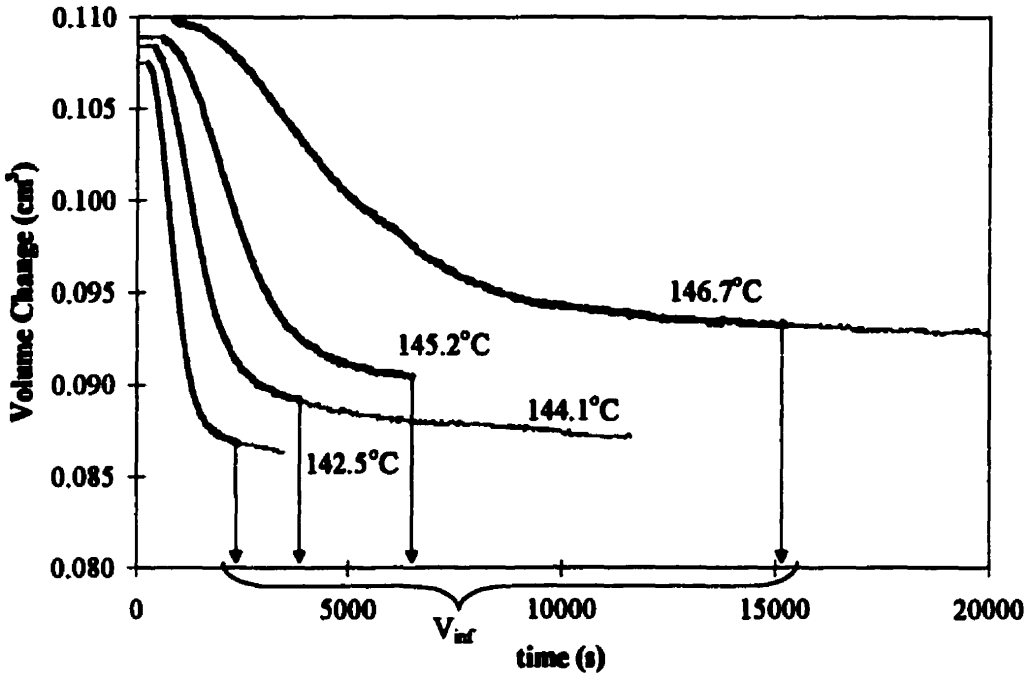

Figure 6.20: Crystallization kinetics experiments for resin H under 100 MPa at various crystallization temperatures. Bold lines indicate the part of the curve that was fitted to the Avrami equation.

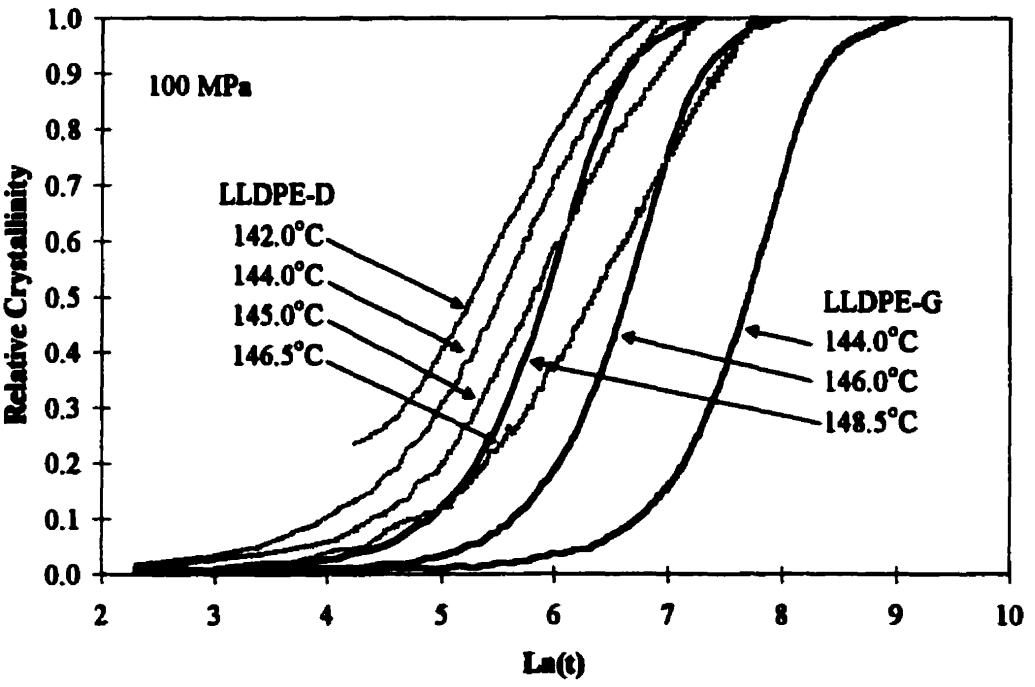

Figure 6.21: Crystallization Kinetics experiments under 100 MPa at various temperatures for the resins D and G.

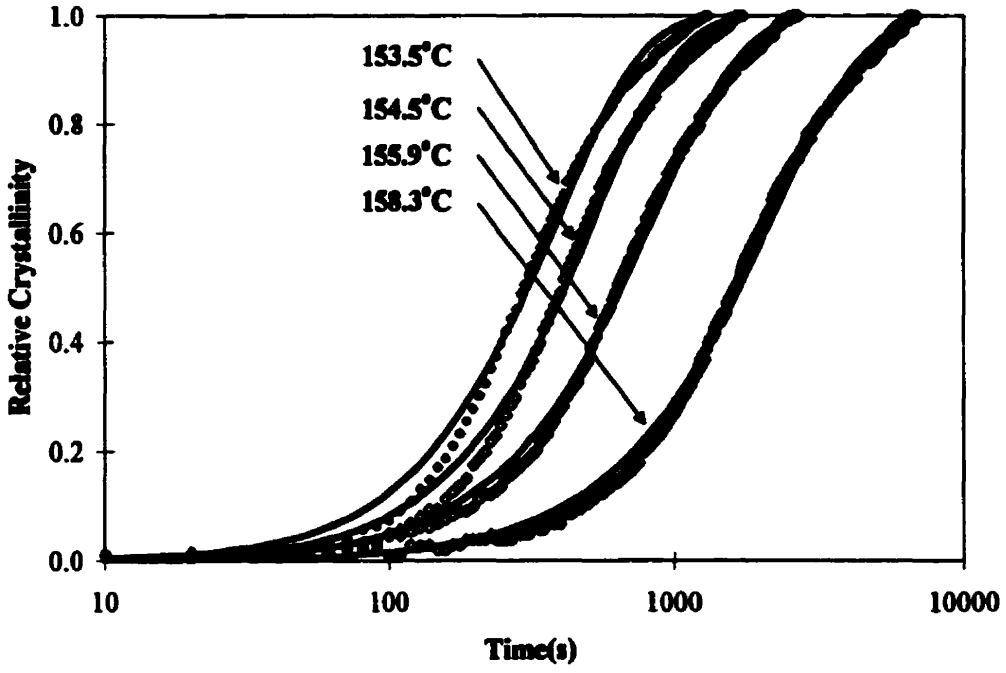

Figure 6.22: Avrami fits for kinetics experiments under 100 MPa at various temperature

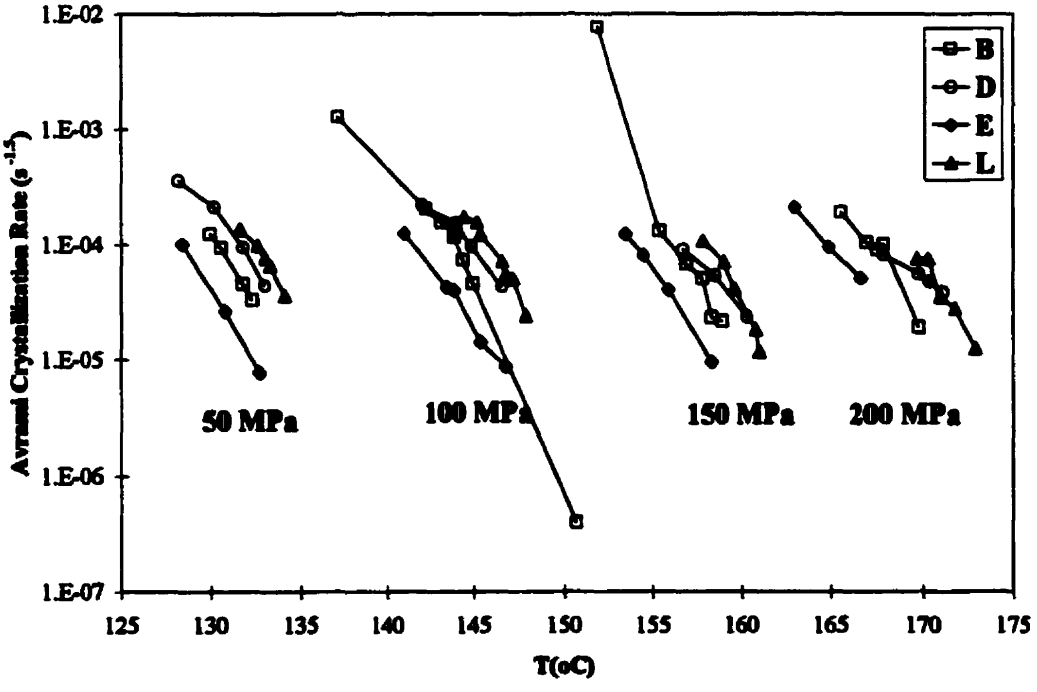

Figure 6.23: Logarithm of the Avrami crystallization rate, $k_{1.5}$, (obtained for n=1.5) versus crystallization temperature under various pressures for resins B, D, E, and L.

runs carried out under 150 MPa at different temperatures, for resin E. This figure also shows that the Avrami equation predicts the experimental data with some error, which was large for some resins, including D, E, F, and K. Large error was also observed for these resins when computing the end of crystallization volume using the "master curve" analysis. It is interesting to note that resins D and E are the only two resins prepared in a gas phase medium with metallocene catalysts., and resins F and K are two LDPEs.

The values of n were found to be in the range from 1.1 to 1.9, and the average values of n for each resin were between 1.2 and 1.8. These values are in good agreement with the ones reported by Brown and Jonas[26]. The lowest average value of n, 1.2 was observed for resin D, and the highest, 1.8 was for resin G. The grades D, E, F, and K, had Avrami exponents between 1.2 and 1.4; for resins I and J, n was around 1.5; for the others resins, n was in the range from 1.6 to 1.8. With the exception of resin C, all the grades exhibiting a high value of n, were prepared by Ziegler-Natta catalysts. On the other hand, the LDPE resin and the metallocene polymers displayed a value of Avrami n below 1.5.

Originally, the value of Avrami n was considered to be a characteristic of the growth mechanism. In this study, the value of n could be idealized to 1, 11/2, or 2 depending on the resin grade. This suggests that the nature of the catalyst, which controls branching uniformity, influences the growth habit of crystals. This can be related to the observation of Bassett[18] that the lamellar thickness was affected by the size and distribution of branches. In addition, the values of n were found to increase with increasing supercooling. This is in agreement with other reported data[8,26].

From the previous figures, it can be observed that crystallization is accelerated by decreasing temperature at constant pressure. This can be verified in Figure 6.23, illustrating the Avrami crystallization rate, $k_{1.5}$, versus crystallization temperature under various pressures for several resins. The value of the Avrami crystallization rate constant is strongly related to the Avrami exponent, n, which is in turn affected by temperature[36], resin grade, and possibly by pressure[24]. Kinetic data were thus compared for the same value of the Avrami exponent n, which was chosen to be equal to the average value of 1.5. From Figure 6.23, the crystallization rate of the various resins seem to be affected

similarly by temperature at constant pressure. The effect of pressure on crystallization rate is now discussed in the section.

6.3.3) Effect of Pressure on Crystallization Kinetics

In agreement with Brown and Jonas[26], the Avrami exponent was found to be independent of pressure in the range investigated. In contrast, for example for resin B in Figure 6.23, it is apparent that the crystallization rate at 150 MPa is significantly faster than that at 100 MPa at constant temperature. In general, this effect is simply and sufficiently explained by the effect of pressure on the melting temperature, which affects the degree of supercooling. Pressure increases the degree of supercooling. However, it has been reported that pressure affects crystallization kinetics even at constant supercooling[16,19,25]. In this project, crystallization half time and induction time were used to represent crystallization kinetics data. This section considers the influence of pressure on half-time of crystallization and induction time at constant supercooling.

The supercooling was defined as the difference between the melting point obtained from isobaric experiments at the pressure investigated and the crystallization temperature. The half-time of crystallization was calculated using the Avrami parameters, as follows:

$$t_{1/2} = \left(\frac{ln\,2}{k}\right)^{\frac{1}{n}} \qquad (6.7)$$

Figure 6.24 displays the results of all the experiments carried out under 100 MPa for each resin. This figure shows explicitly that resins D and G have the two extreme behaviors. Resin D exhibits the fastest crystallization, whereas resin G shows the slowest transformation process. The HDPE grade displays a crystallization behavior as slow as that for the G resin. The same rate order was observed throughout the pressure range investigated. The same graph was plotted for the induction time versus supercooling, as displayed in Figure 6.25. In this figure, resin D shows the shortest induction time,

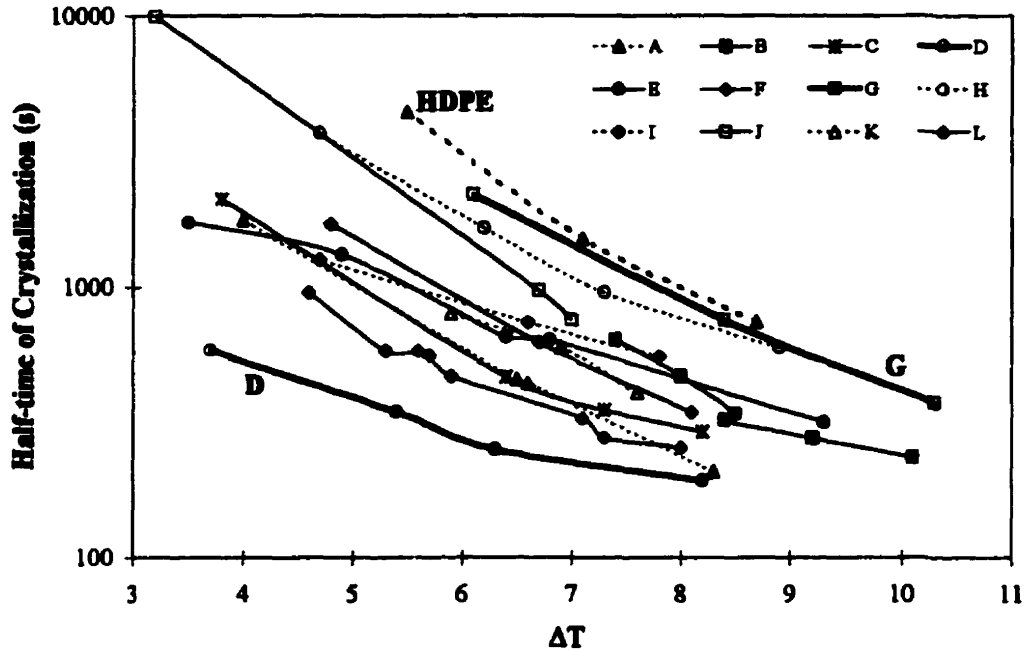

Figure 6.24: Half-time of crystallization vs. supercooling under 100 MPa at various temperatures for all the resins.

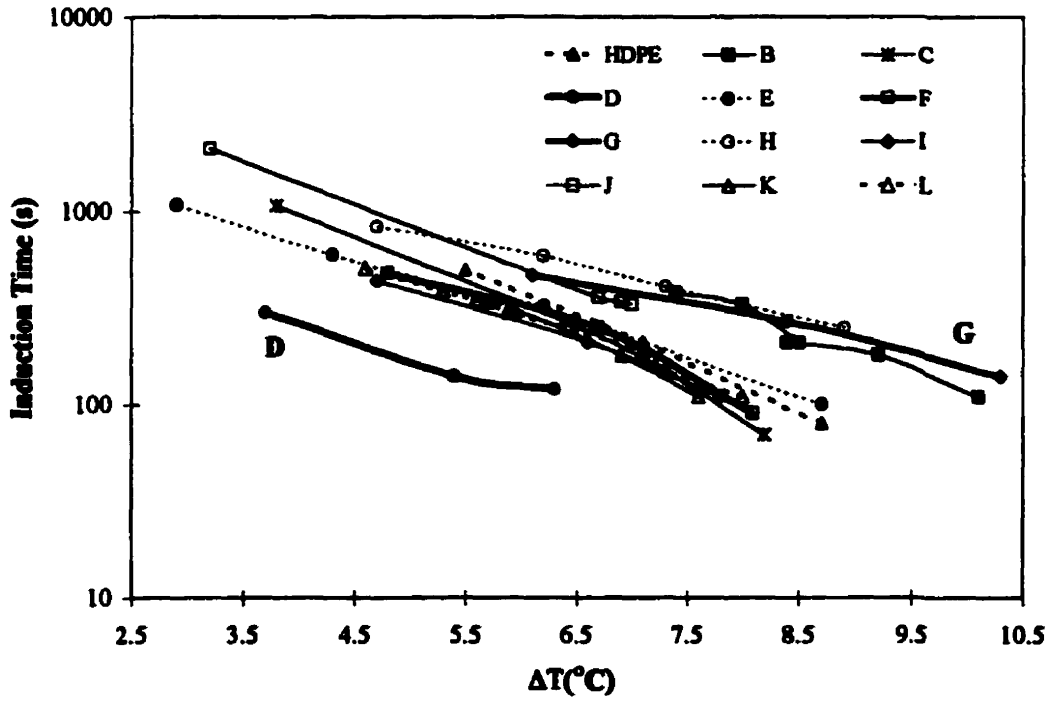

Figure 6.25: Induction time vs. supercooling under 100 MPa at various temperatures for all the resins.

confirming its rapid crystallization behavior. Resins G and H were found to display the longest induction time. This suggests that the nucleation and crystallization might be influenced by molecular chain structure, and especially polydispersity.

Half-time of crystallization and induction time were then plotted versus supercooling for each resin at 50, 100, 150, and 200 MPa. Solely two resins, L and HDPE, showed their crystallization half-time significantly affected by pressure at constant supercooling, as shown in Figures 6.26 and 6.27. In addition, these two polyethylene grades exhibited an opposite behavior. Indeed, the value of $t_{1/2}$ for the L resin was observed to increase with increasing pressure, whereas $t_{1/2}$ of HDPE resin was lowered by increasing pressure. This opposite behavior was confirmed by plotting induction time versus supercooling for both resins, as illustrated in Figures 6.28 and 6.29. The effect of pressure on induction time appears to be somewhat more notable than that on crystallization half-time, since the induction times of resins A, B, G, and H were also increased by pressure.

From these results, it is now clear that pressure affects crystallization kinetics even at constant supercooling. Pressure appears to influence more significantly induction time, thus, nucleation mechanisms, than crystallization rate. Nevertheless, at constant supercooling, crystallization was accelerated by pressure for the HDPE resin, as has been reported by several other workers[19,24,24,26]. On the contrary, the conclusion that crystallization was retarded by pressure for polyethylene has only been mentioned (not investigated) by Wunderlich and Davidson[16]. This contradictory behavior is certainly attributed to the respective singular polymer chain structure of both resins. Since the L and HDPE resins probably differ mainly by their branching content (the L resin structure was not known at the time of writing), this implies that branching significantly influences the effect of pressure on kinetics.

In addition, it can be concluded that the grades prepared by Ziegler-Natta catalysts respond differently to pressure than the metallocene catalyzed resins. For Ziegler-Natta resins, the onset of crystallization is delayed by pressure, whereas the metallocene grades are not significantly affected by pressure up to 200 MPa.

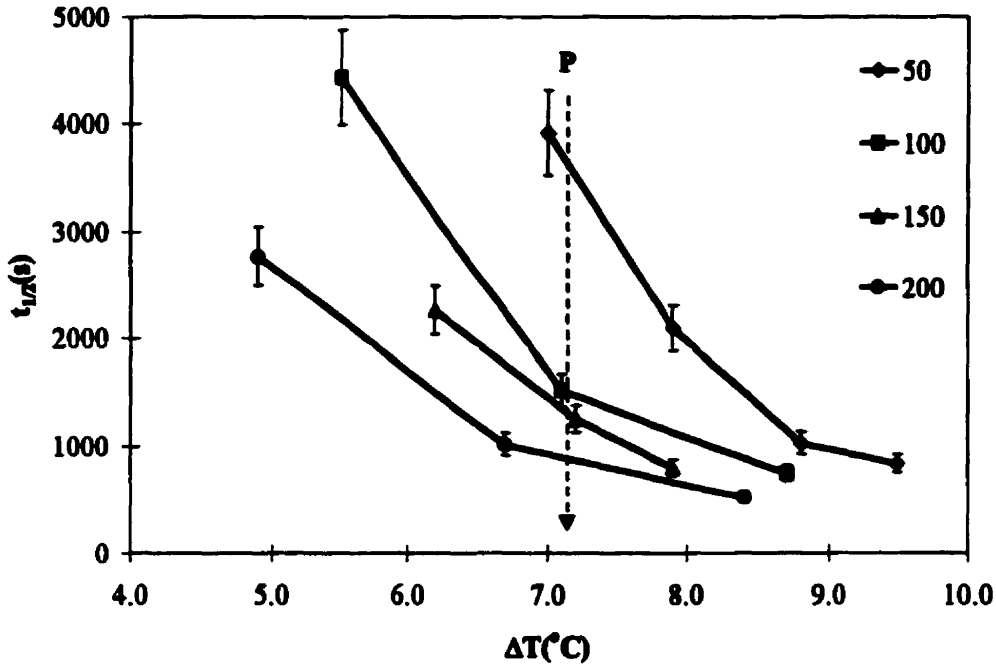

Figure 6.26: Half-time of crystallization vs. supercooling under various pressures and temperatures for HDPE.

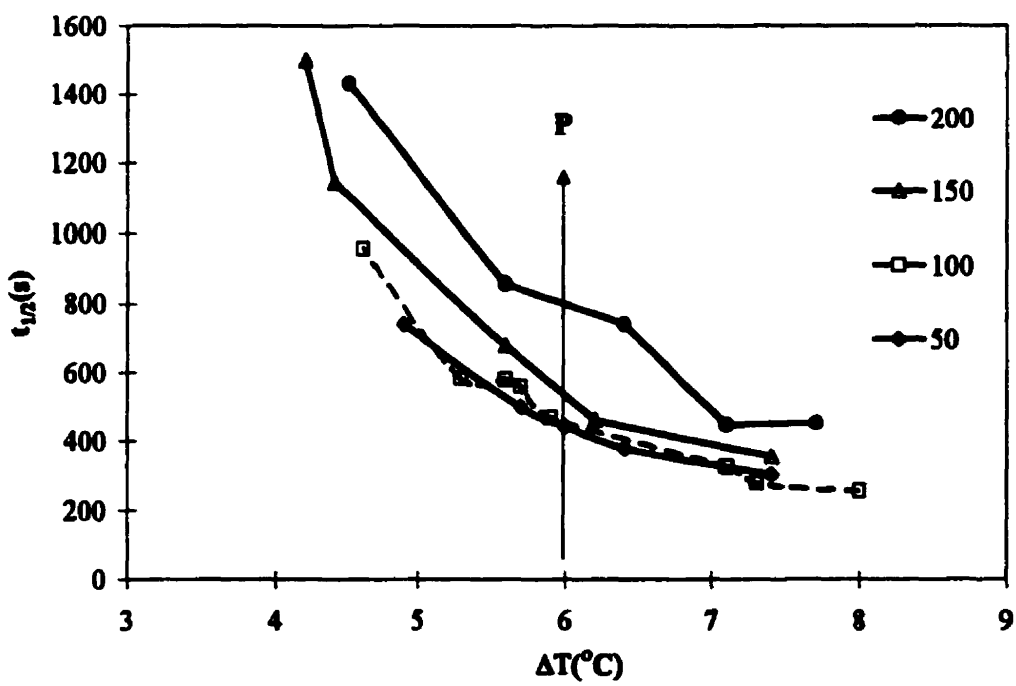

Figure 6.27: Half-time of crystallization vs. supercooling under various pressures and temperatures for resin L.

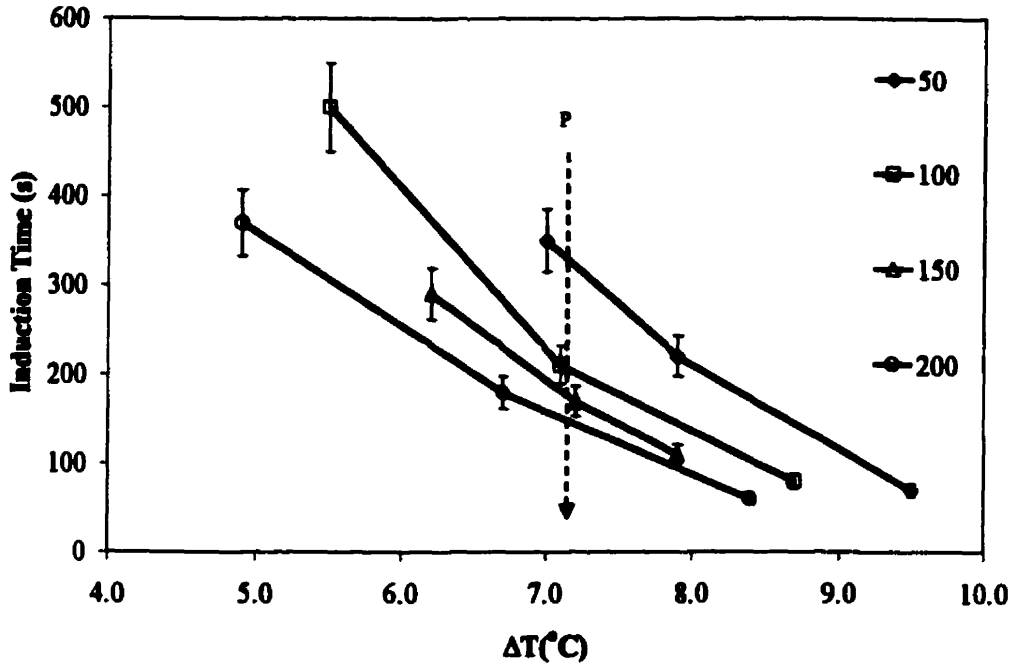

Figure 6.28: Induction time vs. supercooling under various pressures and temperatures for resin HDPE.

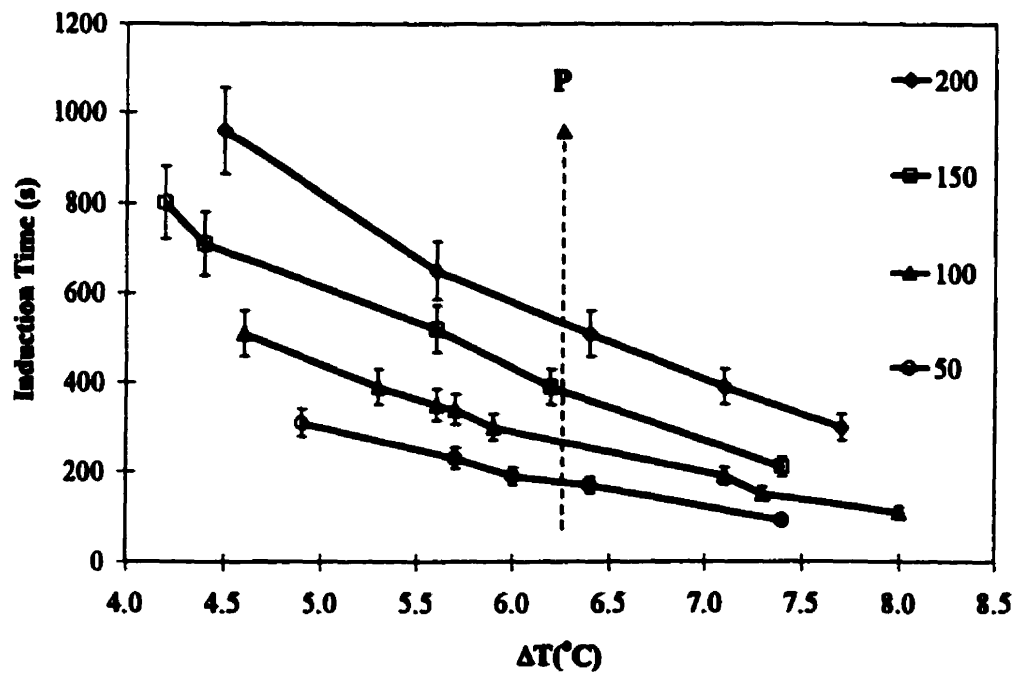

Figure 6.29: Induction time vs. supercooling under various pressures and temperatures for resin L.

This suggests that the effects of the non-uniformity of the branching and molecular weight distribution on the nucleation mechanisms are magnified by pressure.

6.3.4) Further Interpretation

For further interpretation, the theory of Lauritzen, Hoffman and coworkers[3] and the treatment by Mandelkern[1] could be useful here. Mandelkern uses eq. (2.1) for the nucleation rate (for a homogeneous process) to express the overall crystallization rate constant for a rectangular nucleus as

$$k = k_0 \exp\left(\frac{-nE_D}{RT} - [1+(n-1)\bar{a}\frac{\kappa T_m^2}{T(T_m T)^2}\right) \tag{6.8}$$

where E_D is now the free energy of activation for transport across the interface between the nucleus and the polymer melt, $\bar{a}$ is the ratio of critical free energy of secondary nucleation (addition of chains) to that of primary nucleation, and where n is the Avrami exponent. The term κ contains the surface energy and heat of fusion terms

$$\kappa = \frac{16\sigma_u^2\sigma_e}{R\Delta H_u^2} \tag{6.9}$$

where ΔH_u is the heat of fusion per repeat unit, σ_u is the energy of crystal-melt interface parallel to the chain axis, and σ_e is the surface free energy of the crystal fold surface. Mandelkern also described the situation where growth is controlled not by the primary nucleation but by the rate of crystal growth. This secondary nucleation rate (two-dimensional nucleation) was given by Sawada and Nose[25] as

$$k = k_0 \exp\left(\frac{-nE_D}{RT} - \frac{4b\sigma_u\sigma_e}{R\Delta H_u}\frac{T_m}{T(T_m T)}\right) \tag{6.10}$$

where b is the width of the nucleus.

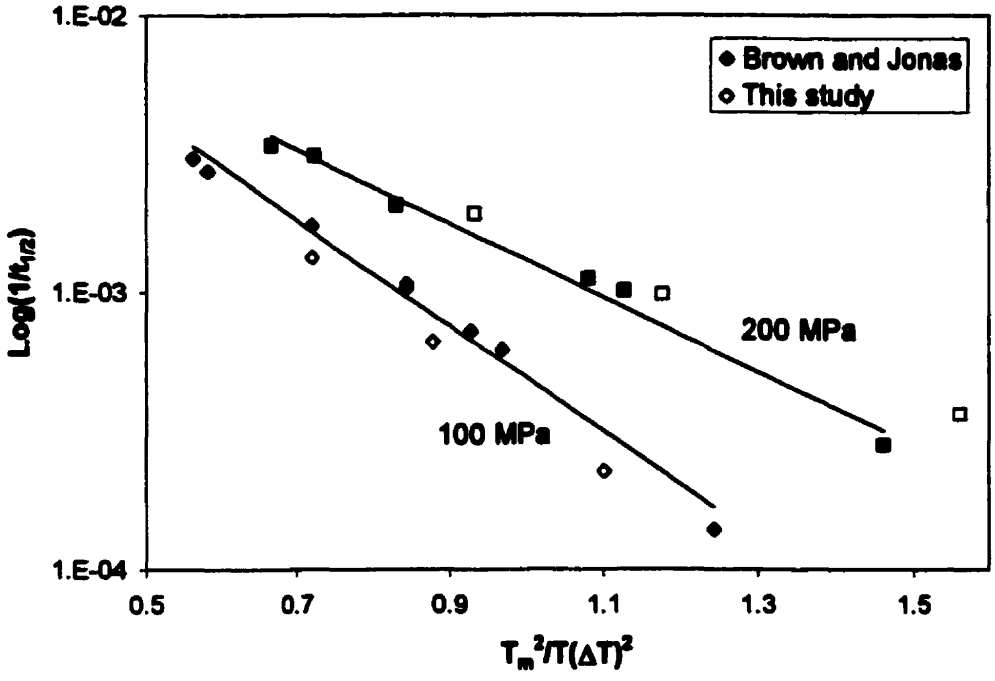

Figure 6.30: Plots of $t_{1/2}^{-1}$ versus undercooling $T_m^2(\Delta T)^2$ for the HDPE resin data and Brown and Jonas[26] data.

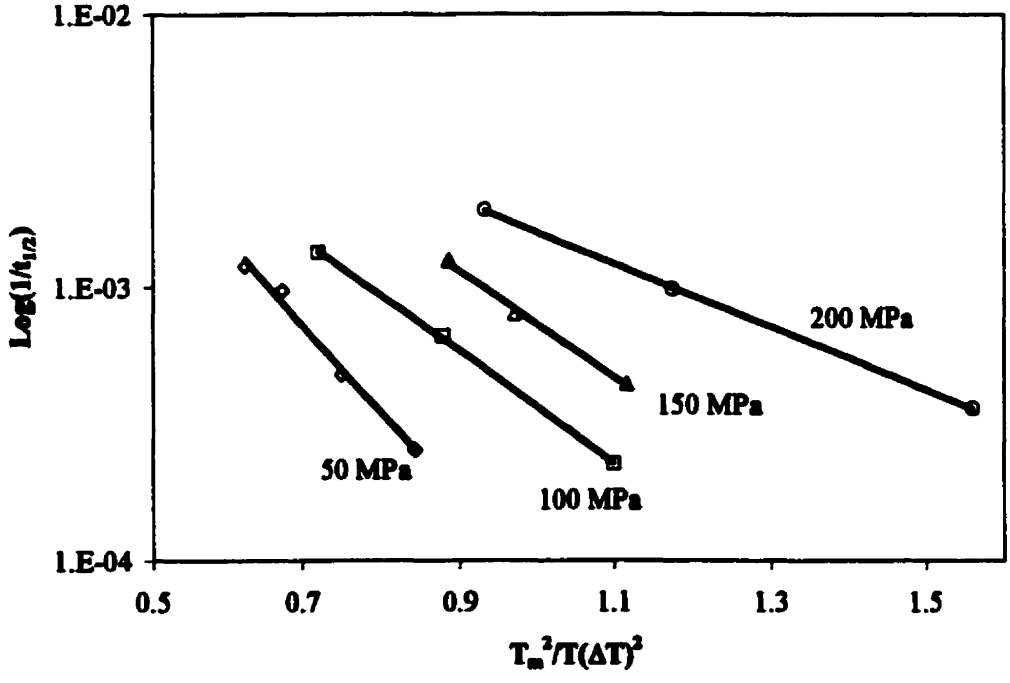

Figure 6.31: Plots of $t_{1/2}^{-1}$ versus undercooling $T_m^2(\Delta T)^2$ for the HDPE resin at various pressures.

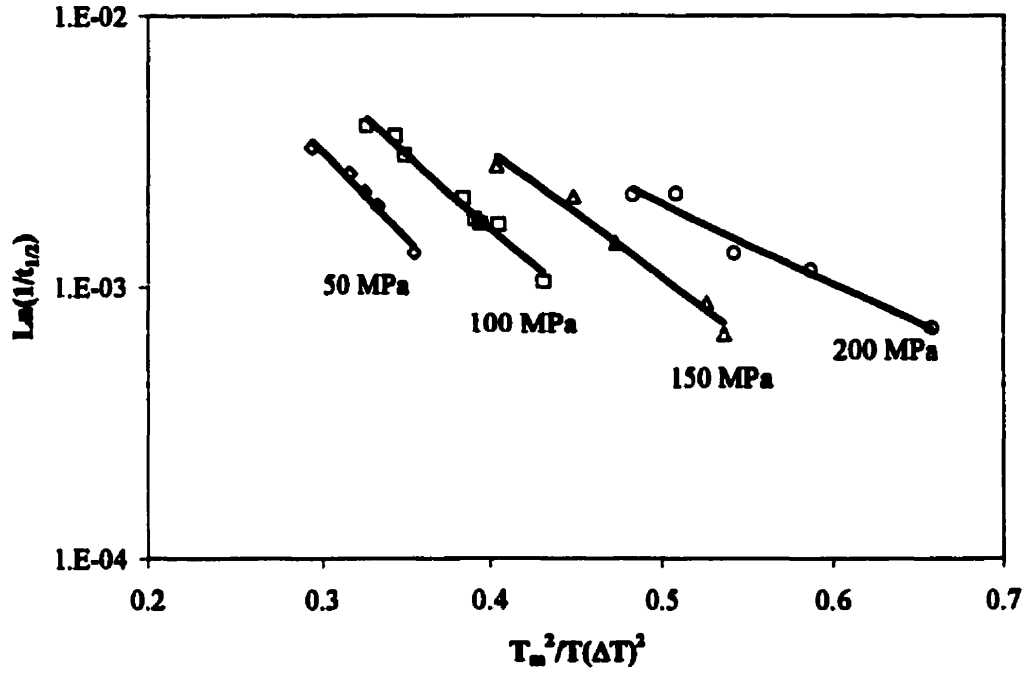

Figure 6.32: Plots of $t_{1/2}^{-1}$ versus undercooling $T_m^2(\Delta T)^2$ for the LLDPE-L resin.

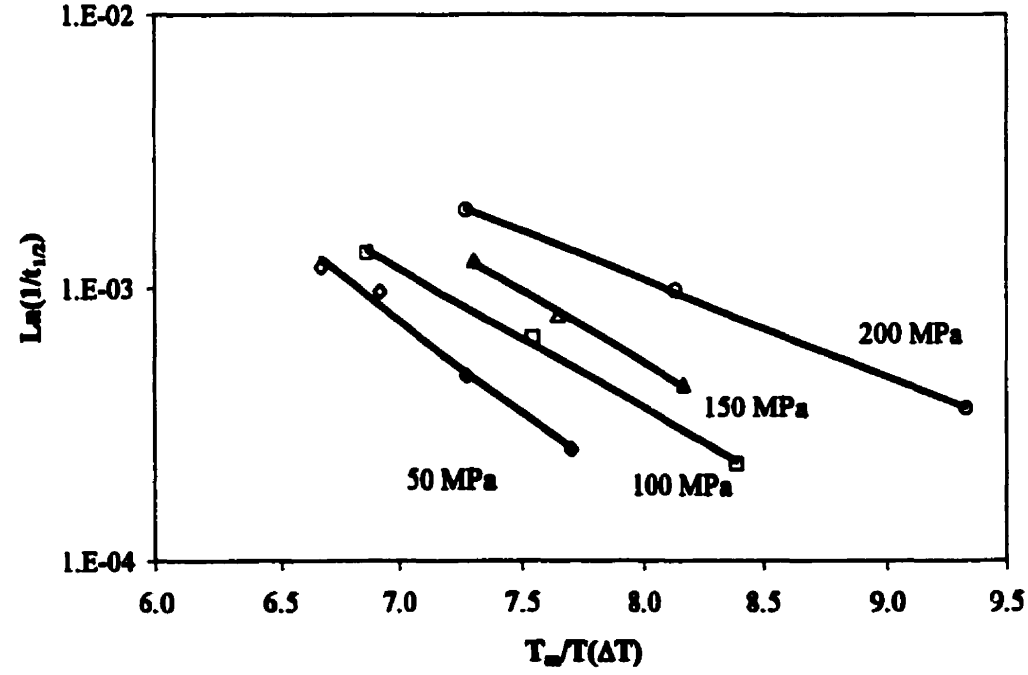

Figure 6.33: Plots of $t_{1/2}^{-1}$ versus undercooling $T_m(\Delta T)$ for the HDPE resin.

In order to discern if the crystallization rate was controlled by the process of diffusion or by the nucleation and growth process, the plots of log $t_{1/2}^{-1}$ versus $T_m^2(\Delta T)^2$ were first traced for the HDPE resin and compared with the results of Brown and Jonas[26], as shown in Figure 6.30.

The plots presented here are known to be strongly dependent on temperature[1]. In this study, the values of T_m were taken from the data of Wunderlich and Davidson[16]. The melting points reported by these authors are for extended-chain crystals that were prepared by crystallization under 5 kbar at 214°C. These temperatures are an approximation of the equilibrium melting point under pressure. These data were also chosen for the sake of comparison of our values with those of Brown and Jonas[26].

Figure 6.30 shows that the kinetics results from this study are in good agreement with those from literature[26]. The straight lines, which are an exponential fitting of Brown and Jonas data, indicate that the rate is controlled by the surface energy and heat of fusion term in eq. (6.8). This figure and Figure 6.31 show a decrease of the slopes with increasing pressure, implying a decrease in the energetic term in eq. (6.9). Only the surface energies are likely to change. This is in agreement with the decrease in the surface energy observed by Kyotani and Kanetsuna[24], Sawada and Nose[25], and Brown and Jonas[26]. However, this indicated decrease contradicts the observation of Calvert and Uhmann[35] of an increase of surface energy σ_e with pressure.

The plot of log $t_{1/2}^{-1}$ versus $T_m^2(\Delta T)^2$ was then traced for all the LLDPE resins. They all exhibited the same tendency as above. The decrease of the slopes with pressure was more or less noticeable depending on the resin. As an example, Figure 6.32 presents the results for the L resin.

The plots of log $t_{1/2}^{-1}$ versus $T_m/T(\Delta T)$ also yielded straight lines, as illustrated for the HDPE resin in Figure 6.33. However, the decrease of the slopes with pressure was less obvious or even not present for the LLDPE resins. From eq. (6.10), this slight decrease indicates that the secondary nucleation is controlled by the surface energy term and not by diffusion.

6.3.5) Summary

The investigation of crystallization kinetics furnished notable information on the effect of pressure and chain structure on crystallization. It was confirmed that the LLDPE resins exhibit a two-step crystallization process, primary and secondary crystallization.

The analysis of the Avrami fitting showed that the Avrami parameter *n* was influenced by the nature of the catalyst employed in the polymerization reaction.

The study of the effect of pressure on half-time of crystallization and induction time demonstrated that resins D and G had a noticeable distinct behavior. Resin D exhibited the fastest crystallization behavior, whereas resin G displayed the slowest crystallization.

The investigation of the effect of pressure at constant supercooling led to contradictory results, depending on resin grade. Crystallization was accelerated by pressure for the HDPE resin, while on the contrary it was delayed for only one LLDPE resin, the L grade. In addition, the onset of crystallization was only observed to be retarded by pressure for the resins prepared by Ziegler-Natta catalysts.

Finally, the interpretation of the results by the Lauritzen-Hoffman theory indicated that some resins, such as HDPE and L, exhibit a decrease in the surface free energy of the crystal nucleus with pressure. It also appears that, for most LLDPE resins, this effect is not observable.

The above results indicate that the polyethylene chain structure influences crystallization kinetics in different ways. It can be concluded that the branching non-uniformity and molecular weight distribution, which are determined by catalyst type and polymerization medium have a significant influence on the nucleation and growth mechanisms. Furthermore, this effect on nucleation seems to be magnified by pressure. Pressure effects on crystallization kinetics depend on chain structure, particularly branching and ist uniformity and molecular weight distribution. Finally, pressure causes the lowering of the surface free energy of the crystal nucleus. This effect of pressure depends on the chain structure and molecular weight distribution.

CHAPTER 7

SUMMARY, CONCLUSIONS, AND FURTHER WORK

7.1) Summary and Conclusions

The main results obtained in the present study for all the resins are summarized in Table 7.1. It includes the thermal expansion coefficient, α_0, and the Tait Parameter, B_0, from the PVT melt behavior; the pressure dependence of the melting point; the average value of the Avrami exponent, *n*; and it indicates the tendency of the pressure effect on crystallization half time and induction time, at constant undercooling.

Table 7.1: Main results achieved in the present study for all the resins.

Resin Code	Polym. Medium	Catalyst Type	Co-monomer	Density	α_0 ($^oC^{-1}$)	B_0 (MPa)	dT_m/dP (^oC/MPa)	*n*	*Effect of Pressure* $t_{1/2}$	t_i
A	Gas	ZN	Hexene	0,9208	7,52	195	0,26	1,6	--	↗
B	Gas	ZN	Butene	0,9194	7,46	194	0,26	1,6	--	↗
C	Solution	Met	Hexene	0,9234	7,54	199	0,26	1,7	--	--
D	Gas	Met	Hexene	0,9192	7,42	200	0,25	1,2	--	--
E	Gas	Met	Hexene	0,9194	7,44	196	0,24	1,4	--	--
F	Gas	-	LDPE	0,9190	7,40	197	0,23	1,3	--	--
G	Solution	ZN	Octene	0,9200	7,55	198	0,26	1,8	--	↗
H	Solution	ZN	Butene	0,9190	7,39	200	0,25	1,7	--	↗
I	Solution	Met	Octene	0,9070	7,26	194	0,22	1,5	--	--
J	Solution	Met	Octene	0,9180	7,35	195	0,24	1,4	--	--
K	Gas	-	LDPE	0,9198	7,53	198	0,23	1,3	--	--
L	Solution	-	LLDPE	0,9222	7,56	204	0,26	1,6	↗	↗
HDPE	-	-	-	0,9620	7,68	197	0,24	1,7	↘	↘

From the isothermal experiments, it was observed that the general PVT behavior was similar for all the LLDPE grades, but it differed for the HDPE resin in the transition region. The PVT melt behavior of all resins was found to be almost identical. This was verified with the fitting results of the Tait and Inverse-Volume equations, which represented accurately the behavior in the melt state. In addition, the isothermal compressibility and thermal expansion coefficient were also not especially affected by the grade of polyethylene resin. The Tait and Inverse-Volume equations were found to poorly predict these two derivatives. However, only, the Inverse-Volume equation could predict the tendency of the thermal expansion coefficient to increase with temperature. From these results, it can be concluded that the polyethylene chain structure, as reflected by comonomer content and type, branching size, and molecular weight and their distributions, does not affect significantly the PVT behavior of the melt state, the compressibility and the thermal expansion.

The investigation of the isobaric experiments lead to the conclusions that the melting and crystallization temperatures of LLDPE and HDPE resins are linearly and similarly dependent on pressure up to 200 MPa. This dependence was estimated at 0.25°C/MPa. Moreover, the curve shapes of the melting and crystallization processes of the LLDPE resins contributed to a better understanding of the differences in crystallization and melting behavior attributed to their branching size and uniformity, molecular weight and polydispersity.

The fitting of the crystallization kinetics data to the Avrami equation yielded interesting results. The average value of the Avrami exponent n was found to vary from 1.1 to 1.8 depending on the polyethylene resin. Furthermore, Ziegler-Natta catalyzed resins clearly exhibited a value of n superior to 1.6, whereas the metallocene catalyzed resins showed values ranging between 1.1 and 1.5, with the exception of resin C. This suggests that the branching size and its uniformity, determined by the type of catalyst, affect crystallization, and especially, the crystal growth and its shape.

The study of the half time of crystallization and induction time at constant supercooling indicated and confirmed that the metallocene resin D and the Ziegler-Natta resin G exhibit different and extreme crystallization kinetics properties, compared to the

other grades. This implies that the polymer chain properties, and subsequently the polymerization process parameters influence crystallization kinetics.

The evaluation of the effect of pressure on crystallization kinetics at constant supercooling yielded the following results: crystallization was accelerated by pressure for the HDPE resin, and in contrast, crystallization and more significantly crystallization onset were delayed by pressure for the Ziegler-Natta catalyzed LLDPE resins. This indicates that the effects of the non-uniformity of branching on the nucleation mechanisms are magnified by pressure.

The interpretation of the results by the Lauritzen-Hoffman theory pointed out that pressure induces a decrease of the surface free energy of the crystal nucleus. This could explain the increase in crystallization rate with pressure for the HDPE resin. A less noticeable decrease of the surface energy was observed for most LLDPE resins. For these resins, this suggests that the influence of pressure on the surface energy is less important than the other effects of pressure on the nucleation mechanisms.

From the present work, the ultimate conclusions concerning the effect of pressure and polymer chain structure on crystallization are summarized below. The polymerization process conditions, such as polymerization medium, catalyst, and comonomer, affect the polymer chain structure, which in turn affect crystallization kinetics. With pressure, the retardation effect of branching and branching non-uniformity on the nucleation and crystallization process seems to be magnified and to overcome the other, opposite effect of pressure on crystallization. Indeed, pressure also influences crystallization by decreasing the surface energy of the crystal nucleus, which seems to induce an acceleration of crystallization.

7.2) Recommendation for Further Work

In order to further explain the results obtained in the present study, and to extend the investigation of the effect of processing and polymerization conditions on crystallization mechanisms, some morphological and thermal studies should be carried out.

As for thermal studies, the numerous data generated in this work should be employed to investigate the non-isothermal kinetic behavior of the resins under pressure. The large range of undercooling covered by non-isothermal experiments under pressure would certainly bring valuable information to confirm and, eventually, to extend the conclusions of this report. Furthermore, using the same experimental technique, the study of the effect of pressure on the secondary crystallization process could provide important information for the understanding of LLDPE crystallization. In addition, an extensive work using differential scanning calorimetry should be performed to assess isothermal and non-isothermal crystallization kinetic data at atmospheric pressure, for comparison with high pressure data. It could also be employed to measure the melting behavior of high pressure crystallized sample.

Morphological investigation of the samples crystallized under pressure using optical microscope and X-rays would be very helpful to observe the correlated effect of pressure and chain structure on morphology and crystallinity.

REFERENCES

1) L. Mandelkern, *Crystallization of Polymers*, McGraw-Hill, New York, 1964.

2) F. Khoury and E. Passaglia, *Treatise on Solid State Chemistry*, vol. 3, N. B. Hanny, Ed., Plenum Press, New York, 1976.

3) J. D. Hoffman, G. T. Davis, and J. L. Lauritzen, *Treatise on Solid State Chemistry*, vol. 3, N. B. Hanny, Ed., Plenum Press, New York, 1976.

4) J. H. Magill, *Properties of solid polymeric materials, Part A*, Treatise on Materials Science and Technology, 10, (J.M. Schultz Ed.), Academic Press, New York, 1977.

5) B. Wunderlich, *Crystal Structure, Morphology, Defects*, Macromolecular Physics, vol. 1, Academic Press, New York, 1973.

6) B. Wunderlich, *Crystal Nucleation, Growth, Annealing*, Macromolecular Physics, vol. 2, Academic Press, New York, 1976.

7) B. Wunderlich, *Crystal Melting*, Macromolecular Physics, vol. 3, Academic Press, New York, 1980.

8) E. Chu, Master of Engineering, McGill University, 1984.

9) L. Mandelkern, Physical properties of Polymers, 2nd ed., ACS Professional Ref Book, ACS, Washington, 1993.

10) G. R. Strobl, *Concepts for understanding their structures and behavior*, The Physics of Polymers, Springer Ed., Berlin, 1996.

11) D. C. Bassett, B. Turner, *On Chain-extended and chain-folded crystallization of Polyethylene*, Phil. Mag., 29, 285 (1974).

12) K. H. Storks, *An Electron-Diffraction Examination of Some Linear High Polymers*, J. Am. Chem. Soc., 60, 1753 (1938).

13) A., Keller, Phil. Mag., 2 1171 (1957).

14) E. W. Fischer, Z. Naturforsh, 12A, 753 (1957).

15) P. H., Jr. Till, J. Polym. Sci., 24, 301 (1957).

16) T. Davidson, B. Wunderlich, *Differential Analysis of Polyethylene under High Pressure*, J. Polym. Sci., Part A2, 7, 377 (1969).

17) Y. Maeda, H. Kanetsuna, K, Tagashira, and T. Takemura, J. Polym. Sci. Polym. Phys. Ed., 19,1313 (1981).

18) J. A. Parker, D.C. Bassett, R. H. Olley, and P. Jaaskelainen, *On high pressure crystallization and the characterization of linear low-density polyethylenes*, Polymer, 35, 4140, (1994).

19) T. Hatakeyama, H. Kanetsuna, H. Kaneda, and T. Hashimoto, *Effect of Pressure on the Crystallization Kinetics of Polyethylene*, J. Macromol. Sci. Phys., B10(2), 359 (1974).

20) T. Kowalewski and A. Galeski, *Crystalization of Linear Polyethylene from Melt in Isothermal Compression*, J. Appl. Polym. Sci., 44, 95 (1992).

21) D, Turnbull and J.C. Fisher, *Rate of Nucleation in Condensed Systems*, J. Chem. Phys., 17, 71 (1949).

22) F. P. Price, *Nucleation in Polymer Crystallization*, in "Nucleation" (A. C. Zettlemoyer, ed.), pp. 405-488 Marcel Dekker, New York (1969).

23) F. P. Price, *Kinetics of Spherulite Formation*, J. Polym. Sci., C, 3, 117 (1963).

24) M. Kyotani and H. Kanetsuna, *Crystallization Kinetics of Polyethylene under Pressure*, J. Polym. Sci. Polyms. Phys., Ed., 12, 2331 (1974).

25) S. Sawada and T. T. Nose, *Crystallization Kinetics of Fractionated Polyethylenes at high pressures by a DTA method*, Polym. J., 11, 477, (1979).

26) D. R. Brown and J. Jonas, *NMR Study of Polyethylene Crystallization Kinetics under High Pressure*, J. Polym. Sci. Polym. Phys. Ed., 22, 655 (1984).

27) H. D. Keith, and F.J., Jr., Padden, Spherulitic *Crystallization from the melt. II. Influence of Fractionation and Impurity Segregation on the Kinetics of Crystallization*, J. Appl. Phys., 35, 1270 (1964).

28) D. W. van Krevelen, *Crystallinity of polymers and the means to influence the crystallization process*, Chimia, 32, 279 (1978).

29) Y. K. Godovsky and G. L. *Slonimsky, Kinetics of Crystallization from the Melt (Calorimetry Approach)*, J. Polym. Sci. Polym. Phys., Ed., 12, 1053 (1974).

30) B. C. Edwards and P. J. Phillips, *High-Pressure Phases in Polymers II...* J. Polym. Sci.: Polym. Phys. Ed., 13, 2117 (1975).

31) J. M. Schultz, J. S. Lin, and R. W. Hendricks, *A dynamic Study of the Crystallization of Polyethylene from the melt*, J. Appl. Cryt., 11, 551 (1978).

32) S. Matsuoka, *Pressure-induced Crystallization in Polyethylene*, J. Polym. Sci., **42**, 511 (1960).

33) G. M Martin and L. Mandelkern, J. Appl. Phys, **34**, 2312 (1963).

34) H. H. Hoehn, R. C. Fergurson, and R. R. Herbert, *Effect of Molecular weight on high pressure crystallization of linear polyethylene. I kinetics and gross morphology*, Polym. Eng. Sci., **18**, 457 (1978).

35) P. D. Calvert and D. R. Uhlmann, *Crystallization of polyethylene at high pressures: A kinetic view*, J. Polym. Sci. A-2, **10**, 1811 (1972).

36) R. Eckel, M. Buback, and G. R. Strobl, Colloid Polym. Sci., **259**, 326 (1981).

37) B. J. Bridges, A. Charlesby, and R. Folland, Proc. R. Soc. Lodon Ser. A, **367**, 343 (1979).

38) M.C. Tobin, J. Polym. Sci.: Polym. Phys. Ed., **14**, 2253 (1976).

39) W. Dietz, *Sphärolithwachstum in Polymeren*, Coll. Polym. Sci., **259**, 413 (1981).

40) Y. A. Malkin, V. P. Beghishev, I. A. Keapin, and Bolgov S. A., Polym. Eng. Sci., **24**, 1396 (1984).

41) S. P. Kim and S. C. Kim, Polym. Eng. Sci., **31**, 110 (1991).

42) K. Nakamura, T. Watanabee, and K. Katayama, J. Appl. Polym. Sci., **16**, 1077 (1972).

43) M. R. Kamal and E. Chu, *Isothermal and Non-isothermal Crystallization of Polytehylene*, Polym. Eng. Sci., **23**, 27 (1983).

44) M. Avrami, J. Chem. Phys., **7**, 1103 (1939).

45) M. Avrami, J. Chem. Phys., **8**, 212 (1940).

46) L. Mandelkern, J. Appl. Phys. **26**, 443 (1955).

47) I. H. Hiller, J. Plym. Sci., A, **3**, 3069 (1965).

48) B. B. Burnett, and W. F. McDevit, J. Appl. Phys., **28**, 1101 (1957).

49) A. Ziabicki, Colloid Polym. Sci., **252**, 207 (1974)

50) S. Saeki, S. Taeki, Y. Ookubo, M. Tsubokawa, T. Yamaguchi, and T. Kikegawa, *Pressure dependence of melting temperatures in branched polyethylene up to 2 GPa*, Polymer, **39**, 4267 (1998).

51) K. Takamizawa, A. Ohno, and Y. Urabe, *Effect of Pressure on Melting Temperatures of Polyethylene Fractions*, Polym. J., 7, 342 (1975).

52) Von F. Simon and G. Glatzel, *Bemerkungen zur Schemelzdruckkurve*, Z. Anorg. Allg. Chem., 178, 309 (1929).

53) C. P. Chiu, K. A. Liu, and J. H. Wei, *A Method for Measuring PVT Relationships of Thermoplastics Using an Injection Molding Machine*, Polym. Eng. Sci., 35, 1505 (1995).

54) Y. A. Fakhreddine and P. Zoller, *Pressure-Volume-Temperature Studies: A Versatile Analytical Tool for Polymers*, ANTEC, Conference Proceedings, 1991, Soc. of Plastics Engineers, Brookfield, CT, USA., 1642 (1991).

55) P. Zoller, "Polymeric Equations of State," *Polymer Handbook*, 3rd Edition, J. Brandup and E. H. Immergut, Editors: Wiley & Sons, (1989).

56) S. K. Bhateja and K. D. Pae, *J. Macromol. Sci. Revs. Macromol. Chem.*, 13, 77 (1975).

57) R. Simha and T. Somcynsky, *Macromolecules*, 2, 342 (1969).

58) R. Simha and R. K. Jain, *J. Polym. Sci. Polym. Phys. Ed.*, 16, p1471-89 (1978).

59) M. R. Kamal and N. T. Levan, *Polym. Eng. Sci.*, 13, p131-138 (1973).

60) P. G. Tait, "*Physics and chemistry of the voyage of H. M. S. challenger*," 2, Pt.4, University Press, Cambridge, p1900 (1888).

61) S. Beret and J. M. Prausnitz, Macromolecules, 8, 536 (1975).

62) *Dilatometry*, Encyclopedia of Polymer Science and Engineering, 2nd Edition, H. Mark, N. Bikales, Ch. Overberger, Ed.; Wiley & Sons, New York, 1986.

63) P. Zoller, *The pressure-volume-temperature properties of three well-characterized low-density polyethylenes*, J. Appl. Polym. Sci., 23, 1051 (1979).

64) P. Zoller, P. Bolli, V. Pahud, and H. Ackerman, Rev. Sci. Instrum., 47, 948 (1976).

65) J. He, Y. A. Fakhreddine, and P. Zoller, J. Appl. Polym. Sci., 45, 45 (1992).

66) *Linear Low Density Polyethylene*, Encyclopedia of Polymer Science and Engineering, 2nd Edition, H. Mark, N. Bikales, Ch. Overberger, Ed.; Wiley & Sons, New York, vol. 17, 756, 1986.

67) M. Samara, PhD's Thesis, McGill University, in print.

68) Levan's Master Thesis, McGill University, 1973.

APPENDIX I

PVT SAMPLE RUNS

This appendix is devoted to describing the detailed procedures of each step required prior to each sample run. It details the procedures for the nickel cup and cell preparation, the cell filling, the apparatus assembling and disassembling, the cell cleaning, and the LVDT calibration. Some recommendations concerning calibration are also included.

I.1) Sample Run Preparation

Note: * *refers to the page number of the PVT manual.*

I.1.1) - Nickel cup preparation (page 52)*

To maintain a hydrostatic pressure on the sample in the solid state and to protect the bellows, a nickel cup is required. A rectangular piece (30×50 mm) is first cut into a 0.001" thick nickel foil. The cup shape is then formed with the use of an aluminum conical mandrel provided with the apparatus. The nickel cup is next weighed to one milligram. All the parts of the cell, including the two gaskets and the steel sealing disk, are also weighed to 0.01 grams. The nickel cup is then entirely filled with the material, which is weighed to one milligram. The cup and the sample are next placed in the sample compartment.

I.1.2) - Bellows preparation (page 64)*

The length of the bellows fixes the overall volume of the cell. It is thus an important step to control the bellows length. The bellows are first mounted on the filler base. The bellows might need to be compressed or stretched in order to obtain the fixed length determined by the set screw of the filler base. Indeed, the set screw should

compress the bellows slightly (about 1/2 mm) when the screw is engaged in the groove of the constraining rod.

I.1.3) - Cell preparation (illustrated page 54-62)*

The different parts of the cell, including the bellows, the central piece, and the sample compartment (containing the sample and the cup), are assembled with the help of the ring nuts. The two gasket rings are placed between parts to ensure a proper sealing of the assembly. The cell parts are tightened with a wrench applied to the central piece. The assembled cell is then mounted on the filler base. To fix the overall volume of the cell, which is extremely important, the constraining rod is inserted and threads into the end of the bellows. The rod position is then adjusted so that the set screw engages exactly the groove in the constraining rod. The cell is then attached to the reservoir with a flexible tube.

I.1.4) - Filling procedure (page 65)*

After having placed the filler base in a tray in a fume hood, fresh, clean confining fluid (about 10-12 cm^3) is poured in the reservoir through the filler base hole, using a syringe. The cell, mounted on the filler base, is next placed in the vacuum vessel, with the reservoir on top and the piezometer cell on the bottom. The vacuum vessel is kept in the 45° position and connected to a vacuum pump in order to obtain a vacuum of better than 4×10^{-2} mm of Hg. When the required vacuum is attained, the vacuum vessel is cautiously tilted past the horizontal, until it comes to rest against the stop provided. Keeping the vacuum pump on the system, the vacuum vessel is maintained tilted for 5 minutes to permit the confining fluid to flow from the reservoir into the sample cell. Without moving the vacuum vessel, the vacuum pump is turned off. Over a period of 15 seconds, the air is admitted through the valve to reduce vacuum to about 15 inches of Hg. The vacuum vessel is then moved back to its original 45° position, and the valve is next opened completely to equilibrate to atmospheric pressure. The filler is now withdrawn carefully

from the vacuum vessel. The flexible tube is disconnected from the reservoir, and the remaining confining fluid is poured into the end of the cell. Employing a suction device, the excess of confining fluid is sucked until the meniscus of the fluid is exactly at the top of the small bore leading into the sample compartment. The steel sealing disk that was previously weighed is placed into the end piece and centered, and the cell closure nut comes to seal the end of the cell. The set screw of the filler base is now unscrewed to release the constraining rod that can be removed from the bellows. The assembled cell is then removed from the filler base. The fully filled cell is finally weighed to 0.01 grams, to evaluate the mass of the confining fluid used. The filling of the cell can be checked with the help of the "fill procedure" section of the PVT software. The repeat fillings of the same cell should have the same volume within 0.03 to 0.05 cm^3.

I.1.5) - Assembling of the apparatus

At this step, the assembled cell, containing the sample, the nickel cup, and the confining fluid, must be mounted on the PVT apparatus. The LVDT core, which is mounted at the end of a long thin tube, is lifted up, far enough, to be capable of screwing its end into the bellows. The sample cell is screwed to the adapter in the base of the PVT apparatus. The pressure vessel, which is a thick steel cylinder with heaters, is cautiously lowered over the sample cell. The control thermocouple is then placed into the side hole of the pressure vessel. The thermocouple block is next placed on top of the pressure vessel, ensuring that the thermocouple tip enters the conical opening of the cell closure nut. The spacer is added to the top of the thermocouple block and finally the finned aluminum heat sink is placed on top of the spacer block. The ram piston is then lowered using the hand pump until the pressure reaches the value of 9000 Psi (around 62 MPa). A pressure of 200 MPa is applied manually to the pressure with the high-pressure pump to fill the vessel with the silicon oil and for inspecting for any possible leakage.

The PVT apparatus is now ready for a calibration or sample run (cf. Paragraph I.2)).

I.1.6) Disassembling of the PVT apparatus

One must be aware of the possible hazards of a PVT run, for example, a leak of confining fluid or generation of gases by decomposition or by chemical reaction. The safety information chapter of the PVT manual should be read before disassembling the apparatus. The disassembling should be done at ambient temperature. Firstly, the electronic boxes are turned off. Secondly, the pressure is released by opening the bottom drain valve. The high-pressure thermocouple and the heater connector are unplugged, and the control thermocouple is removed. Subsequently, the ram piston is raised by releasing the ram pressure slowly. Thirdly, the finned heat sink, the spacer block, the thermocouple block, and the pressure vessel are removed. Finally, the cell is carefully unscrewed and so is the LVDT core. All parts of the PVT apparatus, including the cell, are cleaned with paper towels and acetone.

I.1.7) Cleaning of the cell

The cell can now be disassembled. The cell must be untied by placing it in a strong flexible polyethylene bag in order to prevent spilling of confining fluid, usually mercury. Working over a tray in a fume hood, the bellows are first removed, and then the confining fluid is drained almost completely. After having removed the central part and the ring nuts and drained the remaining confining fluid, the sample, which is usually heavily contaminated with confining fluid, is easily removed thanks to the use of a nickel cup. Finally all parts are abundantly rinsed with acetone, or other suitable solvent, until no more confining fluid can be seen on any part.

I.2) Calibration or Sample Run

If the computer and the two electronic units are turned on, all switches are in the correct position, and the stroke transducer indicates the correct value of 45%, the PVT apparatus is ready to start a new sample run. Every new sample run starts with a LVDT calibration.

I.2.1) - LVDT Calibration (page 27)*

The position of the LVDT, reflecting the position of the bellows end, is measured with a resolution of 0.001 mm, representing a volume change of approximately 0.0001 cm^3/g. The sensitivity of the PVT is calibrated against a precision digital micrometer, which is attached to the LVDT coil. Consequently, before starting a run, the LVDT calibration must be achieved in order to obtain the linear relationship between the output voltage and the micrometer readings. Hence, the output voltage of the LVDT is first set to zero with in 0.001 volt by moving the micrometer. The micrometer is next moved in steps of 1.0 mm (within 0.1 mm) within a range of ±4 mm from the zero point; the corresponding voltage and micrometer readings are recorded. After the final reading, a linear regression is calculated on these recorded data by the PVT software. The LVDT calibration is accepted if the deviation between the experimental and fitted values is less than 0.003 mm; if not, another calibration must be repeated.

I.2.2) - Run information required

The inputting of the run information does not need many explanations. It is, however, important that the specific volume of the sample at ambient temperature is known with reasonable accuracy (2%). Although only volume changes are recorded during experiments, the program still requires the 2% accuracy in order to make certain calculations such as Tait extrapolation to zero pressure.

I.3) Recommendations

The temperature calibration must be performed at least once a month, especially if the apparatus is running constantly. In addition, the data acquisition (DASCON) board must be calibrated every six months, otherwise it could result in large data reading error.

APPENDIX II

ERROR ANALYSIS

Error analysis is the study and evaluation of uncertainty in measurement. Experience has shown that no measurement, however carefully made, can be completely free of uncertainty. This appendix will therefore report how the uncertainties in the PVT measurements were evaluated. Moreover, this section will include the formulae utilized to obtain the uncertainties and standard deviations of the parameters reported.

II.1) Error in the Volume Change Measurement

The change in position of the LVDT core is a measure of the volume change. In fact the volume change corresponds to the difference of position of the LVDT core between a calibration run and a sample run. The difference between the positions of the LVDT core is solely caused by the fact that a certain amount of sample (plus nickel cup) have replaced an amount of confining fluid, and that the sample, nickel cup, and the confining fluid have different PVT properties. The following equation expresses that mathematically:

$$\Delta V = V_s(P,T) - V_s(P_i, T_i) \qquad \text{(II.1)}$$

with $$V_s(P,T) = [1/m_s]\,[A(P,T)\,d(P,T)] - m_{Ni}\,V_{Ni}(P,T) + m_{CF}\,V_{CF}(P,T) \qquad \text{(II.2)}$$

where T_i and P_i are the initialization conditions of the sample run, $A(P,T)$ is the cross-sectional area of the bellows, $d(P,T)$ is the LVDT core position, V is the specific volume and m the mass of the different species; subscript s indicates the sample, Ni indicates the nickel cup and CF the confining fluid.

Equation (II.2) stands at all pressure and so at the initialization conditions. According to equation (II.1), the uncertainty in the volume change can be written as follows:

$$\delta(\Delta V) = \delta V_s(P,T) + \delta V_s(P_i, T_i) \qquad \text{(II.3)}$$

By assuming that errors in the volume values are not dependent on temperature and pressure, it can be written that:

$$\delta(\Delta V) = 2\,\delta V_s(P,T) \qquad \text{(II.4)}$$

For convenience, the volume can also be written: $V_s(P,T) = (1) + (2) + (3)$

which yields the following equation for the uncertainty in the volume:

$$\frac{\delta(V_s)}{V_s} \leq \frac{\delta(1)}{(1)} + \frac{\delta(2)}{(2)} + \frac{\delta(3)}{(3)} \qquad \text{(II.5)}$$

with

$$\frac{\delta(1)}{(1)} = \frac{\delta m_s}{m_s} + \frac{\delta A(P,T)}{A(P,T)} + \frac{\delta d(P,T)}{d(P,T)} \qquad \text{(II.6)}$$

$$\frac{\delta(2)}{(2)} = \frac{\delta m_{Ni}}{m_{Ni}} + \frac{\delta V_{Ni}(P,T)}{V_{Ni}(P,T)} \qquad \text{(II.7)}$$

$$\frac{\delta(3)}{(3)} = \frac{\delta m_{CF}}{m_{CF}} + \frac{\delta V_{CF}(P,T)}{V_{CF}(P,T)} \qquad \text{(II.8)}$$

Providing the following uncertainties:

$\delta m_s = 0.0001$ g,

$\delta m_{Ni} = 0.0001$ g,

$\delta m_{CF} = 0.01$ g,

and assuming that the errors in the specific volume of the different species equal 0.1%, the following values are obtained:

$\delta(1)/(1) = 0.15\%$

$\delta(2)/(2) = 0.32\%$

$\delta(3)/(3) = 0.14\%$.

It yields

$$\frac{\delta(V_s)}{V_s} \leq 1\%.$$

Therefore, the volume accuracy in the temperature range 25-220°C and the pressure range 10-200 MPa is equal to 0.03 cm^3/g.

It should be noted that the above value of the uncertainty corresponds to the systematic error component of the total uncertainty of the volume change. The random error component of the uncertainty, the standard deviation, will then be discussed.

II.2) Repeatability of isothermal measurements

Isothermal experiments consist of recording the volume changes along isotherms with increasing pressure by increments of 10 MPa. In order to estimate the repeatability of those experiments, the data points must be recorded at the exact same temperature. Indeed, a temperature difference of 0.5°C will consequently result in a volume change of 0.0004 cm^3/g. The sensitive part of the experiment is in the melting transition. The biggest discrepancy will be obtained in that region.

The following standard deviation was used to evaluate the repeatability:

$$\sigma = \sqrt{\frac{1}{N-1}\sum_{i=1}^{N}(x_i - y_i)^2} \qquad \text{(II.9)}$$

The average absolute percent deviation, which was utilized to assess the prediction of the isothermal compressibility and thermal expansion coefficient, is defined as:

$$A_{dev} = \sqrt{\frac{1}{N}\sum_{i=1}^{N}\frac{(x_{exp} - x_{pred})^2}{x_{exp}^2}} \times 100 \qquad \text{(II.10)}$$

where x_{exp} is the experimental value, x_{pred} is the value calculated for x_{exp} from the corresponding equation of state, and N is the number of x_{exp} under investigation.

II.3)

APPENDIX III

ISOBARIC EXPERIMENT DATA

III.1) Melting and Crystallization Temperatures

The following table presents the melting and crystallization temperatures obtained from isobaric experiments carried out at 2.5°C/min under 10, 50, 100, and 200 MPa.

Table III: Melting and crystallization temperature obtained from isobaric experiments at 2.5°C/min under various pressures.

P(MPa)	10	50	100	200	10	50	100	200
		A				H		
T_c	118.4	130.2	143.2	166.8	109.9	121.7	135.6	157.7
T_m	130.0	141.8	154.1	178.3	127.2	138.3	151.4	175.4
		B				I		
T_c	114.2	126.1	139.6	162.8	92.2	103.1	114.8	135.7
T_m	127.7	139	152.7	176.7	106.0	117.6	128.4	149.1
		C				J		
T_c	115.5	127.2	140.4	163.4	104.5	115.5	128.1	150.3
T_m	128.2	140.8	153.3	177.4	117.7	127.7	140.9	163.7
		D				K		
T_c	114.4	125.9	139.2	162.7	102.6	113.7	125.8	147.9
T_m	125.9	136.3	150.3	172.3	116.3	126.1	137.9	159.9
		E				L		
T_c	112.5	124.6	137.8	160.8	115.5	127.3	140.9	164.9
T_m	124.2	135.8	149.7	170.9	127.9	139.0	152.5	177.4
		F				HDPE		
T_c	102.1	112.2	124.4	146.0	122.2	134.1	148.1	171.4
T_m	113.8	125.5	137.0	158.9	138.2	149.5	161.7	184.3
		G						
T_c	113.1	125.5	138.9	162.3				
T_m	129.2	141.2	154.5	178.2				

III.2 Crystallization Curves

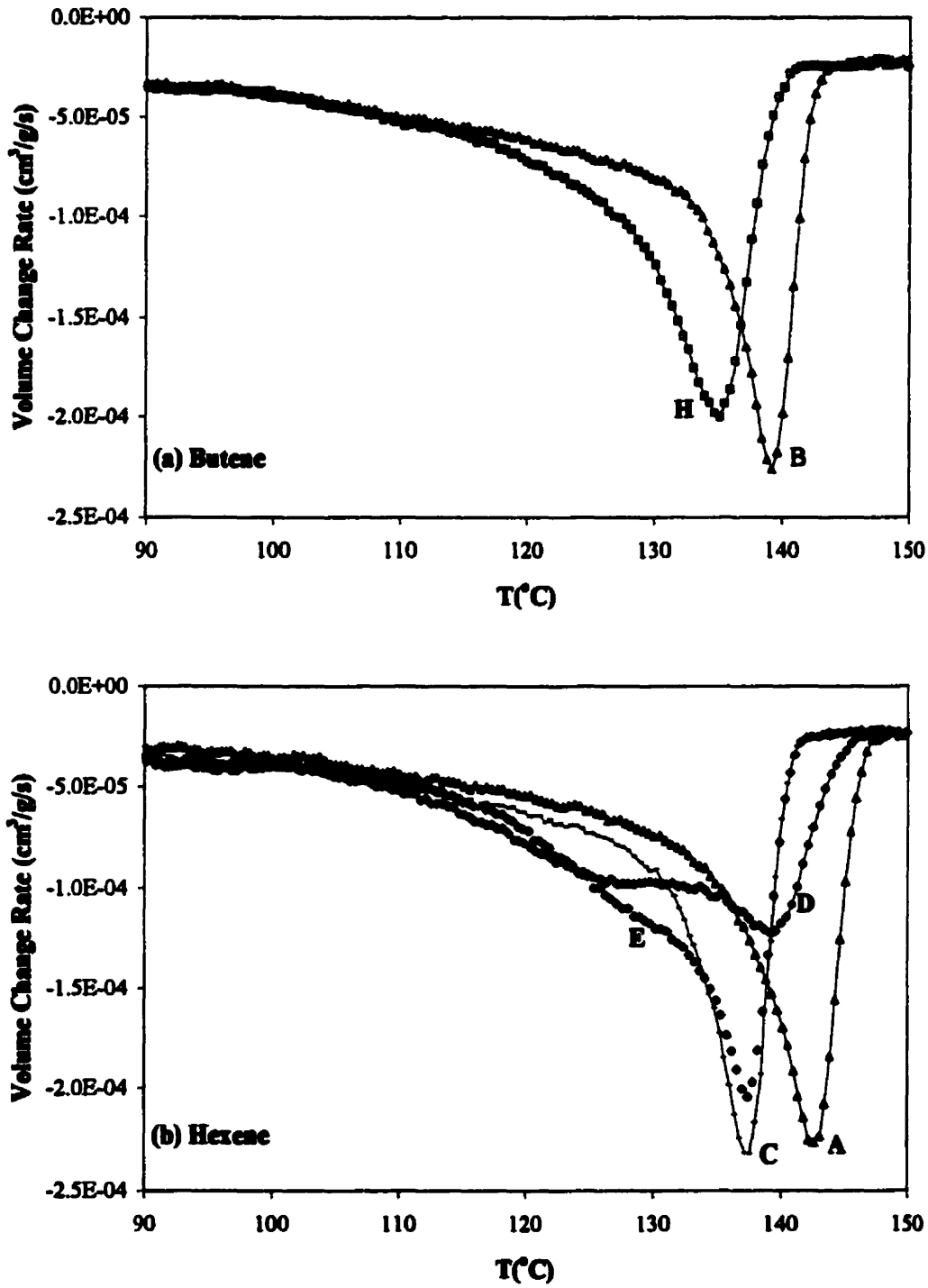

Figure III.1: Volume Change Rate vs. Temperature for the crystallization under 100 MPa at 2.5 °C/min of resins with (a) Butene and (b) Hexene comonomers.

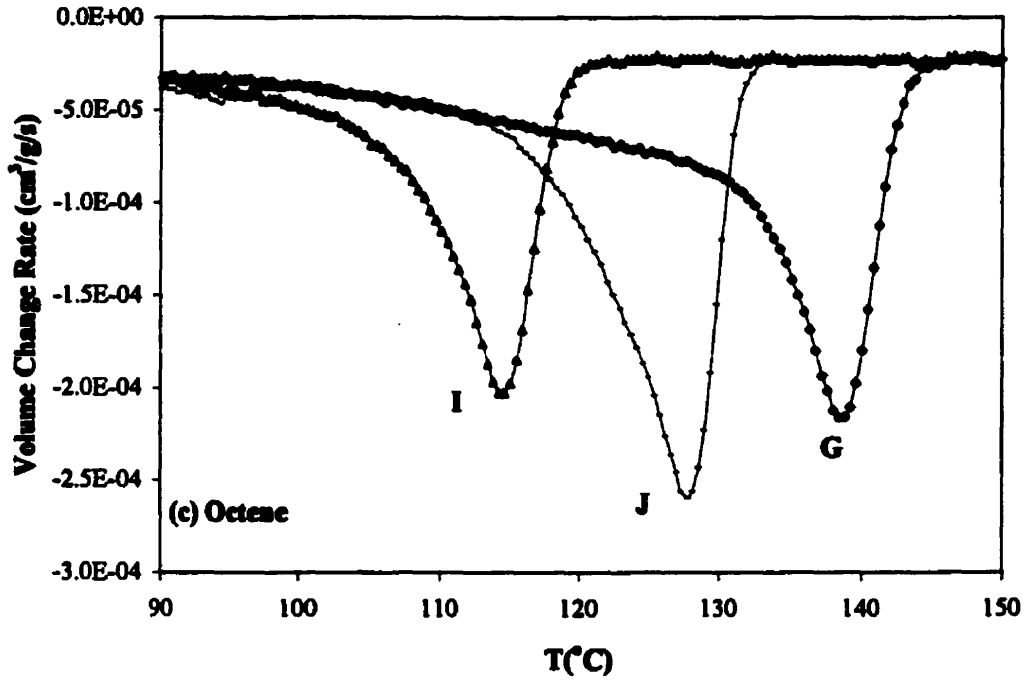

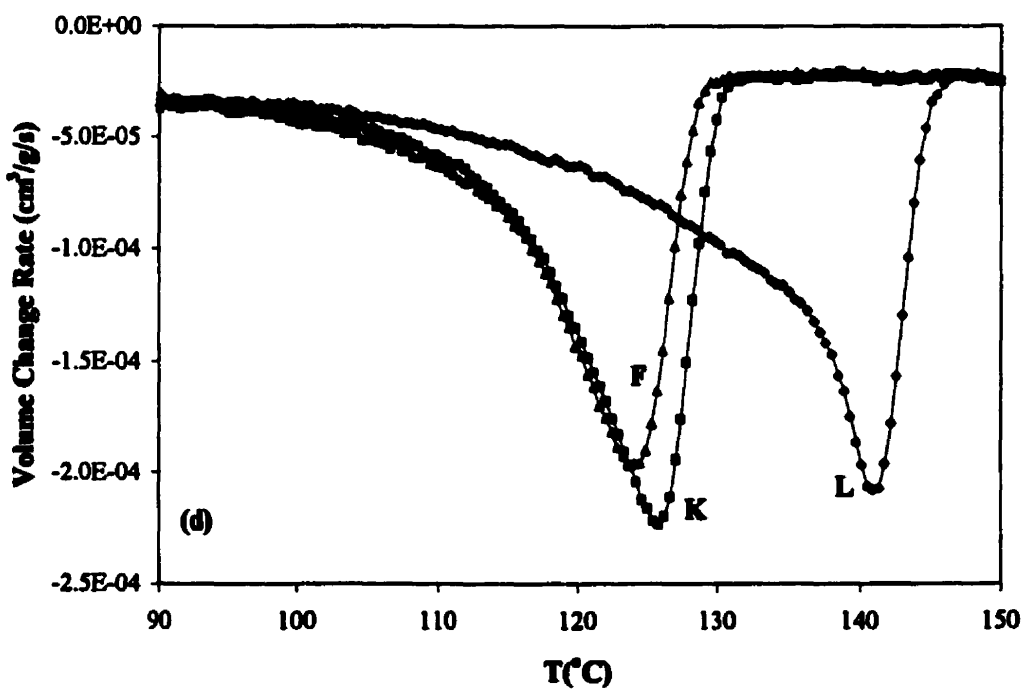

Figure III.1: Volume Change Rate vs. Temperature for the crystallization under 100 MPa at 2.5 °C/min of resins (c) with Octene comonomers and (d) F, K, and L.